REPORT DOCUMENTATION PAGE

Form Approved
OMB No. 0704-0188

1. AGENCY USE ONLY *(Leave blank)*	2. REPORT DATE	3. REPORT TYPE AND DATES COVERED
	May 94	

4. TITLE AND SUBTITLE
Navigation Performance and Integrity Monioring for Ballistic Missiles Using All-In-View GPS

5. FUNDING NUMBERS

6. AUTHOR(S)
Jeff Hossein Hassannia

7. PERFORMING ORGANIZATION NAME(S) AND ADDRESS(ES)
AFIT Student Attending:
Massachusetts Institute of Tech

8. PERFORMING ORGANIZATION REPORT NUMBER
96-006

9. SPONSORING / MONITORING AGENCY NAME(S) AND ADDRESS(ES)
DEPARTMENT OF THE AIR FORCE
AFIT/CI
2950 P STREET, BLDG 125
WRIGHT-PATTERSON AFB OH 45433-7765

10. SPONSORING / MONITORING AGENCY REPORT NUMBER

11. SUPPLEMENTARY NOTES

12a. DISTRIBUTION / AVAILABILITY STATEMENT
Approved for Public Release IAW AFR 190-1
Distribution Unlimited
BRIAN D. GAUTHIER, MSgt, USAF
Chief Administration

12b. DISTRIBUTION CODE

13. ABSTRACT *(Maximum 200 words)*

14. SUBJECT TERMS

15. NUMBER OF PAGES
158

16. PRICE CODE

17. SECURITY CLASSIFICATION OF REPORT	18. SECURITY CLASSIFICATION OF THIS PAGE	19. SECURITY CLASSIFICATION OF ABSTRACT	20. LIMITATION OF ABSTRACT

GENERAL INSTRUCTIONS FOR COMPLETING SF 298

The Report Documentation Page (RDP) is used in announcing and cataloging reports. It is important that this information be consistent with the rest of the report, particularly the cover and title page. Instructions for filling in each block of the form follow. It is important to ***stay within the lines*** to meet ***optical scanning requirements***.

Block 1. Agency Use Only *(Leave blank)*.

Block 2. Report Date. Full publication date including day, month, and year, if available (e.g. 1 Jan 88). Must cite at least the year.

Block 3. Type of Report and Dates Covered. State whether report is interim, final, etc. If applicable, enter inclusive report dates (e.g. 10 Jun 87 - 30 Jun 88).

Block 4. Title and Subtitle. A title is taken from the part of the report that provides the most meaningful and complete information. When a report is prepared in more than one volume, repeat the primary title, add volume number, and include subtitle for the specific volume. On classified documents enter the title classification in parentheses.

Block 5. Funding Numbers. To include contract and grant numbers; may include program element number(s), project number(s), task number(s), and work unit number(s). Use the following labels:

C	- Contract	**PR**	- Project
G	- Grant	**TA**	- Task
PE	- Program Element	**WU**	- Work Unit Accession No.

Block 6. Author(s). Name(s) of person(s) responsible for writing the report, performing the research, or credited with the content of the report. If editor or compiler, this should follow the name(s).

Block 7. Performing Organization Name(s) and Address(es). Self-explanatory.

Block 8. Performing Organization Report Number. Enter the unique alphanumeric report number(s) assigned by the organization performing the report.

Block 9. Sponsoring/Monitoring Agency Name(s) and Address(es). Self-explanatory.

Block 10. Sponsoring/Monitoring Agency Report Number. *(If known)*

Block 11. Supplementary Notes. Enter information not included elsewhere such as: Prepared in cooperation with...; Trans. of...; To be published in.... When a report is revised, include a statement whether the new report supersedes or supplements the older report.

Block 12a. Distribution/Availability Statement. Denotes public availability or limitations. Cite any availability to the public. Enter additional limitations or special markings in all capitals (e.g. NOFORN, REL, ITAR).

- **DOD** - See DoDD 5230.24, "Distribution Statements on Technical Documents."
- **DOE** - See authorities.
- **NASA** - See Handbook NHB 2200.2.
- **NTIS** - Leave blank.

Block 12b. Distribution Code.

- **DOD** - Leave blank.
- **DOE** - Enter DOE distribution categories from the Standard Distribution for Unclassified Scientific and Technical Reports.
- **NASA** - Leave blank.
- **NTIS** - Leave blank.

Block 13. Abstract. Include a brief *(Maximum 200 words)* factual summary of the most significant information contained in the report.

Block 14. Subject Terms. Keywords or phrases identifying major subjects in the report.

Block 15. Number of Pages. Enter the total number of pages.

Block 16. Price Code. Enter appropriate price code *(NTIS only)*.

Blocks 17. - 19. Security Classifications. Self-explanatory. Enter U.S. Security Classification in accordance with U.S. Security Regulations (i.e., UNCLASSIFIED). If form contains classified information, stamp classification on the top and bottom of the page.

Block 20. Limitation of Abstract. This block must be completed to assign a limitation to the abstract. Enter either UL (unlimited) or SAR (same as report). An entry in this block is necessary if the abstract is to be limited. If blank, the abstract is assumed to be unlimited.

★U.S.GPO:1990-0-273-271

CSDL-T-1219

NAVIGATION PERFORMANCE AND INTEGRITY MONITORING FOR BALLISTIC MISSILES USING ALL-IN-VIEW GPS

by

Jeff Hossein Hassannia

May 1994

Master of Science in Aeronautics and Astronautics
Massachusetts Institute of Technology

The Charles Stark Draper Laboratory, Inc.
555 Technology Square, Cambridge, Massachusetts 02139-3563

NAVIGATION PERFORMANCE AND INTEGRITY MONITORING FOR BALLISTIC MISSILES USING ALL-IN-VIEW GPS

by

Jeff Hossein Hassannia

B.S., Astronautical Engineering,
United States Air Force Academy, May 1992

Submitted to the Department of Aeronautics and Astronautics
in Partial Fulfillment of the Requirements for the Degree of

MASTER OF SCIENCE IN AERONAUTICS AND ASTRONAUTICS

at the

MASSACHUSETTS INSTITUTE OF TECHNOLOGY

May 1994

Signature of Author _____
Department of Aeronautics and Astronautics
13 May 1994

Certified by _____
Professor Richard H. Battin
Department of Aeronautics and Astronautics
Thesis Advisor

Certified by _____
Timothy J. Brand
The Charles Stark Draper Laboratory, Inc.
Technical Supervisor

Certified by _____
Stanley W. Shepperd
The Charles Stark Draper Laboratory, Inc.
Technical Supervisor

Accepted by _____
Professor Harold Y. Wachman
Chairman, Department Graduate Committee

NAVIGATION PERFORMANCE AND INTEGRITY MONITORING FOR BALLISTIC MISSILES USING ALL-IN-VIEW GPS

by

Jeff Hossein Hassannia

Submitted to the Department of Aeronautics and Astronautics
on May 13, 1994 in Partial Fulfillment of the Requirements for the Degree of
Master of Science in Aeronautics and Astronautics

ABSTRACT

The proven success of the Global Positioning System (GPS) and recent technological innovations have resulted in a call for incorporation of the system into more advanced applications. One example has been the recent upgrading of navigation systems in ballistic missiles to include GPS technology. Advances have also included the development of receivers with enough channels to use all satellites in the field of view. The intent of this thesis is to analyze the performance of a ballistic missile using an all-in-view GPS receiver versus the more common satellite selection algorithms, most often four or five satellites chosen by their geometry. The performance will be measured by the navigational capabilities of the missile and the vehicle's ability to mitigate the effects of a bad GPS satellite. This latter performance indicator is not integrity monitoring as commonly interpreted, although one plausible form of it.

The performance of the ballistic missile is measured through the use of a linear covariance analysis simulation. In general it is shown that significant performance enhancements are available by using an all-in-view receiver. In terms of navigation, it is shown that an all-in-view receiver can expect to achieve as much as a 35 and 45 % improvement in Circular Error Probable (CEP) versus a five and four channel receiver, respectively. It is also demonstrated that all-in-view capabilities can allow a missile to overcome the degradation seen in four and five channel receivers when a GPS satellite goes bad. The research further suggests that all-in-view can mitigate the effects of even a worst case scenario. However, with the assumptions in the thesis it is believed that the final results are optimistic. This therefore calls for more in-depth research and study.

Thesis Advisor: Professor Richard H. Battin
Adjunct Professor of Aeronautics and Astronautics
The Massachusetts Institute of Technology

Technical Supervisor: Timothy J. Brand
Principal Member Technical Staff
The Charles Stark Draper Laboratory, Inc.

Technical Supervisor: Stanley W. Shepperd
Principal Member Technical Staff
The Charles Stark Draper Laboratory, Inc.

ACKNOWLEDGMENTS

My sincerest thanks is given to all of the individuals who helped me to complete the work in this thesis. Of primary note is Stanley W. Shepperd. Not only has Stan directly helped me through my two years as an engineer at Draper and a student at MIT, but has been a role model as a person. Stan has shown me what it takes to be an excellent engineer--solid knowledge and a striving for excellence--while at the same time offering a humbleness and concern for others seldom seen. For this he has my utmost respect.

I would like to thank Donald J. Pasik for the contributions he has made to my thesis. Through the many days and late evenings Don acted as a mentor to me, offering practical engineering advice, timely words of encouragement, and most importantly, an everlasting supply of peanuts. To James B. Matthews, Timothy J. Brand, and Katherine M. Bruni I also express my gratitude. Both James and Tim offered helpful insight and guidance to my research. Katherine's utter love of the aerospace world and unselfish devotion of time provided me with much support.

Additionally, I would like to thank Dr. Richard H. Battin. I was fortunate enough to take two courses with Professor Battin, gaining invaluable insight into the mathematics involved in astrodynamics, as well as first-hand recollections of the U.S. space program in the "good old Apollo days."

Finally, my family deserves the most thanks. Throughout my life Mom and Dad have given me their unconditional love and support. It was my parents who bought me that first telescope, spurring my interest in space. It was my parents who guided and directed me through my education. It was my parents who shined the light on the "right" course in life. Thank you Mom and Dad.

This thesis was prepared at The Charles Stark Draper Laboratory, Inc., under the Navy DASO-33X Project, Contract No. N00030-94-C-0001.

Publication of this thesis does not constitute approval by Draper or the sponsoring agency of the findings or conclusions contained herein. It is published for the exchange and stimulation of ideas.

I hereby assign my copyright of this thesis to The Charles Stark Draper Laboratory, Inc., Cambridge, Massachusetts.

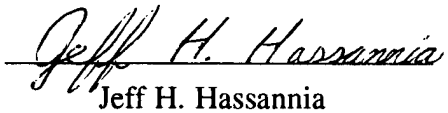

Jeff H. Hassannia

Permission is hereby granted by The Charles Stark Draper Laboratory, Inc., to the Massachusetts Institute of Technology to reproduce any or all of this thesis.

TABLE OF CONTENTS

List of Illustrations 13
List of Tables 15
Nomenclature 17
Chapter 1 Introduction 19
1.1 Introduction and Motivation 19
1.2 Objectives 20
1.3 Overview of Content 21
Chapter 2 The Global Positioning System (GPS) 23
2.1 Introduction 23
2.2 GPS Overview 23
2.3 The GPS Evolution 23
2.3.1 Program Development 24
2.3.2 Current and Future Users 25
2.4 System Components 26
2.4.1 Segments 26
2.4.2 Codes and Messages 29
2.5 User Navigation 31
2.5.1 Tracking Loops and Measurements 31
2.5.2 "Snapshot" Solutions 33
2.5.3 Kalman Filter Estimation 35
2.6 Satellite Selection Methods 36
2.6.1 Dilution of Precision 36
2.6.2 Quick GDOP Method 39
2.6.3 All-In-View 40
2.7 User Navigation Error Sources 40
2.7.1 Space Segment Errors 41
2.7.2 Control Segment Errors 42
2.7.3 User Segment Errors 42
2.7.4 Summary of Segment Errors 44
2.8 Summary of GPS Assumptions 45
Chapter 3 The Ballistic Missile User 47
3.1 Introduction 47

3.2 The Missile Trajectory 47
3.3 Mission Scenarios 48
3.3.1 "Traditional" Scenario 49
3.3.2 "Advanced" Scenario 50
3.4 Hardware Assumptions 51
3.4.1 Antenna Design 51
3.4.2 Receiver Type 52
3.5 Mission Assumptions 52
3.5.1 Measurement Accuracies (Noise) 53
3.5.2 Tumbling and Residual Thrusting 53
3.5.3 Atmospheric Effects 54
3.5.4 GPS Non-Visibility Region 55
3.5.5 Deployment Velocity Errors 55
3.5.6 Jamming 55
3.6 The Navigation System: An Integrated GPS/INS 56
Chapter 4 Filter Development 59
4.1 Introduction 59
4.2 Covariance Analysis 59
4.2.1 Covariance Analysis vs. Kalman Filtering 59
4.2.2 Covariance Equations and the Estimation Process 60
4.2.3 Optimal-Suboptimal Filters 63
4.3 Missile Environment States 66
4.4 The Sensitivity Vector 70
4.4.1 Pseudorange Measurements 70
4.4.2 Integrated Doppler Measurements 71
4.5 State Error Dynamics 73
4.5.1 Modeling of the State Errors 73
4.5.2 Higher-Order Gravity (HOG) Process Noise Matrix 79
4.6 Runge-Kutta Numerical Integration 84
Chapter 5 Navigation Performance of an All-In-View Receiver 87
5.1 Introduction 87
5.2 Circular Error Probable (CEP) 87
5.3 "Traditional" and "Advanced" Cases Analyzed 89
5.4 The Baseline Input Deck 90
5.4.1 Consider States 90
5.4.2 Initial Covariance Matrix 91

5.4.3 Additional Inputs 92
5.5 Baseline Navigation Results 93
5.6 Non-Baseline Cases and Navigation Results 103
5.6.1 No Integrated Doppler Measurements 103
5.6.2 Deployment Velocity Errors 105
5.6.3 Pseudorange Bias States Considered 107
5.6.4 Quick 4 Selection Method 109
Chapter 6 The Integrity Monitoring Issue 111
6.1 Introduction 111
6.2 Why the Integrity Concern? 111
6.3 Integrity Monitoring History and Techniques 113
6.3.1 Historical Development 113
6.3.2 "Snapshot" Techniques 114
6.3.3 A Kalman Filter Approach 117
6.4 All-In-View Integrity Monitoring 118
Chapter 7 Integrity Monitoring Performance for an All-In-View Receiver 121
7.1 Introduction 121
7.2 Integrity Monitoring Input Deck 121
7.3 Baseline Integrity Monitoring Results 122
7.4 Non-Baseline Integrity Monitoring Results 125
7.4.1 Best 5 Selection Method with No Switching 125
7.4.2 Pseudorange Bias States Considered 126
7.4.3 Worst Case Scenarios for All-In-View 128
Chapter 8 Conclusions 133
8.1 Summary of Navigation Performance Results 133
8.2 Summary of Integrity Monitoring Results 134
8.3 Recommendations for Future Research 135
Appendix A Time History of State Uncertainties 139
Appendix B Values of Physical Constants Used in the Simulations 155
References 157

LIST OF ILLUSTRATIONS

Figure 2.1 Dilution of Precision (DOP) in 2D 37
Figure 4.1 Higher-Order Gravity (HOG) Noise vs. Altitude 81
Figure 5.1 The Three Missile Locations (Viewed Down From North Pole) 89
Figure 5.2 Baseline Best 4: CEP vs. Measurement Time 95
Figure 5.3 Baseline Best 5: CEP vs. Measurement Time 99
Figure 5.4 Baseline All-In-View: CEP vs. Measurement Time 101
Figure 5.5 Improvement in CEP Using All-In-View vs. Best 4 102
Figure 5.6 Improvement in CEP Using All-In-View vs. Best 5 103
Figure 5.7 Non-Baseline at Location A: No Doppler Measurements 104
Figure 5.8 Non-Baseline All-In-View: 1/20 m/s Deployment Velocity Uncertainties 106
Figure 5.9 Non-Baseline All-In-View: 1/10 m/s Deployment Velocity Uncertainties 107
Figure 5.10 Non-Baseline at Location A: Pseudorange Bias States Considered 108
Figure 5.11 Non-Baseline Quick 4: CEP vs. Measurement Time 110
Figure 7.1 CEP vs. Measurement Time with Satellite #11 Bad 123
Figure 7.2 CEP Degradation for Each Selection Method with Satellite #11 Bad 124
Figure 7.3 CEP for Best 5 (Switching vs. No Switching) 126
Figure 7.4 CEP Degradation with Pseudorange Bias States Considered 127
Figure 7.5 CEP Degradation for All-In-View Cases I and II 130

LIST OF TABLES

Table 2.1 Classical Orbital Elements for Idealized GPS Constellation 28
Table 2.2 Summary of GPS Segment Errors ("Authorized" Users) 45
Table 3.1 Orbital Elements for Ballistic Missile Trajectory 48
Table 4.1 Summary of Environment States 69
Table 4.2 Summary of First-Order Markov Process State Errors 79
Table 5.1 Initial Covariance Matrix for Simulations 92
Table 5.2 Baseline Best 4: GPS S/C Used and Average GDOP 93
Tables 5.3 Transition (Sensitivity) Matrices for Locations A, B, and C 97
Table 5.4 Baseline Best 5: GPS S/C Used and Average GDOP 98
Table 5.5 Baseline All-In-View: GPS S/C Used and Average GDOP 100
Table 5.6 Non-Baseline Quick 4: GPS S/C Used (Quick vs. Best 4) 109
Table 5.7 Non-Baseline Quick 4: Average GDOP (Quick vs. Best 4) 110
Table 7.1 Satellite # 11's Baseline Markov Process and Clock Values 122
Table 7.2 Sat # 11's Non-Baseline Markov Process and Clock Values
(Cases I & II) 129

NOMENCLATURE

Operator	Description
lower case	scalar
bold lower case	vector
bold upper case	matrix
f(x), h(x)	a function of x
$\equiv$	defined as
$\times$	multiplication; cross-product
$\bullet$	dot product
$\mathbf{x}^T$, $\mathbf{X}^T$	transpose of vector **x**, or matrix **X**
$\mathbf{X}^{-1}$	inverse of **X**
$\lvert\mathbf{x}\rvert$	magnitude of **x**
$\left.\frac{\partial x}{\partial y}\right\rvert_{y=z}$	partial derivative of x with respect to y at y = z
$\dot{x}$, $\frac{dx}{dt}$	time derivative of x
$[\mathbf{y}\times]$	cross-product matrix of **y**
N(x,y)	normal distribution with mean = x and variance = y
E[x]	expected value of x
cov(**x**)	covariance matrix for **x**

CHAPTER 1

INTRODUCTION

1.1 Introduction and Motivation

The Global Positioning System (GPS) is a space-based radio navigation system offering extremely accurate position, velocity, and timing information to a variety of users. This user community has grown extensively over the last few years, with the navigation system being incorporated into an ever-widening variety of applications. One such proposed GPS application has been the upgrading of navigation systems of U.S. missiles, such as the Navy's Trident I ballistic missile fleet, to include the new technology. In the past these systems have relied exclusively on the use of Inertial Navigation Systems (INS). However, with the proven success of GPS (highlighted by the Persian Gulf Conflict) and further technological innovations there has recently been a call to integrate GPS into the missiles' on-board systems to improve their performance [3].

In addition to aiding in the expansion of GPS into applications such as ballistic missiles, recent technological improvements have also advanced the capabilities of the receivers. One of the most prominent changes has been an increase in the number of channels available in the receivers. Each channel allows the user to incorporate measurements from a specific satellite, to "track" that satellite. In the past most receivers were equipped with only four or five channels, giving them the ability to track only four or five satellites in the navigation solution (if time-sharing techniques were not used). Yet, several manufacturers of GPS receivers have recently designed receivers with enough channels to use all the satellites in the field of view. These are termed "all-in-view" receivers.

With this advance in the capabilities of GPS receivers comes a natural question: how much enhancement can be obtained from the use of an all-in-view receiver on a ballistic missile versus other satellite selection methods (typically four or five satellites giving the best geometry)?

1.2 Objectives

The missile's "enhancement" will be evaluated by two distinct measures. First, how does the navigation performance improve by using all of the GPS satellites in view? Secondly, how can the use of an all-in-view receiver aid in integrity monitoring? Determining when a GPS satellite is broadcasting an erroneous signal is a significant concern among the user community as more applications become dependent on the system. "Integrity monitoring" in the truest sense--detecting a failure and possibly isolating the bad satellite--will not be undertaken in this thesis. Instead, how the use of more satellites in the missile's navigation solution can help to make it more resilient to a bad satellite will be analyzed.

The objectives of this thesis are summarized as follows:

- Develop a linear covariance analysis simulation, written in Ada, to model a ballistic missile using an integrated GPS/INS navigation system with the capability to use as many satellites as are in view.

- Compare and quantify the navigation performance of a ballistic missile using an all-in-view receiver versus other common satellite selection algorithms (specifically, four and five channel receivers).

- Compare and quantify the ability of a ballistic missile using an all-in-view receiver (versus other common satellite selection algorithms) to aid in integrity monitoring.

1.3 Overview of Content

This thesis documents the research towards the accomplishment of the stated objectives. Chapter 2 provides a thorough, but basic, description of the Global Positioning System (GPS). The history and growth of the system is presented, with emphasis on its recent application to ballistic missile navigation. The chapter gives a detailed explanation of how GPS can be used for navigation and errors sources present in the system. An entire section is also devoted to describing various satellite selection methods. A comparison of these methods and all-in-view is the thrust of the thesis.

A description of the ballistic missile user for this thesis is presented in Chapter 3. The missile's trajectory and mission scenarios used for the research are presented, as well as assumptions made about the hardware of the missile. The chapter concludes with an explanation of navigation systems that rely on the use of both GPS and an Inertial Navigation System (INS). Such an integrated system is assumed to be present on the ballistic missile.

Chapter 4 of this document provides a detailed description of the development of the covariance filter used in this thesis. It first describes the rationale behind the choice of linear covariance analysis as opposed to using a Kalman Filter for the simulations. The basic covariance analysis equations are presented, highlighting the special form used for the research. The chapter then outlines the states included in the environment model and describes how they were modeled. This chapter is the heart of the thesis, fulfilling the first of the thesis objectives.

The ballistic missile's navigation performance is presented in Chapter 5. A description of the figure of merit, Circular Error Probable (CEP), for the simulations is discussed. The performance enhancements of using an all-in-view receiver is then highlighted through numerous cases. A set of baseline cases is first analyzed, then a group of cases with slight differences from the nominal set are presented. This completes

the second of the stated thesis objectives.

Chapters 6 and 7 complete the last of the thesis objectives, determining how an all-in-view receiver can aid in integrity monitoring. The first chapter details the history of integrity monitoring, including the reasons driving the concern among the user community and schemes that have been developed. It then concludes with a description of the approach taken in this thesis, not integrity monitoring in its truest sense, but one potential form of it. Chapter 7 then presents the integrity monitoring results by comparing an all-in-view receiver with other common satellite selection algorithms. As with the navigation results, several baseline and non-baseline cases are analyzed.

The body of the thesis closes with a summary of the navigation performance and integrity monitoring results for a ballistic missile using all-in-view GPS, Chapter 8. A list of recommendations for future research is also outlined.

Attached as appendices to the thesis are two sections. The first appendix, Appendix A, gives the navigation performance results of the ballistic missile in terms of each of the on-board system's states. Finally, Appendix B gives the values of the physical constants used in the simulations.

CHAPTER 2

THE GLOBAL POSITIONING SYSTEM (GPS)

2.1 Introduction

This second chapter discusses the basics of GPS, from the evolution of the system to the mechanics of how signals are incorporated into a navigation solution. An emphasis is placed on the application of GPS to a ballistic missile user. A summary of the assumptions made in the chapter are presented in the last section.

2.2 GPS Overview

The NAVigation Satellite Timing And Ranging (NAVSTAR) Global Positioning System (GPS) is a space-based 1-way radio navigation system managed by the U.S. Air Force. The 24 satellite constellation offers highly accurate position, velocity, and timing information to ground, sea, and aerospace users in Earth vicinity. With a single position fix "authorized" users can expect to receive accuracies on the order of 10 meters, spherical error probable (SEP) [5]. This precise navigation information is available twenty-four hours a day around the world. Moreover, the system is resilient to poor weather conditions, attempts at interference by outside sources, and handles any number of users. Such capabilities have expanded the use of GPS into more advanced applications, including its incorporation into the navigation systems of ballistic missiles.

2.3 The GPS Evolution

In a mere 20 years the United States has developed and deployed a fully operational space-based navigation system. As a result, the use of GPS has caused most of the more

traditional forms of navigation to either be integrated with the new system or totally discarded. This can be seen in both the military and civilian arenas, where the use of the NAVSTAR satellites has been growing at an unprecedented rate. As technology and familiarity with the system continues to grow, so will the potential applications of GPS.

2.3.1 Program Development

Since the early 1960's the U.S. military and NASA have been pursuing navigation programs based in space. The Navy's TRANSIT program was one of the earliest of these space-based systems. Still operational today, the system is capable of providing maritime users with accurate latitude and longitude information. The early success of this program led the Navy and Air Force to begin simultaneous studies on more advanced and flexible systems. Their objective was to produce a navigation system capable of providing continuous three-dimensional information to high dynamic users. These two fragmented studies were eventually incorporated into a single program in early 1973. This consolidated program, spearheaded by the Air Force, was designated to oversee the development of a comprehensive navigation system called NAVSTAR GPS [2].

The development of GPS from its official inception to the present can be characterized by three distinct phases. The first phase of the program, 1973 to 1979, essentially entailed a concept validation. During this phase testing was undertaken to determine the feasibility of creating the envisioned system. These tests included building prototype satellites, test ranges, and control and monitoring stations. The conclusion of this first phase was marked by the launching of four satellites in 1978. These earliest GPS spacecraft allowed for three-dimensional position and time information to be available from space for the first time [2]. The conceptual idea being validated, the program was ready to enter the next phase.

The period between 1979 and 1985 can be described as the full scale development and testing portion of the GPS program. During this phase contracts were awarded for

the production of the remaining satellites. The size of the constellation was also increased, allowing for a more detailed and thorough testing of the system [2]. The accomplishments during the second phase led the program into its current period, the operational stage.

The last phase of the GPS program, beginning in 1985, encompassed the production and deployment of the second (termed Block II) generation of satellites. These advanced satellites would provide more accurate navigation solutions and have longer life expectancies than their predecessors. The combination of these upgraded satellites with the original ones marked the completion of the entire constellation of 24 spacecraft. With the complete system deployed, GPS receivers could be used in operational vehicles for the first time [2].

2.3.2 Current and Future Users

The GPS evolution has created a broad-based set of users, both civilian and military. In the non-military arena, GPS receivers are being used for any application where precise tracking or navigation is needed. This includes everything from navigating sea vessels and aircraft, to more esoteric uses such as guiding archaeological expeditions and tracking hazardous icebergs [3]. In the future, GPS receivers will most likely make their way into the daily lives of most Americans. In fact, automobile manufacturers are currently installing receivers in the cars and trucks, "space guided" vehicles [20]. Not only has the civilian community found the potential uses of GPS to be boundless, the military is also finding many new uses for the system.

The use of GPS in the military was first limited to low dynamic applications. Early examples included soldiers in the field and the positioning of artillery launchers. However, as receivers improved in size, weight, and performance the use of GPS spread quickly into more advanced applications such as aircraft navigation. As with earlier uses, GPS was extremely successful in helping even the most advanced aircraft to navigate. In

fact, the system was so successful that recently the Department of Defense has called for the phasing out of other military electronic systems such as TACAN, VOR/DME, OMEGA, LORAN-C, and TRANSIT [1]. Only recently, however, has the use of GPS been considered for wide-spread integration into cruise and strategic missiles.

The success of the GPS system in the Persian Gulf Conflict resulted in a call for its incorporation into the navigation systems of missiles. This is in part because of the accomplishments of the Army's Standoff Land-Attack Missiles (SLAM). Two of the Army's missiles were guided to their Iraqi targets with extreme precision using signals from the NAVSTAR satellites [3]. The armed forces now want to upgrade other missiles in the inventory with similar GPS technology. The Navy's Trident ballistic missiles and Tomahawk cruise missiles are prime candidates [3]. The proposed idea is to incorporate a GPS receiver into the inertial navigation systems (INS) of the missiles. In this fashion the GPS receiver and the INS's gyros and accelerometers could be integrated to ultimately improve impact accuracy. Quantifying the relationship between the impact accuracy and various GPS navigation algorithms using such an integrated system is the primary goal of this thesis.

2.4 System Components

The components of the GPS system include three physical segments and the codes and messages between them. Each of these elements are vital to the success of the system as a whole. The components will be addressed in detail below, with assumptions being drawn that are pertinent to the application of this thesis.

2.4.1 Segments

The Global Positioning System is typically divided into three segments, each of which performs a distinct function. These segments include space, control, and user.

Space Segment

The idealized GPS space segment consists of 24 satellites with four in each of six equally spaced orbit planes. The spacecraft are placed into 12-hour circular orbits, inclined at 55 °. They are distributed in these orbital planes such that a minimum of four satellites are always observable from anywhere on the Earth [2]. At the same time, the constellation is also optimized so as to provide the best performance with one, two, or three satellite failures. The constellation is therefore not fully optimized for the 24 satellites [4].

The actual GPS space segment has witnessed the launching of a total of 34 satellites. The first 11 were Block I satellites launched by Atlas F vehicles. The remaining spacecraft were the more advanced Block II's and had to be placed into orbit by Delta II launch vehicles. Currently only 26 of the satellites remain active, 3 Block I's and 23 Block II's. The Air Force plans to launch another Block II spacecraft shortly to make up a complete constellation of only the more advanced satellites. As satellites begin to age or fail the program is prepared to maintain the constellation. In fact, five backup Block II's are ready for launch, and 20 of the newest generation vehicles, Block IIR's, have recently been ordered [4].

For the purposes of this thesis an idealized constellation from November 26, 1989 will be used [6]. The six classical orbital elements--semi-major axis (a), eccentricity (e), inclination (i), longitude of ascending node (Ω), argument of perigee (ω), and true anomaly (f)--for the 24 satellites in this constellation are presented in Table 2.1 (see next page). Notice that because the orbits are circular the argument of perigee is undefined and the true anomaly has been replaced with the argument of latitude (U), defined as the angle, in the plane of the orbit, between the ascending node and the satellite position vector.

Table 2.1 Classical Orbital Elements for Idealized GPS Constellation

SATELLITE #	a (km)	e	i (deg)	Ω (deg)	ω (deg)	U (deg)
1	26609.0	0.0	55.0	325.730284	undefined	190.96
2	26609.0	0.0	55.0	325.730284	undefined	220.48
3	26609.0	0.0	55.0	325.730284	undefined	330.17
4	26609.0	0.0	55.0	325.730284	undefined	83.58
5	26609.0	0.0	55.0	25.730284	undefined	249.90
6	26609.0	0.0	55.0	25.730284	undefined	352.12
7	26609.0	0.0	55.0	25.730284	undefined	25.25
8	26609.0	0.0	55.0	25.730284	undefined	124.10
9	26609.0	0.0	55.0	85.730284	undefined	286.20
10	26609.0	0.0	55.0	85.730284	undefined	48.94
11	26609.0	0.0	55.0	85.730284	undefined	155.08
12	26609.0	0.0	55.0	85.730284	undefined	183.71
13	26609.0	0.0	55.0	145.730284	undefined	312.30
14	26609.0	0.0	55.0	145.730284	undefined	340.93
15	26609.0	0.0	55.0	145.730284	undefined	87.06
16	26609.0	0.0	55.0	145.730284	undefined	209.81
17	26609.0	0.0	55.0	205.730284	undefined	11.90
18	26609.0	0.0	55.0	205.730284	undefined	110.76
19	26609.0	0.0	55.0	205.730284	undefined	143.88
20	26609.0	0.0	55.0	205.730284	undefined	246.11
21	26609.0	0.0	55.0	265.730284	undefined	52.42
22	26609.0	0.0	55.0	265.730284	undefined	165.83
23	26609.0	0.0	55.0	265.730284	undefined	275.52
24	26609.0	0.0	55.0	265.730284	undefined	305.04

Control Segment

The control segment for GPS acts in a monitoring and maintenance fashion. Numerous stations around the world track the GPS satellites, collecting ranging data and satellite clock information. This data is then forwarded for processing to the Master Control Station (MCS) at Falcon Air Force Base, CO. The MCS uses the information to

predict the satellites' future ephemeris and clock drift parameters. At least once a day these updated values are sent to the spacecraft so that accurate data can be broadcast to users [2]. The control segment also serves to monitor the health and status of the satellites in the constellation [4].

User Segment

The final segment of the GPS system consists of the navigators who are equipped to receive and process the signals. This includes numerous organizations and individuals throughout the world, both civilian and military.

2.4.2 Codes and Messages

Each GPS satellite uses two L-band carrier frequencies, L1 at 1575.42 MHz and L2 at 1227.6 MHz, to modulate a variety of codes and messages [3]. This modulated data includes Coarse Acquisition code (C/A-code), Precise code (P-code), and a navigation message. These codes and messages are ultimately received by the user in order to develop a navigation solution. However, the data may be intentionally degraded by a technique called Selective Availability (S/A).

Coarse Acquisition Code (C/A-code)

The C/A-code is a 1023 pseudorandom bit code transmitted at a clock rate of 1.023 MHz [5]. It therefore takes one millisecond for the entire code to be broadcast. This code is termed pseudorandom because even though there is an apparent high degree of randomness in the sequence of 1's and 0's, it is developed from totally predictable mathematical models. In this manner the user can generate an identical replica of the code. The code is usually only modulated onto the L1 carrier and is unique for each satellite. It is available to any user of GPS, typically civilians.

Precise Code (P-code)

The satellites also broadcast a second code, termed P-code. It is a 267 day long pseudorandom sequence, with each satellite given a unique one week segment of the code. The clock rate for modulation is set at 10.23 MHz, 10 times faster than the C/A-code [3]. Modulation occurs on both the L1 and L2 frequencies. This signal can be protected against spoofing (deliberate transmission of incorrect GPS information) by encryption of the P-code, a technique termed Anti-Spoofing (A/S). This encrypted code is then referred to as Y-code.

Selective Availability (S/A)

A potential problem with the use of the GPS signals is their intentional degradation by the Department of Defense, termed Selective Availability. This is done to limit the potential accuracies that an enemy could achieve using the system. S/A is accomplished by disrupting the satellites' on-board clocks and/or degrading the navigation message (see next section). "Authorized" users can overcome this degradation by using a "de-cryption" key that removes the S/A on the P-code. This is typically only given to military users, so the civilian community must endure the degraded accuracy from S/A.

The Navigation Message

The navigation message is superimposed on both of the codes at a data rate of 50 bits/s. It contains information that the user needs to compute a navigation solution. The message includes information on the satellite status such as health, clock correction parameters, ephemeris data, ionospheric models, and information to jump from C/A to P-code. It also contains an almanac of ephemeris data about all of the other satellites in the constellation, critical for satellite acquisition [2].

Code Assumptions for Thesis

A ballistic missile using GPS would most likely use a P-code receiver. Accuracies are improved using P-code because of the ability to eliminate S/A (assuming an

"authorized" user), the smaller clock (chipping) rate, and the capability to reduce ionospheric effects by using both the L1 and L2 frequencies. Therefore, in the simulation section of this thesis measurement accuracies will reflect the better values obtainable from P-code.

2.5 User Navigation

Measurements from the GPS satellites take the form of either 1-way ranges or range rates (actually delta ranges). These measurements are processed by tracking loops in the receiver before being incorporated into the user's navigation solution. Navigation solutions can be either single time ("snapshot") solutions, or filtered solutions by optimal weighting of current and past information.

2.5.1 Tracking Loops and Measurements

GPS receivers use two primary tracking loops for the processing of measurements. A code tracking loop is used for measuring range, and a carrier tracking loop is used for range rate determination.

Code Tracking Loop

The code tracking loops determine the transmission time for the signal from satellite to user by tracking the C/A or P-codes. This is done by gradually shifting the code received from the satellite with the identical code replicated by the receiver. The receiver's code is slewed until all of the binary ones and zeros are brought into correspondence with the satellite's code (the cross-correlation function approaches one). Once this has been accomplished it is then possible to determine the transmission time of the signal. This time is then converted to a range, yet this is not the true range [3].

The true range has not been measured because of user clock errors. For cost reasons most receivers are equipped with quartz clocks, instead of the atomic clocks

present on the GPS satellites. Because of this, a clock offset typically exists between the user and the satellites. Since the codes are generated based on the timing of these clocks, the user clock error must also be estimated and subtracted from the range measurements. Hence, range measurements are termed "pseudorange" since the true range can not be determined until the user clock offset is established [3].

These pseudorange measurements are also "raw" in the sense that corrections have yet to be added. These corrections to the pseudorange measurements are timing errors caused by effects such as tropospheric and ionospheric delays, and satellite clock errors from true GPS time. These errors and the resulting corrections are discussed in Section 2.7.

Carrier Tracking Loop

The second tracking loop, the carrier, is responsible for determining line-of-sight velocities between the user and the satellites. This loop essentially tracks the L1 or L2 carrier signals broadcast by the GPS satellites. Two forms of carrier tracking are available for velocity determination.

The first form of carrier tracking is the frequency-locked loop. This loop provides line-of-sight velocities by determining frequency shifts in the carrier signal, a technique termed instantaneous Doppler. It does not provide a great deal of accuracy because of jittering in the frequency, so is typically used as a "stepping-stone" to the second form of carrier tracking [5].

The more commonly used form of carrier tracking is the phase-locked loop. In this loop two successive phase measurements are taken over a small time interval. The relative difference between these measurements provides a highly accurate measure of range change. When combining this range change with the measurement time span it is possible to determine an average velocity for the measurement interval [5]. This form of velocity determination, often termed carrier phase or integrated Doppler, will be used by the ballistic missile analyzed in this thesis.

2.5.2 "Snapshot" Solutions

"Snapshot" solution methods use GPS measurements at only one single point in time. There is no memory of prior navigation states and no use of dynamics to propagate the estimate forward in time. Because of this, only quantities that are directly observable from GPS are estimated. Thus, position and user clock offset states are estimated directly from pseudorange measurements. Likewise, velocity and user clock offset rate states are determined from range rate measurements [5].

In the most common form of "snapshot" solutions only pseudorange measurements are taken. Assuming an idealized scenario with no external delays, the true range from the user to a specific satellite, satellite k, is represented by

$$r_k = c(t_u - t_k) \tag{2.1}$$

where: r_k = true range from the user to satellite k
t_u = user's true (GPS system) time at signal reception
t_k = satellite k's true (GPS system) time at signal transmission
c = speed of light

This can also be written in terms of the times that the receiver actually receives the signal and satellite k actually transmits the signal as

$$t_u^* = t_u + \Delta t_u \tag{2.2}$$

$$t_k^* = t_k + \Delta t_k \tag{2.3}$$

$$r_k = c(t_u^* - t_k^*) - c\Delta t_u + c\Delta t_k \tag{2.4}$$

where: t_u^* = user's erroneous signal reception time
Δt_u = error in user time from true (GPS system) time
t_k^* = satellite k's erroneous signal transmission time
Δt_k = error in satellite k's time from true (GPS system) time

But, the actual pseudorange measurement, p_k, to satellite k processed by the receiver is just

$$p_k = c(t_u^* - t_k^*) + v_k \tag{2.5}$$

where: v_k = pseudorange measurement noise (zero mean) to satellite k

which can be written as

$$p_k = r_k + c\Delta t_u - c\Delta t_k + v_k \tag{2.6}$$

or, in terms of the user and satellite position vectors at the time of measurements, $\mathbf{r}_u$ and $\mathbf{r}_{sat\,k}$, as

$$p_k = |\mathbf{r}_u - \mathbf{r}_{sat\,k}| + c\Delta t_u - c\Delta t_k + v_k \tag{2.7}$$

Given four noiseless pseudorange measurements, the three elements of position and the user clock offset could be solved for exactly using (2.7). This is just four equations and four unknowns, since the satellite's clock offset from GPS system time and position vector would be given (contained in the navigation message). The equations would be non-linear and some sort of iterative numerical method like Newton's Method would typically have to be used.

With noisy measurements the solution is usually determined by a linearization of (2.7), resulting in corrections to some nominal state. This same procedure would be undertaken if more than four satellites were used in a navigation solution. In this case the equations would be overdetermined and would usually be solved in a least-squares sense.

Assuming n satellites are used in the solution, the linearization scheme begins by putting (2.7) into vector notation (minus the quantities contained in the navigation message) as

$$\mathbf{x} = \begin{bmatrix} r_{ui} \\ r_{uj} \\ r_{uk} \\ c\Delta t_u \end{bmatrix} \quad \mathbf{p} = \begin{bmatrix} p_1 \\ \vdots \\ p_n \end{bmatrix} \quad \mathbf{v} = \begin{bmatrix} v_1 \\ \vdots \\ v_n \end{bmatrix} \tag{2.8}$$

and

$$\mathbf{p} = \mathbf{f}(\mathbf{x}) + \mathbf{v} \tag{2.9}$$

Now, writing the user's state as a nominal state plus a small correction, $\mathbf{x} = \mathbf{x}^* + \Delta\mathbf{x}$, the pseudorange measurement vector can be written as

$$\mathbf{p} = \mathbf{f}(\mathbf{x}^* + \Delta\mathbf{x}) + \mathbf{v} \tag{2.10}$$

Assuming that $\Delta\mathbf{x}$ is small, (2.10) can be expanded as a Taylor Series to first-order

$$\mathbf{p} = \mathbf{f}(\mathbf{x}^*) + \left.\frac{\partial \mathbf{f}(\mathbf{x})}{\partial \mathbf{x}}\right|_{\mathbf{x}=\mathbf{x}^*} \Delta\mathbf{x} + \mathbf{v} \tag{2.11}$$

or simply

$$\Delta\mathbf{z} = \mathbf{H}(\mathbf{x}^*)\Delta\mathbf{x} + \mathbf{v} \tag{2.12}$$

where: $\Delta\mathbf{z} = \mathbf{p} - \mathbf{f}(\mathbf{x}^*)$ = noiseless pseudorange measurement residual vector

$\mathbf{H}(\mathbf{x}^*) = \left.\frac{\partial \mathbf{f}(\mathbf{x})}{\partial \mathbf{x}}\right|_{\mathbf{x}=\mathbf{x}^*}$ = the sensitivity matrix

For this particular scenario the rows of the sensitivity matrix would contain the unit line-of-sight vectors from the user to the GPS satellites and a one at the end for the user's clock offset. Thus, **H** is of size n by 4, with n being the number of satellites used.

The correction to the state can then be found in a least-squares sense as

$$\Delta\hat{\mathbf{x}} = (\mathbf{H}^T\mathbf{H})^{-1}\mathbf{H}^T(\Delta\mathbf{z} - \mathbf{v}) \tag{2.13}$$

where: $\Delta\hat{\mathbf{x}}$ = least-squares estimate of state correction

The least-squares solution reduces the effects of measurement noise as the number of satellites used in the solution increases. Also notice that if only four satellites are used in the solution, (2.13) simply reduces to the well-known expression

$$\Delta\hat{\mathbf{x}} = \mathbf{H}^{-1}(\Delta\mathbf{z} - \mathbf{v}) \tag{2.14}$$

2.5.3 Kalman Filter Estimation

For a user desiring numerous navigation solutions the Kalman Filter offers a much better method than just taking sequential "snapshot" solutions. A Kalman Filter essentially allows for the combining of past information with current measurements to derive a "statistically" optimal estimate at the current time. This estimate can then be propagated forward in time based on the dynamics of the user vehicle. By maintaining all of this past information it is also possible to estimate more navigation states than with using only "snapshot" solutions.

The Kalman Filter is the tool of choice among navigation and guidance applications.

This thesis will use the Kalman Filter (actually linear covariance analysis, described in Section 4.2) to simulate the performance of a ballistic missile using an integrated INS/GPS navigation system.

2.6 Satellite Selection Methods

If a user has a limited number of channels to devote to measuring range and range rates, the set of satellites chosen plays a tremendous role in the accuracy achieved. There are numerous methods in which to choose the set of satellites to be used in a navigation solution. The most common selection method relies on the relative geometry of the user and the GPS satellites to determine the set to be used. More advanced algorithms can combine the geometry with other inputs to derive an even better set. A common example of this technique is combining geometry with User Range Accuracy (URA). URA is a statistical indicator in the navigation message describing the ranging accuracies available from a specific satellite [7].

Another satellite selection method chooses the set of satellites such that Circular Error Probable (CEP) at impact is minimized. This would most likely be used by a missile, concerned with achieving the highest probability of impact with the intended target.

However, the satellite selection methods analyzed in this thesis will be limited to those based only on geometry. This is the most common method used in today's aerospace arena. This section discusses these geometry-based selection methods.

2.6.1 Dilution of Precision

Dilution of Precision (DOP) is a numerical indicator of the effect of geometry on a navigation solution. In essence it describes how the relative orientation of the user and the satellites affect the solution accuracy. An intuitive example of DOP is easily shown in 2-dimensional space, Figure 2.1 [2]. Given only two pure range measurements, with

uncertainties in each, a user's position estimate is best when the measurements are at right angles. As the angle between the measurements becomes smaller, position uncertainties grow. In the extreme, maximum position uncertainty is reached when the measurements come from the same direction.

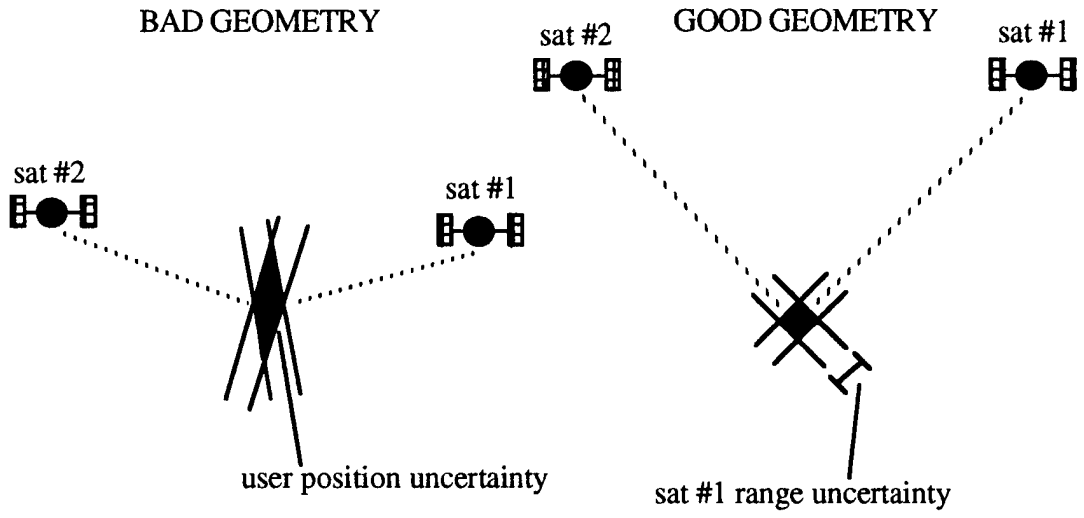

Figure 2.1 Dilution of Precision (DOP) in 2D

DOP is formed by minimizing the covariance matrix for the user's state errors. This can be derived by starting with the least squares solution to the navigation equation, (2.13), developed in Section 2.5.2

$$\Delta\hat{\mathbf{x}} = (\mathbf{H}^T\mathbf{H})^{-1}\mathbf{H}^T(\Delta\mathbf{z} - \mathbf{v}) \tag{2.15}$$

The errors in this estimate are

$$\partial\Delta\hat{\mathbf{x}} = \Delta\hat{\mathbf{x}} - E[\Delta\hat{\mathbf{x}}] = -(\mathbf{H}^T\mathbf{H})^{-1}\mathbf{H}^T\mathbf{v} \tag{2.16}$$

The covariance matrix for the user's state errors is then found by

$$\text{cov}(\partial\Delta\hat{\mathbf{x}}) = E[(\partial\Delta\hat{\mathbf{x}})(\partial\Delta\hat{\mathbf{x}})^T] = (\mathbf{H}^T\mathbf{H})^{-1}\mathbf{H}^T\mathbf{R}((\mathbf{H}^T\mathbf{H})^{-1}\mathbf{H}^T)^T \tag{2.17}$$

where

$$\mathbf{R} = \text{cov}(\mathbf{v}) = E[(\mathbf{v})(\mathbf{v})^T] \tag{2.18}$$

Now, making the assumption that the pseudorange measurement noises are uncorrelated between satellites and equal for each satellite, the pseudorange measurement

noise covariance matrix reduces to

$$\mathbf{R} = \sigma_n^2 \mathbf{I} \tag{2.19}$$

where: σ_n^2 = pseudorange measurement noise variance to GPS satellites

Thus, the covariance matrix becomes

$$\text{cov}(\partial\Delta\hat{\mathbf{x}}) = \sigma_n^2(\mathbf{H}^T\mathbf{H})^{-1}\mathbf{H}^T((\mathbf{H}^T\mathbf{H})^{-1}\mathbf{H}^T)^T \tag{2.20}$$

or simply

$$\text{cov}(\partial\Delta\hat{\mathbf{x}}) = \sigma_n^2(\mathbf{H}^T\mathbf{H})^{-1} \tag{2.21}$$

The user's state error variances are along the diagonals. Thus, DOP is defined as

$$\text{GDOP} = \sqrt{\text{trace}(\mathbf{H}^T\mathbf{H})^{-1}} \tag{2.22}$$

and the best solution to the state minimizes this value.

This particular form of DOP is called Geometric Dilution of Precision (GDOP) because the satellite geometry selected minimizes the user's three components of position and clock offset. DOP's also exist to minimize just position, PDOP, or time, TDOP. These would be computed by taking the trace of only the first three diagonals of $(\mathbf{H}^T\mathbf{H})^{-1}$ for PDOP, or only the last diagonal for TDOP. In general, user's are concerned with minimizing both position and time uncertainties (time uncertainties are usually not critical for the user's mission, but indirectly affect the user's ability to estimate position). This is the case for a ballistic missile user since both position and time errors affect impact accuracy. Thus, GDOP will be the selection criteria for the ballistic missile user analyzed in this thesis.

Regardless of the DOP desired, at least four satellites must be used to avoid singularity of $(\mathbf{H}^T\mathbf{H})^{-1}$. A similar singularity problem arises when the line-of-sight vectors to the satellites used for DOP determination all lie on a cone.

If four satellites were used in the solution set, a high correlation exists between GDOP and the volume of a tetrahedron formed by the points of unit vectors from the user to these satellites. In fact, minimizing GDOP is roughly equivalent to maximizing the volume of this tetrahedron [3]. The best geometry therefore exists when the satellites are

widely dispersed, with large angles between the line-of-sight vectors to them.

Also notice that GDOP yields the best set of satellites if the user's current covariance matrix is ignored. It is actually for users with no knowledge of their location and requiring a single position fix, a "snapshot" solution. On the other hand, if the user had a particular covariance matrix it would be possible to choose a set of satellites with another method that would reduce the uncertainties more significantly than with the GDOP algorithm alone, or a CEP selection method. However, this is a time consuming process and GDOP tends to produce almost optimal results.

A typical receiver will cycle through all possible sets of visible satellites until a set is found that minimizes GDOP. The size of the set is dependent on the number of channels in the receiver. The limited channel cases presented in this thesis will be for four and five channel receivers. These represent some of the most common receivers.

2.6.2 Quick GDOP Method

In the four satellite selection method an alternative exists to finding the best GDOP by the common practice of cycling through the many combinations of satellites. This new method was developed by J.A. Soltz at The Charles Stark Draper Laboratory to reduce the computation time needed to determine the best set [8].

The procedure is as follows:

(1) Determine the set of visible satellites and their line-of-sight vectors from user to satellites, **s**'s.

(2) Select the satellite, S1, most directly overhead. That is, the satellite whose position vector makes the smallest angle with the user's position vector.

(3) Select the satellite, S2 ($\neq$S1), such that **s2** makes an angle closest to 90° with **s1**. Specifically, choose S2 such that (**s2** • **s1**) has minimum absolute value.

(4) Select the satellite, S3 ($\neq$S2,$\neq$S1), so that **s3** makes the largest absolute angle with the plane formed by **s1** and **s2**. Specifically, choose satellite S3 such that

($\mathbf{s3} \bullet \text{UNIT}(\mathbf{s2} \times \mathbf{s1})$) has maximum absolute value.

(5) Finally, find the satellite, S4 (≠S3,≠S2,≠S1), so that GDOP is minimized.

Instead of cycling through all possible combinations, this method relies on the geometrical interpretation of GDOP to pick the first three satellites. The algorithm attempts to pick the three satellites so that their line-of-sight vectors are mutually orthogonal. This helps to maximize the volume of the ensuing tetrahedron. The final results produce a set of satellites giving a GDOP very close, if not the same, to the best GDOP, with far less computations. An even better algorithm has recently been proposed by Soltz in reference [9]. This selection method chooses the best set of five satellites using a very simple, fast, and good algorithm with universal applications [9].

Results from using this "Quick GDOP Method" will be looked at briefly in Section 5.6.4 of the thesis.

2.6.3 All-In-View

All-in-view GPS receivers possess the capability to receive measurements from every satellite in the field of view. Thus, although the receiver becomes more complex because of the added channels, the time intensive DOP algorithms are not needed for satellite selection. Even more significant is the navigation improvements and integrity monitoring capabilities inherent in all-in-view receivers. These will be the primary issues analyzed in this thesis.

2.7 User Navigation Error Sources

There are many error sources in the GPS system directly affecting a user's navigation accuracy. These error sources are typically lumped into one of the three GPS segments: space, control, or user. Each of these segments is presented in the following section, with the errors limited to those experienced by an "authorized" user (one using P-code with S/A compensation). These errors will be used later in the thesis for

determining measurement accuracies and the modeling of certain states.

2.7.1 Space Segment Errors

The space segment errors include the unmodeled forces that drive the GPS satellites away from their predicted orbits. It also includes unintentional errors in the satellite broadcast signals such as clock and electronic anomalies.

Satellite Orbital Fluctuations

The first space segment error source is from unmodeled or unpredictable motion of the satellites. These effects are typically a result of solar pressure, higher-order gravity, vehicle stabilization and control, and unmodeled gas venting (caused by heating and pressurized tanks) in the satellite. The Control Segment attempts to eliminate these effects by tracking and updating the satellites with fresh ephemeris data on a daily basis, but residual errors remain. Studies have shown that the errors are periodic and contribute to a time-averaged pseudorange error standard deviation of roughly 1.5 m [5].

Satellite Clocks

Time is established on the GPS satellites through the use of four atomic clocks, two Cesium and two Rubidium. Ideally these are synchronized with GPS system time (a common time established for the entire system and monitored on the ground). Yet, in reality these clocks tend to drift from true GPS time. These drift characteristics are monitored by the Control Segment, which then sends clock correction parameters back to the satellites at least once per day. The parameters are then broadcast to users via the navigation message. Although most errors in the clocks are corrected by these parameters, residual errors remain that ultimately affect the user's range computations. Empirical evidence has shown that, over short periods of time, a satellite clock error is best modeled as a zero-mean random bias whose standard deviation is 3.0 m [5].

Satellite Electronics Group Delay (Tgd)

The final space segment error is caused by the passage of a signal through a satellite's equipment. This results in a time delay, termed group delay (Tgd). Errors from these delays are typically quite small since ground tests of satellites' equipment can determine their magnitudes. The group delays are then accounted for by adding them into the clock correction parameters of the satellites. Because of this, it is difficult to separate the group delay's individual contribution to ranging errors from that of the satellite clock correction parameters. Their contribution has therefore been included in the clock correction parameter's uncertainty [5].

2.7.2 Control Segment Errors

Control segment errors result from the differences between the Control Segment's estimates of satellite ephemeris and clock correction parameters and the true values. This is a result of errors in the ground's ability to track the satellites and inadequate models. The contributions of these errors are coupled with the errors resulting from the space segment. They have therefore been included in the space segment errors.

2.7.3 User Segment Errors

When the transfer time for a signal between a GPS spacecraft and the receiver differs from the free-space value, a user segment error has occurred. This is not only due to the internal elements of a receiver, but is also a function of the receiver's location relative to the GPS satellite and nearby physical objects. Typical transfer time errors are a result of such things as ionosphere and troposphere errors, multipath, and receiver noise [5].

Ionospheric Effects

The effect of a RF signal passing through the electrically charged region above the

Earth, the ionosphere, is to alter the signal. This region, stretching from roughly 50 to 1,000 km, causes the speed of a signal to be reduced and some ray bending [5]. Fortunately, the delay in the signal is directly related to its transmission frequency. Thus, with two frequencies available to P-code users it is possible to nearly eliminate the ionospheric delay. Unfortunately, receiver noise (bandlimited white) is generated with the incorporation of the tracking loops to eliminate these ionospheric errors. This noise generally has a standard deviation of about 1.5 m [5].

Tropospheric Effects

The troposphere is an electrically neutral band of un-ionized air stretching from the ground up to altitudes between 9 and 16 km. Transmission delay and bending are not a function of the frequency of the signal, so it is not possible for a P-code receiver to reduce its effects. It is also difficult to accurately model the troposphere because it is a function of the air's temperature, humidity, and pressure [5].

As will be discussed in the Chapter 3, the mission scenarios for the ballistic missile user considered in this thesis are such that measurements will never be taken through the troposphere. It therefore does not contribute any errors.

Receiver Noise

The processing of signals by the receiver's hardware and software creates receiver noise (bandlimited white). In general, the amount of noise generated is dependent on the such factors as the tracking loop bandwidths and algorithms, integration times, and antenna gains. It therefore tends to vary between different receivers. Recent improvements in technology have resulted in P-code receiver noise on the order of roughly 1.0 m [5].

Multipath

Multipath is an error that is caused by the distortion of an original signal due to "false" signals generated from other propagation paths. The additional propagation paths

are typically created from reflections off of objects near the receiver, sometimes even the user's own vehicle. In general, P-code users are less susceptible to the effects of multipath because of code correlation differences [5]. For the ballistic missile user examined in this thesis multipath errors were not considered.

There were three primary reasons for not choosing to include the effects of multipath. First, the effects of multipath for a user in open space would be small compared to other error sources. Next, conservative values for some of the previous error sources would act to absorb any multipath biases present. Finally, little was known of the physical structure of the ballistic missile user needed to develop accurate multipath models.

2.7.4 Summary of Segment Errors

A summary of the GPS errors present in each of the segments is presented in Table 2.2. These values will be used later in the thesis for determining pseudorange measurement accuracy (noise) and creating states for modeling the pseudorange errors.

Recalling the DOP equations derived in Section 2.6.1, it is possible to calculate an average 3-dimensional position error, the RSS 3D position error as

$$1\sigma \text{ RSS 3D position error} = \text{PDOP} \times (1\sigma \text{ ranging error}) \tag{2.23}$$

This equation represents the accuracies a user would expect for a "snapshot" estimate of position. PDOP would be derived based on the geometry of the satellites chosen for a particular solution. Assuming that the errors presented in Table 2.2 are uncorrelated, the 1σ ranging error would come from RSS'ing all of the error sources

$$1\sigma \text{ ranging error} = \sqrt{1.5^2 + 3.0^2 + 1.5^2 + 1.0^2} = 3.8 \text{ m} \tag{2.24}$$

With a typical value of PDOP around 2.6 for 4 satellites [3], this results in a 1σ RSS 3D position error on the order of 10 meters.

Table 2.2 Summary of GPS Segment Errors ("Authorized" Users)

SEGMENT	ERROR SOURCE	ERROR MODEL	1 σ VALUE (m)	NOTES
space	satellite orbital fluctuations	time-averaged pseudorange error	1.5	
	satellite clocks	zero-mean random bias	3.0	
	Tgd	-----	-----	included in the satellite's clock uncertainties
control	-----	-----	-----	included in the space segment errors
user	ionospheric effects	bandlimited white noise	1.5	L1 and L2 tracking loops generate noise
	tropospheric effects	-----	-----	missile never looks through the troposphere
	receiver noise	bandlimited white noise	1.0	
	multipath	-----	-----	assumed to be negligible

2.8 Summary of GPS Assumptions

Several assumptions for the thesis have been made in this chapter about GPS and a ballistic missile's direct interaction with GPS. These are summarized below.

(1) An idealized GPS constellation from November 26, 1989 will be used for the simulations [6].

(2) The ballistic missile will use a P-code receiver with S/A compensation.

(3) Velocity measurements will be taken by integrated Doppler techniques.

(4) Kalman filter estimation will be used, as opposed to sequential "snapshot" solutions.

(5) Geometry-based satellite selection algorithms of best four GDOP, best five GDOP, and the quick GDOP method will be compared to all-in-view in the simulations.

(6) The errors presented in Section 2.7 are assumed to be realistic for a ballistic missile. These values will later be used for determining pseudorange measurement accuracies (noise) and creating states to model the pseudorange errors.

CHAPTER 3

THE BALLISTIC MISSILE USER

3.1 Introduction

This thesis will focus on the use of GPS by a ballistic missile. As a result, numerous assumptions had to be made about the specifics of this missile for the simulation work. This chapter describes these assumptions: beginning with a description of the trajectory and mission scenarios, followed by a discussion of assumptions about the hardware and mission, and concluding with the selection of the missile's navigation system.

3.2 The Missile Trajectory

A single ballistic missile trajectory was chosen to be used by the simulations presented in this thesis. This trajectory represents the flight path of a "typical" ballistic missile, such as a Navy Trident I missile.

The orbital elements for this trajectory were found by first choosing two key missile parameters: how far downrange should the missile travel and at what angle should it impact the ground? These were set at realistic values of 4000 nautical miles downrange and 45° for an impact angle. From these parameters the semi-major axis (a) and eccentricity (e) were then directly found as 5282 km and 0.722, respectively. The semi-major axis and eccentricity completely define the size and shape of the orbit. The trajectory's orientation in space and the missile location in the orbit would be defined by the other four orbital elements.

The inclination of the trajectory was chosen as 45°. This gave a trajectory that was not geometrically biased towards any specific region of the GPS constellation. The

longitude of ascending node (Ω) and argument of perigee (ω) were both chosen as 0°. The value for ω would ensure a trajectory that was symmetric about the equator, again to avoid any biases. The final orbital element to be chosen was the true anomaly (f). For all of the mission scenarios (discussed in detail in Section 3.3) the simulations start at one million ft (304.8 km) altitude. With this altitude the initial value for f turned out to be 149°. Table 3.1 lists the six orbital elements.

Table 3.1 Orbital Elements for Ballistic Missile Trajectory

ORBITAL ELEMENT	VALUE
a (km)	5281.79199249
e	0.72217919368
inc (deg)	45.0
Ω (deg)	0.0
ω (deg)	0.0
initial f (deg)	149.438389705

3.3 Mission Scenarios

Missile trajectories are usually characterized by four distinct phases: boost, post-post/deployment, coast, and re-entry. The boost phase covers the period of time between launch and termination of the final main stage. This is the thrusting portion of the trajectory and typically ends at roughly one million ft (304.8 km) altitude. In the next phase, the post-boost/deployment portion, the vehicle is first prepared to deploy the re-entry bodies (r.b.'s). This includes such activities as expulsion of any remaining stages, attitude control, and correction of errors in the Inertial Navigation System (INS). The phase concludes with the firing of the vehicle's maneuvering thrusters and the actual deployment of the r.b.'s. The third phase, coasting, consists of the period of time when the r.b.'s proceed toward the target under the influence of gravity alone. Finally,

the re-entry phase begins when the r.b.'s first experience the effects of the atmosphere, typically at an altitude of 400,000 ft (121.92 km).

Navigation with GPS is generally used only during the post-boost/deployment region of the trajectory. During the boost phase of a missile the high dynamics involved create tracking problems for GPS receivers. Consequently, the INS is the sole provider of navigation information during this phase. GPS is also not used during the coast or re-entry phases because the r.b.'s have no maneuvering capabilities, thus making any navigation useless. This thesis will therefore simulate a ballistic missile using GPS only during the post-boost/deployment region of the trajectory.

In most cases, a ballistic missile initiates the post-boost/deployment phase immediately after the boost segment. However, it is possible for the vehicle to travel in a free-fall fashion before initiation of the second phase, thus shortening the coast phase for the r.b.'s. Several advantages and disadvantages are present in the two methods. Both of these cases will be addressed in the thesis, identified as the "traditional" and "advanced" scenarios.

3.3.1 "Traditional" Scenario

The "traditional" mission scenario initiates the post-boost/deployment phase at one million feet, the termination point of the boost phase. It is assumed that this phase includes the following sequence of events:

(1) expulsion of the final main stage, typically the third stage, leaving only the bus (the r.b.'s are attached to the bus)

(2) the firing of attitude jets to stabilize the bus

(3) the use of a star tracker to correct propagated errors in the INS

(4) the use of maneuvering thrusters to properly guide the bus for the sequential deployment of the r.b.'s

The GPS receiver will be activated at the beginning of this sequence and will provide navigation information throughout the phase. It will be assumed that this phase lasts only 100 s, a typical minimum value for ballistic missiles. It will also be assumed that the bus' maneuvering thrusters will be activated during the entire phase, providing thrust at 0.1 g's in the direction of the velocity vector.

There are several advantages to deploying the r.b.'s early in the trajectory. First, the earlier the deployment of the warheads the less chance for failures in the bus. Also, the use of GPS early in the trajectory reduces the susceptibility of the receiver to jamming near the target. Finally, early deployment is typically undertaken as a means to reduce power consumption, thus minimizing the number of batteries to be carried. However, as the next scenario will address, deploying the r.b.'s later in the trajectory means less time for initial state uncertainties to grow from orbital dynamics, higher-order gravity unknowns, and especially deployment velocity errors.

3.3.2 "Advanced" Scenario

The "advanced" scenario is identical to the "traditional" case except for the timing of the post-boost/deployment phase. Unlike the "traditional" scenario, the second phase is not initiated directly after the boost phase. Instead, the final main stage and bus free-fall for a period of time before the second phase is initiated. The length of this free-fall period is variable, with a maximum such that enough time remains to complete the 100 s post-boost/deployment phase before entering the atmosphere. As in the "traditional" case, the use of GPS and deployment thrusting will be limited to these 100 s.

In this scenario it is also possible for GPS measurements to be taken prior to initiation of the post-boost/deployment phase of the trajectory. This would give more time for the receiver to take measurements with potential navigation improvements. However, with the extreme accuracy of GPS a user's state uncertainties approach steady-state conditions in a very short period of time. Also, GPS measurements taken

for an extended period of time would result in increased power and fuel consumption. Electrical power would be drained by the use of the GPS receiver and the additional burdens placed on the on-board computer, although quite small. Fuel would also be needed to provide attitude control so the GPS signals could be tracked (tumbling is discussed in Section 3.5.2). Although, with band antennae GPS might be usable even if the vehicle is tumbling.

The thesis will limit the "advanced" scenario to the use of GPS only during the 100 s of the post-boost/deployment phase. This is a reflection of the issues discussed above and also allows for a more direct comparison between the "traditional" and "advanced" scenarios.

3.4 Hardware Assumptions

Several assumptions about the hardware of the ballistic missile presented in this thesis were made. These include assumptions about the design of the antenna and the type of receiver used.

3.4.1 Antenna Design

Antenna type and placement on the user vehicle is critical to the successful use of GPS. The L-band transmissions arrive at extremely low power densities so efficient and properly placed antennae are required to pick up the modulation on the signals [3]. Antennae currently come in a variety of shapes, sizes, and capabilities. The choice of an antenna and its placement are dependent on the intended application. The ballistic missile user will be assumed to have antennae such that the signals to all of the satellites in view can be tracked and processed.

3.4.2 Receiver Type

There are two primary types of GPS receivers available. The first type of receiver is often termed a "sequential" receiver because it tracks the GPS satellites one at a time. Only one or two hardware channels are time-shared between the satellites. A slow "sequential" receiver sequences through the set of satellites until all of the pseudoranges and range rates have been measured. These measurements are then combined to form a navigation solution. Consequently, the resulting accuracy is poor and the receiver cannot be used for high dynamic applications. A fast "sequential" receiver sequences through the satellites at a rate such that the data from all of the satellites is continuously sampled. This requires some form of multiplexing, but offers better accuracy than a slow sequencing receiver [2].

A "continuous" receiver is more complex and expensive than a "sequential" one, but provides the highest accuracy. This type of receiver devotes one hardware channel to each of the satellites being tracked. As a result, a receiver using four satellites would have at least four channels and an all-in-view receiver could theoretically have as many as 24 channels. This type of receiver is best suited for high dynamic users like the military. It also offers additional jamming protection [2].

It will therefore be assumed that the ballistic missile will use a continuous GPS receiver. It will also be assumed that measurements to the GPS satellites will be taken every second. This is typically the time interval needed to raise the signal-to-noise ratio of the GPS signal components to support measurement processing [5].

3.5 Mission Assumptions

There are several assumptions that will be made about both the "traditional" and "advanced" mission scenarios. These help to clarify the conditions under which the ballistic missile was analyzed for this thesis.

3.5.1 Measurement Accuracies (Noise)

Pseudorange Measurements

Pseudorange measurement noise can be calculated directly from the GPS segment errors presented in Section 2.7. Each of the segment errors leads directly to pseudorange uncertainties, but only the errors modeled as noise would be included in the measurement noise terms to be used in a Kalman Filter. These are the terms that truly act as bandlimited white noise in the receiver, instead of biases or slowly wandering errors. These later terms would best be accounted for with a state in the filter.

The 1σ value for measurement noise can be calculated by RSS'ing the noise generated from the L1 and L2 tracking loops (used to eliminate ionospheric effects) and the receiver noise

$$1\sigma \text{ pseudorange measurement noise} = \sqrt{1.0^2 + 1.5^2} = 1.8 \text{ m} \qquad (3.1)$$

Integrated Doppler Measurements

Even though carrier phase measurements can be as accurate as 1/100 of a cycle in a lab environment, equating to 0.002 m/s integrated Doppler accuracy for the L1 carrier, in real-life applications this performance is degraded. For example, The Interstate Electronics Corporation (IEC) typically uses values on the order of 0.02 m/s or greater for the 1σ measurement noise [12]. This is primarily a result of the significant flexing and body rate uncertainties associated with a ballistic missile. Therefore, a conservative value of 0.02 m/s will be used in this thesis.

3.5.2 Tumbling and Residual Thrusting

Tumbling is often a concern for ballistic missiles. It is typically caused by the thrusters of the final main stage exerting an unwanted torque on the vehicle at burnout. The errors in the thrusters are driven by the control loops, which, as the final main stage

burns the last elements of fuel, have difficulty aligning the thrust through the true center of mass of the vehicle. The Trident program specifies that the residual torques can exert as much as 30 deg/s of spin rate to the vehicle. The spin axis of the tumbling is impossible to predict, except that it will likely not be about the roll axis [10].

For the "traditional" case in this thesis tumbling will not be a concern. This is because there is no free-fall portion between termination of the boost phase and initiation of attitude control as part of the post-boost/deployment phase. Any tumbling will be immediately eliminated. On the other hand, the vehicle (the final main stage and bus) of the "advanced" mission scenario will experience tumbling because of the free-fall phase.

In addition to the tumbling experienced by the '"advanced" scenario, the vehicle will also produce residual thrusting. This is caused by outbursts of thrust from the final main stage even after it has burnt out. Because it is a solid rocket motor it is impossible to perform a perfectly "clean" termination of thrust. The magnitude and duration of this residual thrusting is difficult to predict [10]. Its effects will be to cause an increase in the user's position and velocity uncertainties during the free-fall phase. Only the "advanced" scenario will be affected by residual thrusting since the "traditional" one ejects the final main stage immediately after burnout. The residual thrusting will also intensify the tumbling of the vehicle.

3.5.3 Atmospheric Effects

The atmosphere causes significant impact errors for a re-entry body. This is primarily due to the drag and ablation experienced by the vehicle while traveling through this region. The simulations in this thesis will neglect the effects of the atmosphere on the ballistic missile. This is because the scope of the thesis is governed by the relationship between navigational errors, various satellite selection methods, and some figure of merit like CEP.

3.5.4 GPS Non-Visibility Region

It will be assumed that the ballistic missile will not take measurements if the GPS signal would pass closer than 16 km above the Earth's surface. This altitude represents the outer boundaries of the troposphere. As discussed in Section 2.7.3, the troposphere can cause errors in range and range rate measurements.

3.5.5 Deployment Velocity Errors

When the bus jettisons the r.b.'s toward their respective targets, errors in the mechanics of the deployment system cause velocity errors to be placed on the bodies. These velocity errors ultimately result in position errors at impact.

Even though the issue of deployment velocity errors strays from the focus of the thesis, it will be briefly addressed in Section 5.6.2. The effects of these errors will be analyzed by using two sets of deployment velocity errors, 1/20 and 1/10 m/s (1σ) in each of the three orthogonal directions. The reason for its discussion is twofold. First, it is a significant contributor, if not the largest, to the impact position error. Next, the resulting impact errors are a function of where in the orbit the r.b.'s are deployed. This then ties in with the "advanced" mission scenario.

3.5.6 Jamming

Jamming is a concern among military users of GPS. For a ballistic missile the potential for jamming would grow as the missile approaches the target. For this reason jamming is not much of an issue in the "traditional" mission scenario. On the other hand, the "advanced" scenario could be susceptible to the effects of jamming, especially if the post-boost/deployment phase was not initiated until the later part of the trajectory.

Various schemes can be undertaken by the missile to mitigate the effects of jamming. This includes such techniques as masking the terrain, using advanced

antennae, and carefully integrating GPS with INS. P-code and continuous tracking receivers (both assumed to be used on the ballistic missile) are also less prone to the effects of jamming. Because of this, the simulations in this thesis will not include the effects of jamming, but only mention it as an area of concern for the "advanced" scenarios.

3.6 The Navigation System: An Integrated GPS/INS

Many navigation systems, both past and present, rely solely on the use of an Inertial Navigation System (INS). This typically consists of a gyroscopically stabilized platform onto which three accelerometers are mounted in orthogonal directions, often termed a "gimbaled" INS. In this fashion it is possible to measure sensed inertial accelerations (i.e. thrust). These instantaneous accelerations can then be integrated once to determine velocity, and twice for position. The vehicle's attitude relative to the platform can also be obtained from the gyroscopes. More recently, accelerometers have been mounted onto three mutually orthogonal directions of the parent vehicle, a "strapdown" INS. The attitude can then be measured through gyroscopic sensing techniques. "Gimbaled" systems are typically more accurate, but "strapdown" systems are cheaper and getting better all the time. The "strapdown" system is also computation intensive.

In both of the INS configurations external measurements are periodically required to update the system. Because an INS is a dead-reckoning system (current position and velocity is based on old values through integration of the sensed accelerations) any errors tend to grow over time. These errors are typically caused by gyroscope drift and accelerometer biases. Additionally, higher-order gravity and numerical integration errors also contribute to INS inaccuracies. It is therefore necessary to correct for errors in the INS with external measurements of the vehicle's state. For missile applications a single IMU realignment using a star tracker is done in the post-boost/deployment phase.

This attitude measurement then feeds into the other states through correlations that have built up.

A significant accuracy improvement in a navigation system can be obtained by integrating the INS with GPS. In an integrated or "tightly coupled" GPS/INS system a continually improving state solution is found by incorporating both the GPS and INS information. A GPS/INS navigation filter is able to use both the sensed accelerations from the INS and the position and velocity measurements from GPS to provide a better solution. Not only is this due to the direct measurements provided by both of the systems, but also because an integrated filter can estimate the errors in the INS' gyroscopes and accelerometers.

An integrated GPS/INS system also maintains the benefits unique to each independent system. For example, the accuracy of the GPS measurements are evident in the navigation solution. Additionally, an instantaneous navigation solution is available at any time, unlike using GPS alone. This is because of the continuous sensed acceleration measurements provided by the INS. These accelerations also help to increase the user's dynamic operating range because the information from the INS can help the GPS tracking loops. Finally, jamming capabilities are improved, compared to using GPS alone, because of the tightened tracking loops afforded by INS aiding and the ability to screen out deceiving information coming in.

The covariance filter developed in this thesis is based upon a ballistic missile using an integrated GPS/INS system. The INS is assumed to be "gimbaled." This filter is described in the next chapter.

CHAPTER 4

FILTER DEVELOPMENT

4.1 Introduction

This chapter focuses on the development of the filter used in the ballistic missile simulations. It begins with a discussion of covariance analysis and how the analysis is applied to the ballistic missile simulation. The states assumed to be present in the environment or "truth" model and their relationship with GPS measurements are then discussed. Finally, the dynamics and process noise models for the states are presented.

4.2 Covariance Analysis

Covariance analysis provides a "quick and dirty" method of assessing the potential performance of a navigation system. It relies on the use of the Kalman Filter equations, yet only is concerned with the statistics of the errors in a user's state, instead of maintaining the best estimate of the state itself. A description of covariance analysis and the equations used in the ballistic missile simulations are presented in this section.

4.2.1 Covariance Analysis vs. Kalman Filtering

Covariance analysis can best be described as an analysis of the errors in a user's state along a nominal trajectory. This analysis is accomplished via the use of a covariance matrix, which describes the statistics (variances and covariances) of the user's state errors. This matrix is improved by measurements, and extrapolated to represent the error statistics at a future point in time. However, information about the state errors is never used to alter the states themselves.

On the other hand, a Kalman Filter goes one step further by using the information contained in the covariance matrix to improve the estimate of the user's state. This update results in a "best" estimate of the state at all times (in a least squares sense). In an on-board navigation system Kalman Filtering would be used because the user wishes to maintain this best state estimate. However, in both covariance analysis and Kalman Filtering the primary concern still lies in the accuracy of the errors in the state, represented by the covariance matrix.

If the corrections to the state are small, the covariance matrix will behave in a similar fashion whether the state is updated (Kalman Filter) or not (covariance analysis). This is a result of the linearizations made as part of the development of the Kalman Filter equations. Furthermore, this also allows for the use of conic trajectories to represent the nominal orbit, instead of more realistic trajectories based on higher-order gravity. This is again a result of the fact that the state errors will behave similarly on all nearby orbits. However, if non-linearities are present then covariance analysis cannot be used. Instead, a Monte Carlo (many individual runs of the on-board system) approach would be necessary to determine the statistics of the errors.

The ballistic missile studies presented in this thesis will make use of linear covariance analysis. The linearization assumptions are valid, so this provides an accurate portrayal of the accuracy obtainable from using GPS.

4.2.2 Covariance Equations and the Estimation Process

The linear covariance equations used in the simulations are for continuous dynamics and discrete measurements. That is, the dynamics driving the states are continuous in nature, i.e. the equations of motion. On the other hand, measurements to the GPS satellites will not be taken continuously, but at discrete times. The time interval for discrete measurements has been set to one second for the missile simulations, as discussed in Section 3.4.2.

[19] provides a description of the linear covariance equations, beginning with the system and measurement models. The continuous system model can be described as

$$\dot{\mathbf{x}}(t) = \mathbf{f}(\mathbf{x}(t), t) + \mathbf{u}(t) \tag{4.1}$$

where: t = time
$\mathbf{x}(t)$ = state vector
$\mathbf{u}(t)$ = bandlimited white noise vector

The discrete measurement model for scalar measurements is represented as

$$z_m = h_m(\mathbf{x}(t_m)) + v_m \tag{4.2}$$

where: t_m = discrete measurement time
z_m = a scalar measurement at time t_m
v_m = bandlimited white noise at time t_m;

The statistics of the white noise processes, $\mathbf{u}(t)$ and v_m, are defined as

$$\mathbf{u}(t) \equiv N(\mathbf{0}, \mathbf{Q}(t)) \tag{4.3}$$

$$v_m \equiv N(0, \alpha_m^2) \tag{4.4}$$

$$E[\mathbf{u}(t)\, v_m] = \mathbf{0} \text{ for all times t and } t_m \tag{4.5}$$

where: $\mathbf{Q}(t)$ = the process noise matrix; a power spectral density matrix
α_m^2 = variance of measurement noise at time t_m

It is also assumed that there are no cross-correlations between the elements of $\mathbf{u}(t)$, or v_m's for measurements occurring at the same or different times.

The update of the covariance matrix for scalar measurements can be written for any weighting or gain vector, $\tilde{\mathbf{w}}_m$, as

$$\mathbf{P}_m^+ = (\mathbf{I} - \tilde{\mathbf{w}}_m \mathbf{b}_m^T)\mathbf{P}_m^-(\mathbf{I} - \tilde{\mathbf{w}}_m \mathbf{b}_m^T)^T + \alpha_m^2 \tilde{\mathbf{w}}_m \tilde{\mathbf{w}}_m^T \tag{4.6}$$

where: $\tilde{\mathbf{w}}_m$ = any weighting or gain vector
$\mathbf{P}_m^+$ = state error covariance matrix after update
$\mathbf{P}_m^-$ = state error covariance matrix prior to update

$$\mathbf{b}_m(\mathbf{x}(t_m)) = \left(\frac{\partial h_m(\mathbf{x}(t_m))}{\partial \mathbf{x}(t_m)} \right)^T = \text{sensitivity vector}$$

and is usually referred to as the Joseph Form of the update equation.

If the weighting vector is optimal (i.e. chosen such that the mean-square estimation error is minimized) then the covariance update equation becomes

$$\mathbf{P}_m^+ = (\mathbf{I} - \mathbf{w}_m \mathbf{b}_m^T)\mathbf{P}_m^- \tag{4.7}$$

where: $\mathbf{w}_m = \dfrac{\mathbf{P}_m^- \mathbf{b}_m}{\mathbf{b}_m^T \mathbf{P}_m^- \mathbf{b}_m + \alpha_m^2}$ = the optimal or Kalman weighting vector

In the covariance analysis for the ballistic missile simulations an update equation of the form

$$\mathbf{P}_m^+ = \mathbf{P}_m^- - k_m \mathbf{w}_m \mathbf{w}_m^T + k_m (\mathbf{w}_m - \tilde{\mathbf{w}}_m)(\mathbf{w}_m - \tilde{\mathbf{w}}_m)^T \tag{4.8}$$

where: $k_m = \mathbf{b}_m^T \mathbf{P}_m^- \mathbf{b}_m + \alpha_m^2$

will be used. Developed by Stanley W. Shepperd, this equation is equivalent to (4.6), thus good for any gain or weighting vector, yet offers a more computationally efficient form of the update equation for scalar measurements [12]. Its equivalence to (4.6) can be proven by substituting k_m and $\mathbf{w}_m$ into (4.8) and performing the vector and matrix multiplications. Also notice that the first two terms are the optimal contribution to the update and are algebraically equivalent to (4.7), while the last term represents the suboptimal contribution to the update (a worsening of the covariance because the last term is added and its diagonals are non-negative regardless of the values of $\mathbf{w}_m$ and $\tilde{\mathbf{w}}_m$).

The extrapolation portion of covariance analysis involves the propagation of both the state and covariance matrix. The state is simply propagated using the system model, (4.1), minus the noise, as

$$\dot{\mathbf{x}}(t) = \mathbf{f}(\mathbf{x}(t), t) \tag{4.9}$$

The covariance matrix is extrapolated using the well-known Riccati Equation as

$$\dot{\mathbf{P}} = \mathbf{F}\mathbf{P} + \mathbf{P}\mathbf{F}^T + \mathbf{Q} \tag{4.10}$$

where: $\mathbf{F}(\mathbf{x}(t), t) = \dfrac{\partial \mathbf{f}(\mathbf{x}(t), t)}{\partial \mathbf{x}(t)}$ = the dynamics matrix

Recall in covariance analysis that the state need not be updated with the measurements (as in a Kalman Filter), but only propagated about some nominal trajectory. Therefore, the dynamics matrix (**F**) and sensitivity vector (**b**) are formed from points along this nominal path.

The estimation process for covariance analysis begins with a "best guess" of the initial state and state error covariance matrix. This covariance matrix is then updated using (4.8) for a scalar measurement. The update would be repeated if several measurements were taken at the same moment in time. This is the case for the simulations because a minimum of eight measurements will be taken at every time step (for the best four satellite case four pseudorange and four integrated Doppler measurements are taken). The updated covariance matrix is then extrapolated to a future time using (4.10). The state is also propagated from (4.9). Because of non-linearities and coupling both (4.9) and (4.10) are integrated using a numerical integrator, discussed in Section 4.6. This entire process is then repeated for a new set of measurements.

4.2.3 Optimal-Suboptimal Filters

An environment state vector, and its associated covariance matrix, represents a model in which all of the real or "truth" states have been included. This can never truly be achieved, since it is impossible to model everything in the real world. However, a good estimate of the primary contributors to errors can be made, with a little process noise included to account for unmodeled states. If an on-board system has the capability to carry all of the environment states in its filter, then the covariance update equation using the optimal weighting vector, (4.7), can be used. This would provide optimal results since it is assumed that the on-board filter models everything in the "truth" environment.

In practice it is seldom possible for the user's navigation system to represent all of the states present in the environment model because of the computational burdens it would place on the computer. The size of the filter would be too large and burdensome to carry as an on-board system. Instead, only the most important states are carried in the on-board filter, therefore it is termed a suboptimal filter.

As a first step in creating an on-board system, the performance of the suboptimal filter in the "truth" environment must be analyzed. One technique is to maintain both the environment and suboptimal filters separately. Then, compute the weighting vector for the suboptimal filter, again using the optimal weighting vector equation. Next, add zeros to this vector to increase its size to that of the dimension of the environment model. This weighting vector can then used as the gain for the environment filter model. Because of the addition of the zeros this weighting vector is now suboptimal, requiring the covariance update to use the Joseph Form. The resulting covariance update generated from the environment filter would then represent the statistical performance of the suboptimal filter in the assumed environment. This accurately depicts how the real user's system would perform. This technique is generally referred to as "off-line system error analysis [19]."

However, the on-board system is not limited to the results from the above analysis. In a procedure termed "tuning," process noise and/or underweighting (equivalent to degrading the estimates of measurement noise) can be added to the suboptimal filter to improve its performance as determined by the environment. This tuned suboptimal filter would ultimately be used as the final on-board system.

There are numerous methods by which to tune the suboptimal filter. If the user was most concerned with minimizing a particular state (for example, position or velocity) then it could be tuned until the desired results were achieved. On the other hand, if the user was concerned about minimizing all of the suboptimal filter's states then it should be tuned to best match the results of the environment model. However, it

is not theoretically possible to achieve the environment performance because of the missing states in the suboptimal filter. As shown by (4.8), the only way to eliminate the third term in this equation, giving an optimal update, is for the optimal and suboptimal weighting vectors to be identical. Clearly, the missing states in the suboptimal filter make this impossible [12].

On the other hand, if the suboptimal weighting vector was identical to the optimal one, except for the missing states, in (4.8) then the contribution of the third term would be minimized. This could be accomplished by computing the optimal weighting vector from the environment, then zeroing out the states present in the environment but not contained in the on-board system. This thus represents the best performance, in principle, that could be achieved by the suboptimal filter working in the truth surroundings described by the environment model, hence the term "optimal" suboptimal. This also represents the best possible tuning of the on-board filter [12].

Optimal-suboptimal analysis can be accomplished completely through the use of (4.8). In this equation $\mathbf{w}_m$ would represent the optimal weighting vector for the environment model. That is, $\mathbf{w}_m$ would be created as described in (4.7). The suboptimal weighting vector, $\tilde{\mathbf{w}}_m$, is then created by zeroing out the elements of $\mathbf{w}_m$ that are not included as on-board filter states. Note from (4.8) that the net effect of doing this is to zero out all suboptimal contributions from the third term of (4.8), except for the elements of $\mathbf{w}_m$ which have been zeroed out. The consequence of zeroing out states in the optimal weighting vector, also termed "considering" them out, is to not estimate them, yet still allow correlations with other states to grow [12].

Because of the manner in which the gain is computed, an optimal-suboptimal filter is somewhat optimistic. However, for practical purposes it can offer a valuable "first cut" look at a problem. The reasons are twofold. First, it is easy to implement because only one covariance model needs to be maintained. This can be seen through the use of (4.8). Secondly, through the use of an optimal-suboptimal filter the best

possible results of a tuned on-board filter are determined. In essence it is self-tuning. It can therefore be used as an initial feasibility study and to identify critical states for a specific application [12].

An optimal-suboptimal filter will be used in the simulations for the ballistic missile. All of the states present in the environment model are discussed in the next section. Those states to be considered out, representing those assumed not present in the ballistic missile's on-board navigation filter, will be discussed in the results chapter.

4.3 Missile Environment States

Typical integrated GPS/INS on-board navigation filters contain between 11 and 17 states. The minimum 11-state filter would consist of states for position, velocity, attitude (platform misalignment), and clock offset and rate. A more advanced 17-state filter might add states for accelerometer biases and attitude rates (platform drift). These filters are often termed "aided" since the IMU would be providing sensed accelerations directly to the filter. On the other hand, in an "unaided" filter the user's acceleration would replace attitude in the 11-state filter.

The covariance simulations presented in this thesis will make use of a 44-state "aided" filter. It was assumed that this was the number of states needed to accurately model the real environment. An actual on-board navigation system would most likely carry much fewer states in order to reduce the computational burdens. The potential performance of the on-board navigation system will be analyzed in the results section by "considering out" certain states not carried by the missile (an optimal-suboptimal filter).

The 44 states for the environment are presented below. Recall that in covariance analysis the statistics for the errors in these states will analyzed.

Position

The missile's Earth Centered Inertial (ECI) position vector represents the first three states. The 1σ errors in these states will be resolved into their downrange, vertical, and crosstrack (local-vertical/local-horizontal (LVLH)) components for the simulation output.

Velocity

The missile's ECI velocity vector makes up the next three states. Again, the 1σ errors in these states will be resolved into the LVLH frame for output.

Attitude

The attitude of a platform IMU represents its offset from some inertial attitude, typically initialized on the ground. Even though gyroscopes tend to be quite stable, over time they drift. These changes in the gyroscopes' attitudes represent unknown misalignments, typically measured as three Euler angle errors (small angle approximations) from the inertial axes. Since the ballistic missile will require thrusting and accurate pointing for deployment of the r.b.'s, attitude information is critical.

The IMU misalignments can be directly estimated by taking optical measurements with a star tracker. Yet, in an integrated GPS/INS system some attitude error information is also indirectly observable from the radiometric measurements. This information is created when the missile thrusts, causing correlations to build between the attitude and position/velocity states. These correlations are driven by the fact that the missile believes it is thrusting in a certain direction, while in fact IMU attitude errors are steering the vehicle in a skewed direction. The resulting position and velocity offset is visible through measurements to GPS. In fact, the larger the misalignments and thrusting, the more visible these attitude errors become. The statistics for the attitude errors will be presented in units of arcsec.

Attitude Rate

Three states are needed to model the attitude drift of the IMU, the Euler angle rates. These attitude rate states are generally much more difficult to detect than the attitude states themselves. However, over time the uncertainties in the rate errors also propagate into position and velocity errors, and can be observed. The 1σ attitude rate errors will be presented in units of arcsec/s (deg/hr).

Accelerometer Bias

Although accelerometers are typically calibrated on the ground by measuring their biases, errors still exist. Three states are therefore needed to model these biases whenever sensed accelerations from the accelerometers are being fed into the navigation system. Like attitude errors, errors in the accelerometer biases become visible through correlations with position and velocity. The statistics of these bias errors will be shown in the results section in units of micro g's.

User Clock Offset

As discussed in Section 2.5.2, the clock contained in the missile's GPS receiver will not be synchronized with true GPS system time. This results in ranging measurement errors to the GPS satellites. A state is thus contained in the filter to estimate the clock offset. The state used in the covariance filter is actually the range equivalent clock offset, i.e. clock offset x speed of light, and is expressed in m.

User Clock Offset Rate

A clock rate state will also be included in the filter to model the drift characteristics of the user's clock. This state will be modeled as the velocity equivalent clock offset rate, i.e. clock offset rate x speed of light, and is expressed in m/s.

Pseudorange Bias

Section 2.7 discusses the different error sources in the GPS system directly affecting a user's navigation accuracy. The errors not modeled as receiver noise will be lumped together into a pseudorange bias state for each of the GPS satellites, thus requiring 24 states. Although the state is termed a "bias", it will be modeled in Section 4.5.1 as a long correlation time (Markov process) pseudorange error, in units of m. However, the correlation time is large enough such that pseudorange bias rate states are not needed. This state therefore only affects ranging measurements.

Residual Thrusting

Three states will be included in the filter for residual thrusting. This is an additional error source present only in the "advanced" mission scenarios, caused by the final main stage being carried along with the bus during the free-fall phase. These states lead directly to acceleration errors for the missile, modeled in units of micro g's. A worst case scenario for the residual thrusting has been assumed and is discussed in more detail in Section 4.5.1.

A summary of the size, symbols, and units associated with each of the environment error states is presented in Table 4.1.

Table 4.1 Summary of Environment States

STATE	SIZE	SYMBOL	UNITS FOR ERRORS
position	3	**r**	m
velocity	3	**v**	m/s
attitude	3	**att**	arcsec
attitude rate	3	**att_rate**	arcsec/s
accelerometer bias	3	**acc_bias**	micro g's
user clock offset	1	$c\Delta t_u$	m
user clock offset rate	1	$c\Delta t_u$_rate	m/s
pseudorange bias	24	**bias**	m
residual thrusting	3	**res_thrust**	m/s^2

4.4 The Sensitivity Vector

The sensitivity vector described in the development of (4.6) is the critical element in the update equation. In essence it describes how a measurement changes for a small change in the state. It was developed as part of the process to derive a linearized Kalman Filter. In the ballistic missile simulations two forms of the sensitivity vector will be used, one for the pseudorange measurements and one for the integrated Doppler measurements.

4.4.1 Pseudorange Measurements

Recalling the development of (2.7), a pseudorange measurement, p_k, from a ballistic missile to GPS satellite k can be written as

$$p_k = |\mathbf{r}_u - \mathbf{r}_k| + c\Delta t_u - c\Delta t_k + v_k \tag{4.11}$$

where: $\mathbf{r}_u$ = user's inertial position vector at measurement time
$\mathbf{r}_k$ = satellite k's inertial position vector at measurement time
$c\Delta t_u$ = range equivalent error is user time from true (GPS system) time
$c\Delta t_k$ = range equivalent error in sat k's time from true (GPS system) time
v_k = pseudorange measurement noise to satellite k; zero mean

and recall that $c\Delta t_k$ and $\mathbf{r}_k$ are given as part of the navigation message.

The pseudorange biases associated with each GPS satellite will also contribute directly to the ranging measurements. Thus, (4.11) now takes the form

$$p_k = |\mathbf{r}_u - \mathbf{r}_k| + c\Delta t_u - c\Delta t_k + \text{bias}_k + v_k \tag{4.12}$$

where: bias_k = pseudorange bias to satellite k

The sensitivity vector (**b**) is formed by taking the partial derivative of the measurement, p_k, with respect to each of the 44 states of the ballistic missile filter. This results in **b** containing non-zero components only for the position states, the clock offset state, and the appropriate pseudorange bias state. The partial derivative with

respect to the user's position is

$$\frac{\partial p_k}{\partial \mathbf{r}} = \left[\leftarrow \mathbf{h}^T \rightarrow \right] \tag{4.13}$$

where: $\mathbf{h}$ = the unit line of sight vector from GPS satellite k to the missile

Next, the partial of the measurement with respect to the user's clock offset is just

$$\frac{\partial p_k}{\partial c\Delta t_u} = 1 \tag{4.14}$$

Likewise, the component of the sensitivity vector for the pseudorange bias state is

$$\frac{\partial p_k}{\partial \text{bias}_k} = 1 \tag{4.15}$$

Combining (4.13) through (4.15) into the proper elements of $\mathbf{b}$ gives the overall sensitivity vector for pseudorange measurements. Notice that the one for the pseudorange bias state must be placed in the element of $\mathbf{b}$ corresponding to the satellite whose pseudorange is being measured.

4.4.2 Integrated Doppler Measurements

The integrated Doppler sensitivity vector will be formed in a similar fashion to that of the pseudorange measurement. First, the equation for an integrated Doppler measurement needs to be formed. In order to simplify the sensitivity vector for this measurement a less complicated form was used. This simplified form defines the velocity measurement as that of the relative velocity along the line of sight vector (actually creating an instantaneous Doppler model for the velocity measurements). However, the advantages of a user processing integrated Doppler can still be achieved by applying the appropriate amount of noise for the more complicated measurements, 0.02 m/s as discussed in Section 3.5.1.

The instantaneous Doppler measurement to satellite k, d_k, can therefore be

defined as

$$d_k = (\mathbf{v}_u - \mathbf{v}_k) \bullet \mathbf{h} + c\Delta t_u\_rate = (\mathbf{v}_u - \mathbf{v}_k) \bullet \frac{(\mathbf{r}_u - \mathbf{r}_k)}{|\mathbf{r}_u - \mathbf{r}_k|} + c\Delta t_u\_rate \qquad (4.16)$$

where: $\mathbf{v}_u$ = user's inertial velocity vector at measurement time
$\mathbf{v}_k$ = satellite k's inertial velocity vector at measurement time
$c\Delta t_u\_rate$ = velocity equivalent user's clock offset rate

Notice that the user's clock offset rate also contributes directly to the line of sight velocity. The next step is to differentiate (4.16) with respect to the user's state. First, define

$$\mathbf{r} = \mathbf{r}_u - \mathbf{r}_k \qquad \partial\mathbf{r} = \partial\mathbf{r}_u - \partial\mathbf{r}_k \qquad (4.17)$$

$$\mathbf{v} = \mathbf{v}_u - \mathbf{v}_k \qquad \partial\mathbf{v} = \partial\mathbf{v}_u - \partial\mathbf{v}_k \qquad (4.18)$$

so (4.16) becomes

$$d_k = \mathbf{v}^T \frac{\mathbf{r}}{r} + c\Delta t_u\_rate \qquad (4.19)$$

This creates an equation that can be differentiated easily for the user's states. The partial derivative with respect to $\mathbf{r}$ is now

$$\frac{\partial d_k}{\partial \mathbf{r}} = \frac{1}{r^3}\left[(\mathbf{r} \bullet \mathbf{r})\mathbf{v} - (\mathbf{v} \bullet \mathbf{r})\mathbf{r}\right]^T = \frac{1}{r^3}\left[(\mathbf{r} \times \mathbf{v}) \times \mathbf{r}\right]^T \qquad (4.20)$$

and similarly for $\mathbf{v}$ is

$$\frac{\partial d_k}{\partial \mathbf{v}} = \frac{\mathbf{r}^T}{r} \qquad (4.21)$$

Recalling that the sensitivity vector measures the magnitude of change in a measurement for a small change in the user's state, both $\partial\mathbf{r}_k$ in (4.17) and $\partial\mathbf{v}_k$ in (4.18) can be set to zero. (4.20) and (4.21) now become the sensitivity vectors for the user's position and velocity states, respectively.

The final element of $\mathbf{b}$ represents the measurement change due to a change in the user's clock offset rate. This can be found as

$$\frac{\partial d_k}{\partial c\Delta t_u\_rate} = 1 \qquad (4.22)$$

4.5 State Error Dynamics

The state error dynamics for covariance analysis describes how the state errors change over time. Often the dynamics of systems can not be described by deterministic models, but instead are best modeled based on evidence from empirical data.

4.5.1 Modeling of the State Errors

The dynamics matrix, **F**, presented in the development of (4.10) describes the dynamics of the user's state errors. The matrix is given as

$$\mathbf{F}(\mathbf{x}(t),t) = \frac{\partial \mathbf{f}(\mathbf{x}(t),t)}{\partial \mathbf{x}(t)} \tag{4.23}$$

creating a linearized system model, (4.9), as

$$\frac{d}{dt}\Delta\mathbf{x} = \mathbf{F}\Delta\mathbf{x} + \mathbf{u} \tag{4.24}$$

where: $\Delta\mathbf{x}$ = the missile's state error
$\mathbf{u}$ = bandlimited white noise vector

The elements of the dynamics matrix associated with each of the user's state errors are presented below.

Position and Velocity Errors

The relationship between position and velocity errors can be developed through the use of the gravity gradient matrix, **G**. This is developed by taking the partial derivative of the conic gravity vector with respect to the missile's position. First, the 2-body gravity vector is written as

$$\mathbf{g} = \frac{-\mu\mathbf{r}}{r^3} \tag{4.25}$$

where: $\mathbf{g}$ = the gravity vector at point $\mathbf{r}$
μ = the gravitational parameter = $3.986012 \times 10^{14}\ m^3/s^2$

and taking the partial derivative with respect to the missile's position gives

$$\mathbf{G} = \frac{\partial \mathbf{g}}{\partial \mathbf{r}} = \frac{-\mu}{r^3}\left[\mathbf{I} - \frac{3\mathbf{r}\mathbf{r}^T}{\mathbf{r}^T\mathbf{r}}\right] \tag{4.26}$$

Thus, the dynamics matrix for the relationship between position and velocity can be written in the form of (4.24) as

$$\frac{d}{dt}\begin{bmatrix}\Delta\mathbf{r}\\ \Delta\mathbf{v}\end{bmatrix} = \begin{bmatrix}\mathbf{0} & \mathbf{I}\\ \mathbf{G} & \mathbf{0}\end{bmatrix}\begin{bmatrix}\Delta\mathbf{r}\\ \Delta\mathbf{v}\end{bmatrix} + \begin{bmatrix}\mathbf{0}\\ \mathbf{u}_{gravity}\end{bmatrix} \tag{4.27}$$

When combining this dynamics matrix into the Riccati Equation, (4.10), there will also be noise driving the velocity channel due to the effects of higher-order gravity. This is addressed in Section 4.5.2.

Attitude and Attitude Rate Errors

The attitude and attitude rate (often termed platform misalignment and drift) errors for the missile's IMU cannot be described by deterministic models. Instead, empirical data suggests a manner in which to model the statistics of the errors. One excellent model for many physical systems driven by random disturbances is a Markov process, which generates an exponentially correlated random variable. This kind of random variable has an autocorrelation function that is a decreasing exponential.

A first-order Markov process can be represented by the state error equation (4.24) as

$$\frac{d}{dt}\Delta x = \frac{-1}{\tau}\Delta x + u \tag{4.28}$$

where: τ = the time constant for the Markov process

Forming the scalar Riccati equation and looking for a steady-state value for the variance by setting $\dot{p}$ equal to zero requires the process noise to be

$$q = \frac{2\sigma_{ss}^2}{\tau} \tag{4.29}$$

where: σ_{ss}^2 = the steady-state or maximum variance for the Markov process

Integrating the Riccati equation provides the response for the variance of Δx, $\sigma^2(t)$, as

$$\sigma^2(t) = \sigma_{ss}^2\left(1 - e^{\frac{-2t}{\tau}}\right) \quad \text{if } \sigma^2(0) = 0 \tag{4.30}$$

Notice that (4.30) is an exponential response, bounded by the steady-state variance, and whose correlation is determined by the time constant. This provides a growth rate error model typical of many physical systems such as gyroscopes, accelerometers, and clocks.

If the attitude rate errors are Markov processes and driving the attitude errors, then the attitude errors become integrated Markov processes, shown in the form of (4.10) as

$$\frac{d}{dt}\begin{bmatrix} \sigma^2_{\Delta att} & \sigma_{\Delta att,\Delta att\_rate} \\ \sigma_{\Delta att\_rate,\Delta att} & \sigma^2_{\Delta att\_rate} \end{bmatrix} = \begin{bmatrix} 0 & 1 \\ 0 & \frac{-1}{\tau} \end{bmatrix}\begin{bmatrix} \sigma^2_{\Delta att} & \sigma_{\Delta att,\Delta att\_rate} \\ \sigma_{\Delta att\_rate,\Delta att} & \sigma^2_{\Delta att\_rate} \end{bmatrix} + \mathbf{P}\mathbf{F}^T + \begin{bmatrix} 0 & 0 \\ 0 & \frac{2\sigma_{ss}^2}{\tau} \end{bmatrix} \tag{4.31}$$

for scalar components.

σ_{ss} and τ are set to 0.02 arcsec/s and 1 day for the ballistic missile simulations, respectively. These values represent the error growth characteristics of a good IMU.

Errors in attitude also create acceleration errors when the missile is thrusting. Clearly, if a vehicle does not know its attitude perfectly it cannot point its jets in the desired directions. The dynamics matrix describing the relationship between attitude errors and the resulting acceleration errors can be derived by first developing an equation relating thrust to acceleration errors. This can be written as

$$\Delta\mathbf{a} = \begin{bmatrix} 0 & -att_k & att_j \\ att_k & 0 & -att_i \\ -att_j & att_i & 0 \end{bmatrix}\mathbf{a}_p \tag{4.32}$$

where: $\Delta\mathbf{a}$ = inertial acceleration errors
att = Euler angle error vector of the inertial offset between the true and estimated platform directions
$\mathbf{a}_p$ = sensed accelerations in the true platform frame

The matrix of platform angular errors is developed by taking the difference between two Euler angle transformation matrices, assuming small angles. The first represents the transformation matrix relating the sensed accelerations in the true platform coordinates to the inertial directions. Likewise, the second matrix represents the estimated (what the missile thinks) platform coordinates to the inertial directions. Taking the difference of the second from the first gives the relationship between the sensed platform accelerations and the inertial acceleration errors due to small IMU misalignments, **att**. This is shown as (4.32).

Multiplying (4.32) out gives

$$\Delta\mathbf{a} = \begin{bmatrix} -\mathbf{a}_{p2}att_k + \mathbf{a}_{p3}att_j \\ \mathbf{a}_{p1}att_k - \mathbf{a}_{p3}att_i \\ -\mathbf{a}_{p1}att_j + \mathbf{a}_{p2}att_i \end{bmatrix} = \begin{bmatrix} 0 & \mathbf{a}_{p3} & -\mathbf{a}_{p2} \\ -\mathbf{a}_{p3} & 0 & \mathbf{a}_{p1} \\ \mathbf{a}_{p2} & -\mathbf{a}_{p1} & 0 \end{bmatrix} \begin{bmatrix} att_i \\ att_j \\ att_k \end{bmatrix} \tag{4.33}$$

or

$$\Delta\mathbf{a} = \frac{d}{dt}\Delta\mathbf{v} = -\left[\mathbf{a}_p \times\right] \begin{bmatrix} att_i \\ att_j \\ att_k \end{bmatrix} \tag{4.34}$$

where: $\left[\mathbf{a}_p \times\right]$ = cross-product matrix of sensed accelerations in the true platform frame

Thus, the relationship between IMU attitude errors and the velocity errors can be written in the form of (4.24) as

$$\frac{d}{dt}\begin{bmatrix} \Delta\mathbf{v} \\ \Delta\mathbf{att} \end{bmatrix} = \begin{bmatrix} \mathbf{0} & -\left[\mathbf{a}_p \times\right] \\ \mathbf{0} & \mathbf{0} \end{bmatrix} \begin{bmatrix} \Delta\mathbf{v} \\ \Delta\mathbf{att} \end{bmatrix} + \begin{bmatrix} \mathbf{0} \\ \mathbf{0} \end{bmatrix} \tag{4.35}$$

Since the cross product matrix is only non-zero when the vehicle is thrusting, attitude induced velocity errors only occur during thrusting mission phases.

Accelerometer Bias Errors

Like the attitude rate errors, the IMU's accelerometer bias errors will also be modeled as first-order Markov processes. A value of 10 micro g's was chosen for the accelerometer bias steady-state standard deviation, σ_{ss}, and one day for the time constant, τ.

Assuming that the missile's platform remains aligned with the inertial directions, accelerometer bias uncertainties will lead directly into acceleration errors when the vehicle thrusts. In the form of (4.10), for scalar components, this is shown as

$$\frac{d}{dt}\begin{bmatrix} \sigma^2_{\Delta v} & \sigma_{\Delta v,\Delta acc\_bias} \\ \sigma_{\Delta acc\_bias,\Delta v} & \sigma^2_{\Delta acc\_bias} \end{bmatrix} = \begin{bmatrix} 0 & 1 \\ 0 & \frac{-1}{\tau} \end{bmatrix}\begin{bmatrix} \sigma^2_{\Delta v} & \sigma_{\Delta v,\Delta acc\_bias} \\ \sigma_{\Delta acc\_bias,\Delta v} & \sigma^2_{\Delta acc\_bias} \end{bmatrix} + \mathbf{P}\mathbf{F}^T + \begin{bmatrix} 0 & 0 \\ 0 & \frac{2\sigma^2_{ss}}{\tau} \end{bmatrix} \quad (4.36)$$

The identity matrix will only be placed in the missile's dynamics matrix when the vehicle is thrusting. It is assumed that the on-board computer ignores accelerometer outputs except when the vehicle is thrusting. Like the IMU's attitude states, the accelerometer biases will then only be estimated during the thrusting portions of the missile trajectory.

User Clock Offset Error and Offset Rate Error

The user clock rate error is again modeled as a first-order Markov process, creating an integrated Markov process for the offset error. A σ_{ss} of $5x10^{-10}$ s/s was chosen, or 0.149898 m/s of velocity equivalent drift rate. This represents a typical frequency drift for quartz clocks over a period of a day, τ equals one day [11]. This is the quality of clock assumed to be used in the GPS receiver on the ballistic missile.

Pseudorange Bias Errors

The next set of error states, the pseudorange bias errors to each of the GPS satellites, will also be modeled as Markov processes. A steady-state value of 3.4 m will be used. This value is derived from RSS'ing the non-noise GPS errors presented in Section 2.7. Specifically, it is the RSS of the 1 σ values for satellite orbital fluctuations

and satellite clocks. A time constant of 1/2 day was assumed, primarily because the GPS satellites are in 12 hour orbits.

Residual Thrusting Errors

The final set of error states, those for residual thrusting, represent an error source present only in the "advanced" mission scenarios. They are caused from leaks or thrust sputtering from the final main stage as it is carried along with the bus during the free-fall portion of the trajectory.

A worst case scenario has been assumed by modeling the residual thrusting as states directly affecting the missile's acceleration errors. In this manner it is assumed that the residual thrusting occurs at a constant rate in some constant direction over the entire free-fall phase. This creates the most pessimistic scenario since the vehicle would most likely be tumbling and sputtering as discussed in Section 3.5.2. Such a scenario would be best modeled as process noise, a more optimistic approach than using filter states. It is also assumed that the residual thrusting is just equal to the steady-state accelerometer bias uncertainties of the IMU (10 micro g's). As a result, the missile would not incorporate the sensed thrusts from the accelerometers, since the addition of the accelerometer bias errors into the missile's acceleration errors are larger (or equal) to the thrust itself. However pessimistic, modeling the residual thrusting errors as states is a valid scenario representing the worst possible situation.

No dynamics are associated with the residual thrusting errors, as the errors will be assumed to be constant over the entire free-fall phase. The 1σ error in each of the inertial directions will be set to 10 micro g's. This state error then directly affects the acceleration errors during the free-fall phase, thus

$$\frac{d}{dt}\begin{bmatrix} \Delta v \\ \Delta res\_thrust \end{bmatrix} = \begin{bmatrix} 0 & I \\ 0 & 0 \end{bmatrix}\begin{bmatrix} \Delta v \\ \Delta res\_thrust \end{bmatrix} + \begin{bmatrix} 0 \\ 0 \end{bmatrix} \tag{4.37}$$

The identity matrix is removed at the beginning of GPS measurements; the final main stage having been ejected. A summary of the states modeled as Markov processes are presented in Table 4.2.

Table 4.2 Summary of First-Order Markov Process State Errors

STATE ERROR	τ	σ_{ss}
attitude rate	1 day	0.02 arcsec/s
accelerometer bias	1 day	10 micro g's
user clock offset rate	1 day	0.149898 m/s
pseudorange bias	1/2 day	3.4 m

4.5.2 Higher-Order Gravity (HOG) Process Noise Matrix

A vehicle in space is subject to gravitational accelerations beyond those modeled in the on-board software. These higher-order gravitational (HOG) accelerations are due to the fact that the Earth is not a perfect spherical body and lacks a uniform mass distribution. In the extrapolation of the missile's covariance matrix it is therefore necessary to account for the position and velocity disturbances resulting from these gravitational effects.

An optimistic, yet simplified, process is undertaken to determine the noise matrix for the effects of higher-order gravity. The primary concern is to provide a process noise matrix that is representative of the position and velocity error growth from the higher-order gravity between GPS measurements, i.e. one second intervals. The process described below provides optimistic values, yet the difference between the resulting effects using these values and those obtainable using more complicated techniques is negligible because of the short propagation time. Additionally, the primary focus of the thesis is to stress the advantages of using all-in-view GPS, not to model gravity perfectly.

HOG Noise Covariance Matrix Development

The unmodeled HOG accelerations can be accounted for in the extrapolation equation, (4.10), through the use of the process noise matrix (**Q**). The effect of adding process noise is to increase the missile's position and velocity uncertainties, thus accounting for the gravitational uncertainties.

The proper **Q** must reflect those HOG terms acting as white noise. Terms not acting as noise can be accounted for in the gravity gradient matrix. Such gravity terms would also be used in the extrapolation of the user's position and velocity states. However, this would typically only be undertaken in an on-board navigation system, where the user is concerned about finding an actual state solution (the vehicle's location). On the other hand, for the purposes of covariance analysis the statistics of the user's errors are being analyzed, and these errors are going to behave similarly on all nearby orbits, as discussed in Section 4.2.1. Therefore, the covariance simulations extrapolate using the 2-body equations of motion and account for the gravitational noise terms through **Q**.

It is assumed in this thesis that terms between a 5x5 and 18x18 model of the Earth's gravitational field can be modeled as white noise over the period of one second, the measurement interval. This is an optimistic assumption because in the distance covered by the ballistic missile in one second these terms would not truly be "white." Essentially, the assumption is being made that the correlation times for these terms are one second, when in fact to be white the correlation time should be on the order of 100 s [13]. However, assuming one second correlation times simplifies the development and implementation of the process noise matrix.

The statistics for the HOG terms acting as noise were determined by a uniform sampling of the Earth. 500 sampling locations were chosen at a common altitude such that each point represented an equal surface area of the Earth. At each of the sampling points a gravity noise vector was computed by differencing an 18x18 Earth gravity

vector (representing the "truth") and a 4x4 gravity vector. From these samples it was then possible to develop a covariance matrix for the HOG noise in a local-vertical/local-horizontal (LVLH) frame. Similar covariance matrices were developed for altitudes between 0 and 3000 km at 100 km increments, covering the missile's flight region.

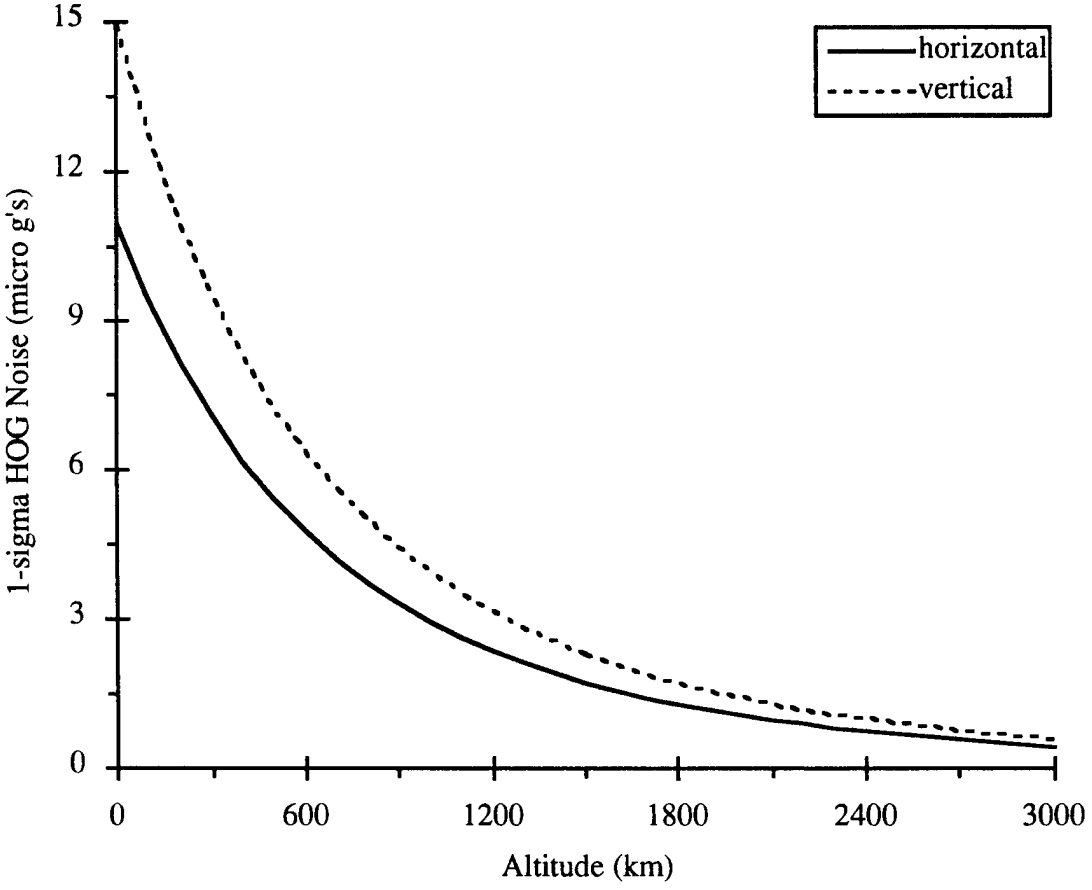

Figure 4.1 Higher-Order Gravity (HOG) Noise vs. Altitude

It was discovered that the horizontal components of each of these matrices were uncorrelated with the vertical component. For example, at ground level the largest correlation coefficient was only 0.008. On the other hand, there was a slight correlation between the horizontal values in each of the matrices. A conservative measure was taken by diagonalizing these horizontal components, thereby assuming that the missile happened to be traveling in the worst horizontal direction. In each of the matrices the

two horizontal variances were also set to the value of the largest one. This again was a conservative measure, essentially creating an isotropic model of the gravity noise field in the horizontal plane. This resulted in a statistical model with no preferential horizontal direction (orbit inclination), being a function of altitude only. The gravity noise statistics as a function of altitude are shown on the previous page in Figure 4.1.

Before the HOG noise covariance matrices can be used in the simulations, the equivalent process noise matrices have to be determined for each altitude.

Relationship to Q

The relationship between the HOG noise covariance matrices and their equivalent process noise matrices (**Q**'s) have to be developed before the extrapolation equation, (4.10), can be used. This relationship can often be difficult to resolve because **Q** is a power spectral density matrix, not a true covariance matrix. Although, several assumptions can be made to arrive at the connection. First, in free-space an acceleration error, $\Delta\mathbf{a}$, creates a velocity error, $\Delta\mathbf{v}$, as such

$$\Delta\mathbf{v} = \Delta\mathbf{a}\, t \tag{4.38}$$

and converted into covariance matrices as

$$\mathbf{P}_{\Delta v} = t^2\mathbf{P}_{\Delta a},\ \text{if } E[\Delta\mathbf{a}] = E[\Delta\mathbf{v}] = \mathbf{0} \tag{4.39}$$

The free-space equation can be used because of the assumption of one second correlation times for the HOG noise. Over this period gravity has little time to act.

The next step is to determine the relationship between the velocity error covariance matrix in (4.39) and **Q**. Using (4.10), with a dynamics matrix void of the gravity gradient (again, one second time steps make the effects of gravity negligible), the velocity error covariance matrix can be found as

$$\mathbf{F} = \begin{bmatrix} \mathbf{0} & \mathbf{I} \\ \mathbf{0} & \mathbf{0} \end{bmatrix},\ \mathbf{P} = \begin{bmatrix} \mathbf{P}_{\Delta r} & \mathbf{P}_{\Delta r \Delta v} \\ \mathbf{P}_{\Delta r \Delta v}^T & \mathbf{P}_{\Delta v} \end{bmatrix},\ \mathbf{Q} = \begin{bmatrix} \mathbf{0} & \mathbf{0} \\ \mathbf{0} & \mathbf{Q}_{HOG} \end{bmatrix} \tag{4.40}$$

$$\dot{\mathbf{P}}_{\Delta v} = \mathbf{Q}_{HOG} \tag{4.41}$$

$$\mathbf{P}_{\Delta v} = \mathbf{Q}_{HOG} t,\ \text{if } \mathbf{P}_{\Delta v}(0) = 0 \text{ matrix} \tag{4.42}$$

Finally, combining (4.39) and (4.42) results in a direct relationship between the HOG noise covariance matrices developed earlier and **Q** as

$$\mathbf{Q}_{HOG} = t\mathbf{P}_{\Delta a} \tag{4.43}$$

with t equal to one second.

In the simulations a table of process noise matrices was created from (4.43) for each of the HOG noise covariance matrices. The ballistic missile could then choose a **Q** to use based upon altitude, interpolating when necessary.

Several issues should be clarified concerning the development of (4.43). First, notice that (4.38) is derived for the relationship between acceleration and velocity errors, instead of acceleration and position errors. It is possible to do the latter, but in the ultimate solution the magnitude of the elements of **Q** would be smaller than (4.43). By instead choosing **Q** to match the velocity error growth, a more conservative approach is used. Additionally, velocity error growth will later be shown to be the driving factor in the size of circular error probable (CEP).

A second issue is the use of the **Q**'s developed above during the free-fall phase of the "advanced" scenarios. These **Q**'s provide rather optimistic results for the position and velocity uncertainty growth due to higher-order gravity during the length of this phase. This is a result of the one second correlation times assumed in their development. Since no GPS measurements are being taken during this phase, longer correlation times could be used to create a better model.

This improved model would generally be created by including gravity error states in the filter as Markov processes. There gravity errors would then directly drive the velocity errors. In this fashion a more representative correlation time could be used for the HOG noise matrix. The state vector form would be

$$\frac{d}{dt}\begin{bmatrix}\Delta v\\ \Delta g\end{bmatrix} = \begin{bmatrix}\mathbf{0} & \mathbf{I}\\ \mathbf{0} & \frac{-\mathbf{I}}{\tau}\end{bmatrix}\begin{bmatrix}\Delta v\\ \Delta g\end{bmatrix} + \begin{bmatrix}\mathbf{0}\\ \mathbf{u}\end{bmatrix} \tag{4.44}$$

where τ would represent the correlation time for the higher-order gravity covariance matrix. With the development of the Riccati equation, the relationship between the gravity covariance matrix and the process noise matrix (driving the gravity channel) could be found [13].

However, a better HOG model for the free-fall phase would only serve to increase the initial covariance matrix of the missile at the start of GPS measurements. The difference between this matrix and the one developed from the **Q**'s for one second intervals would become negligible after only one set of GPS measurements. Additionally, the difference in the size of the covariance matrix using the two methods would be drastically diminished because the missile simulations begin with considerable position and velocity uncertainties. The RSS contribution of gravity noise would therefore be quite small regardless of the **Q** used.

Finally, only HOG noise is chosen to drive the velocity channel of the missile's covariance matrix. It is possible for disturbances from other sources, such as solar pressure and third bodies, to also create uncertainties. Yet, in the case of the ballistic missile these are assumed to be negligible.

4.6 Runge-Kutta Numerical Integration

The integration of the covariance extrapolation equation, (4.10), is accomplished using a 4th-order Runge-Kutta numerical integrator. This same numerical integrator is also used to propagate the entire state for the simulations. Since only the position and velocity states affect pseudorange and integrated Doppler measurements to the GPS satellites, these are the only states propagated (about a nominal orbit). Recall that covariance analysis is not concerned with keeping track of the entire states, but does need reasonable approximations of them to properly compute the coefficients of **F**, **b**, and **Q**. The thrusting of 0.1 g along the velocity vector during the 100 s of GPS

measurements will also be included in this propagation. With one second time steps for the simulations the integrator provides extremely accurate results.

CHAPTER 5

NAVIGATION PERFORMANCE OF AN ALL-IN-VIEW RECEIVER

5.1 Introduction

The navigation performance of a ballistic missile using an all-in-view receiver versus the best four or five satellites is presented in this chapter. A set of baseline cases will be presented, followed by a group of simulations with some of the nominal values or models slightly changed. All of these results are presented in the latter portion of the chapter. They are preceded by a discussion of CEP, the specific cases analyzed, and the input deck to be used by the simulations.

5.2 Circular Error Probable (CEP)

In addition to the state uncertainties of the ballistic missile, circular error probable (CEP) was also used to quantify the performance enhancements of using an all-in-view receiver. CEP gives the radius of a circle on the Earth defining a boundary in which a 50 % probability of impact exists. Since the ultimate goal of a ballistic missile is to accurately strike a target, CEP was a good figure-of-merit for comparing the selection methods.

CEP for this thesis was calculated in several steps. First, a 2-body state transition matrix was used propagate the position and velocity components of the covariance matrix to the impact point of the Earth along the nominal trajectory. The conic equation of motion was chosen since the effects of process noise from higher-order gravity were found to be small. This error ellipsoid was then flattened in the horizontal plane (the

ground) by "flying out" all of the position error vectors to their impact points. This created an ellipse in the horizontal plane.

Because the ballistic missile also has clock offset uncertainties from true GPS time, these errors needed to be accounted for in the calculation of CEP. Specifically, a clock offset on the missile would mean that the true vehicle could be ahead or behind of the nominal impact point (corresponding to a clock that is behind or ahead of true GPS time). However, because of the high velocity of the ballistic missile the clock error contribution to impact accuracy was extremely small. Combining the above steps created a sensitivity matrix defined as

$$\partial \mathbf{r}_{hor} = \Phi \partial \mathbf{x} \tag{5.1}$$

where: $\partial \mathbf{r}_{hor} = \begin{bmatrix} \partial r_{dr} \\ \partial r_{ct} \end{bmatrix}$ = downrange and crosstrack position errors in hor. plane

Φ = 2x7 transition (or sensitivity) matrix

$\partial \mathbf{x} = \begin{bmatrix} \partial \mathbf{r} \\ \partial \mathbf{v} \\ \partial t \end{bmatrix}$ = position, velocity, and clock error at a point on nominal orbit

The transition matrix relates position, velocity, and clock offset errors along the nominal trajectory to impact position errors in the horizontal plane. In terms of the statistics associated with these impact errors, (5.1) could be used to write

$$E\left[\partial \mathbf{r}_{hor} \partial \mathbf{r}_{hor}^{T}\right] = \Phi E\left[\partial \mathbf{x} \partial \mathbf{x}^{T}\right] \Phi^{T} \tag{5.2}$$

This 2 by 2 matrix, $E\left[\partial \mathbf{r}_{hor} \partial \mathbf{r}_{hor}^{T}\right]$, could then be used directly to determine CEP. Finding the eigenvalues of the ellipse, σ_a and σ_b, yields

$$CEP = 0.588 \times (\sigma_a + \sigma_b) \tag{5.3}$$

as one means with which to approximate CEP.

Notice in the calculations of CEP that the effects of the missile traversing through the atmosphere and higher-order gravity were neglected. The CEP thus represents a somewhat optimistic value for real-life scenarios. However, for the purposes of this thesis the calculations of CEP provide an excellent means with which to compare the relative value of using one selection algorithm versus another.

5.3 "Traditional" and "Advanced" Cases Analyzed

Three locations along the ballistic missile's trajectory (described in section 3.2) were used to represent the "traditional" and "advanced" scenarios. Location A models the "traditional" scenario. GPS measurements are taken for 100 s immediately after burnout of the final main stage. This is assumed to begin at an altitude of one million feet.

The second and third locations, B and C, represent "advanced" scenario cases. As discussed in section 3.3.2, it is assumed that the free-fall phase prior to the use of GPS will contain residual thrusting errors from the final main stage. Location B was chosen to begin at the apogee of the trajectory, or roughly 8.9 million ft. Location C was chosen such that 100 s remained before impact with the atmosphere. This led to an altitude of 1.9 million feet for the start of GPS measurements. In both of the "advanced" scenarios residual thrusting occurred from the start of the simulation, an altitude of one million feet. These three locations are depicted in Figure 5.1.

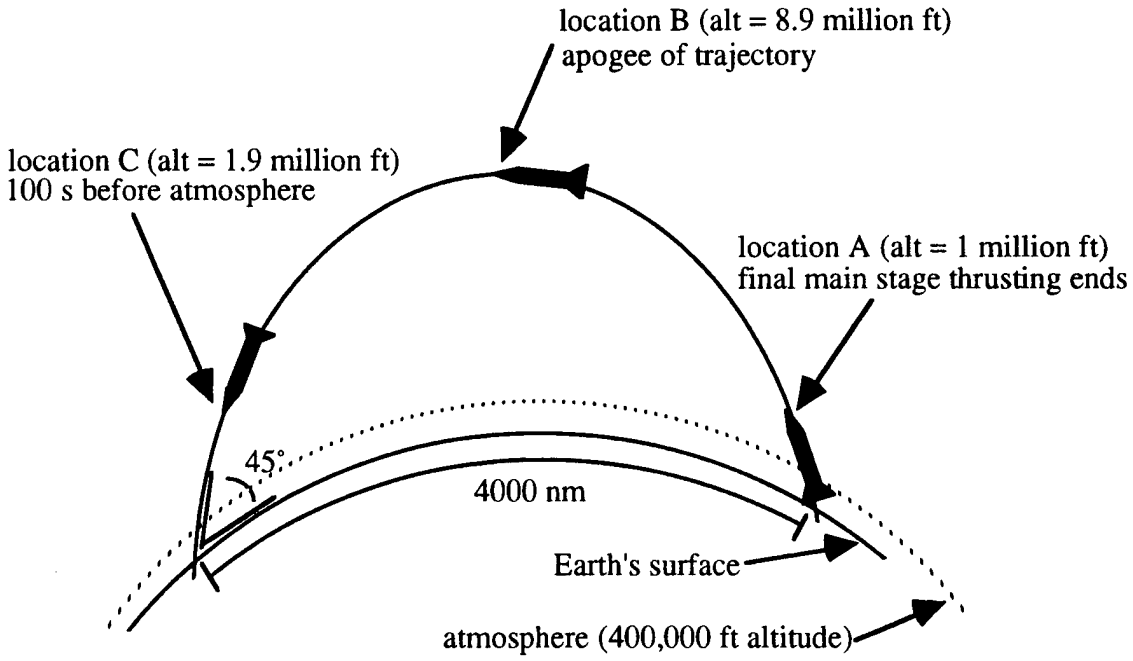

Figure 5.1 The Three Missile Locations (Viewed Down From North Pole)

The three locations were spread over the trajectory for two primary reasons. First, the spread among locations B and C emphasizes the potential effects of errors from residual thrusting and higher-order gravity prior to the start of GPS measurements. The longer the ballistic missile coasts, the more time these effects have to play into position and velocity uncertainties. This then increases the covariance matrix at the beginning of the GPS measurements for these locations. The second reason for dispersing the locations among the trajectory was to emphasize the effects of orbital mechanics on CEP. The farther the GPS measurement phase from the impact point the more time for conic gravity to spread the vehicle's error ellipsoid, increasing the CEP at impact.

The three locations were also rotated such that the same GPS constellation was available to them. Except for altitude differences, this presented the ballistic missile with the same GPS satellite geometry at locations A, B, and C. Because the results for the simulations represent only a single sample, one trajectory at one point in time, this helped to make the cases more comparable.

5.4 The Baseline Input Deck

The baseline input deck consists of the simulation values and other conditions assumed to represent the nominal ballistic missile scenario. This next section describes this input deck; including the states to be "considered out", the initial covariance matrix, and additional values in the covariance analysis simulations.

5.4.1 Consider States

Consider states are those states in the environment model assumed to be excluded from the on-board system. The other states in the suboptimal system are those that would eventually be contained in the on-board navigation filter. As discussed in section 4.2.3, consider states would be created by zeroing out the respective components of the optimal weighting vector, $\mathbf{w}_m$, forming the suboptimal gain, $\tilde{\mathbf{w}}_m$, to be used in (4.8).

The results from the simulations would then represent the theoretical best that the on-board filter could possibly achieve.

For the baseline simulations it was assumed that the only consider states were for residual thrusting. These then represent environmental states not present in the missile's navigation filter.

Estimating all of the pseudorange bias states creates a rather large filter to be carried by an on-board navigation system (17 states + 24 states for the biases). This could create computational problems due to the sheer size of the filter. However, in a real application the number of pseudorange bias states could be limited to the number of satellites used in the selection algorithm. In this fashion a selection algorithm using the best four would only need to carry four additional pseudorange bias states. Likewise, for an all-in-view receiver the maximum number of visible satellites could be precomputed and the appropriate number of states carried in the filter. The only drawback to this method would be a situation in which a satellite was used, then dropped, then used again. Information about the pseudorange errors developed during the first use would be lost the second time around. However, the probability of a satellite being brought back into the navigation solution is extremely small.

5.4.2 Initial Covariance Matrix

The state errors modeled as first-order Markov processes were set to their steady-state values for the initial conditions. This starts the ballistic missile at a worst case situation, a conservative measure. The other state errors were set to values representative of what a missile might possess at the completion of burnout. The initial covariance matrix is summarized in Table 5.1 (see next page).

Table 5.1 Initial Covariance Matrix for Simulations

STATE ERROR	INITIAL 1 σ VALUE	COMMENTS
position	2000 ft	
velocity	2 ft/s	
attitude	50 arcsec	
attitude rate	0.02 arcsec/s	Markov steady-state value
accelerometer bias	10 micro g's	Markov steady-state value
user clock offset	10^{-6} s	
user clock offset rate	5×10^{-10} s/s	Markov steady-state value
pseudorange bias	11.15 ft	Markov steady-state value
residual thrusting	10 micro g's	

5.4.3 Additional Inputs

Additional baseline simulation inputs, discussed in earlier portions of the thesis, are recapped in this section. First, the pseudorange and integrated Doppler measurement noises were set to 1.8 m and 0.02 m/s, respectively. Next, it was assumed that the bus would be thrusting at 0.1 g along the velocity vector during the 100 s of GPS measurements. The thrusting allows for the bus to properly position itself for the deployment of the r.b.'s. The deployments could occur at any time during the 100 s. Finally, for the "advanced" scenarios, locations B and C, it was assumed that residual thrusting would be present at 10 micro g's in each of the inertial directions. This would continue from the start of the simulations, an altitude of one million feet, to the beginning of GPS measurements.

5.5 Baseline Navigation Results

The baseline navigation cases used the input deck described in Section 5.4 at locations A, B, and C. At each of these locations the performance of the missile using various selection methods was analyzed. The navigation performance of four, five, and all-in-view GPS receivers were analyzed in terms of the missile's CEP.

Best 4

The first set of baseline cases represented the performance of the missile using the four satellites giving the best GDOP. The satellites used at each location and their times of use, as well as the average GDOP are given in Table 5.2. Notice that at locations A and B the receiver stayed with the same set of four satellites during the entire 100 s. On the other hand, at location C the receiver found a better set at 94 s. Location B's GDOP was the best, as might be expected from the highest altitude in the trajectory. This gave the missile the most visibility of the GPS constellation.

Table 5.2 Baseline Best 4: GPS S/C Used and Average GDOP

LOCATION	GPS S/C USED AND WHEN	AVERAGE GDOP
A	4-8-11-13 @ start	1.768
B	1-5-7-15 @ start	1.625
C	4-8-11-13 @ start 2-8-11-22 @ 94 s	1.790

Appendix A gives a time history of the state uncertainties during the 100 s of measurements at location A. Locations B and C are not shown since they produce similar results. The first page of Appendix A describes the position and velocity error standard deviations in LVLH coordinates. The position uncertainties approached 2.5 to 4 m, 1σ. These quickly reached a steady-state value, being held up by the inability of a

four satellite receiver to estimate the pseudorange biases. On the other hand, the velocity uncertainties continued to improve, reaching a 1σ of roughly 0.003 m/s at the end of the measurement interval. Notice how quickly the use of GPS brought down the uncertainties in these values; they started at σ's of 2000 ft and 2 ft/s.

The next page of Appendix A describes the uncertainties in the attitude (platform misalignment) and attitude rates (platform drift) of the IMU. As expected, some attitude error information was gained during the interval due to the small amount of deployment thrusting along the velocity vector. Two of the Euler angle errors, the J and K axes, were reduced to 1σ's of 25 arcsec. Notice that very little improvement was seen in the I axis since the velocity vector was primarily in that direction for location A. Additionally, essentially no improvement in the attitude rate errors was seen. It takes larger attitude rate uncertainties, greater thrusting, or more time to estimate these states.

The third page of Appendix A describes the accelerometer bias and clock error uncertainties. Like the attitude states, a small amount of accelerometer error improvement was obtained during the measurement phase. The last two plots on this page describe the range and velocity equivalents of the clock offset and clock offset rate errors, respectively. The range uncertainty of the clock offset error reached just below 2 m, 1σ. The velocity equivalent of the clock offset rate error also improved dramatically, reaching a 1σ of 0.003 m/s.

The last two pages of Appendix A describe the pseudorange bias error uncertainties to each of the 24 satellites. Table 5.2 states that GPS satellites 4, 8, 11, and 13 were used during the entire measurement interval at location A. These plots show that the use of only four satellites in the selection algorithm was not enough to estimate the pseudorange bias errors to the satellites.

Figure 5.2 summarizes the performance of the ballistic missile using the best four satellites in terms of CEP. CEP is calculated every second during the 100 s interval of

measurements, for each of the three locations. Recall that it was assumed that the re-entry bodies could be deployed at any time during this phase.

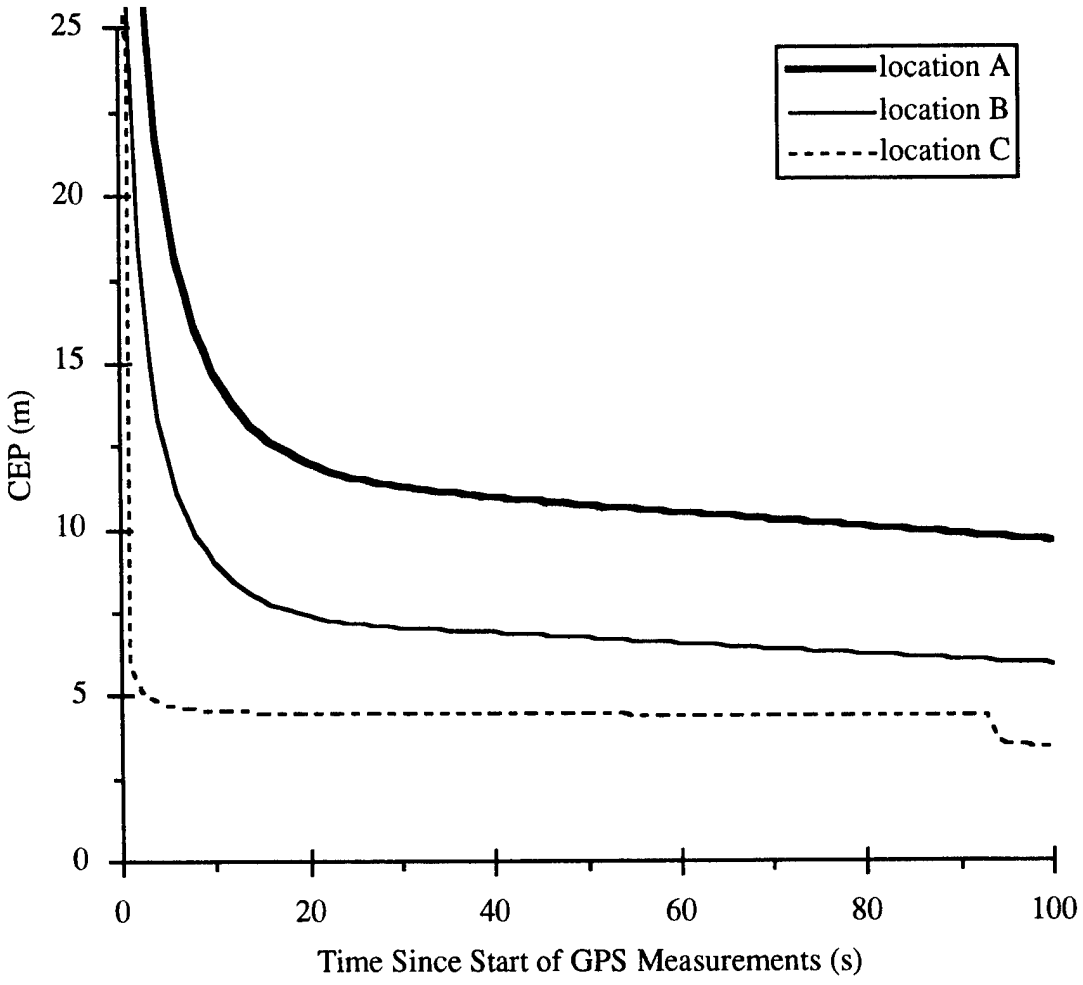

Figure 5.2 Baseline Best 4: CEP vs. Measurement Time

These CEP's reveal excellent performance for the ballistic missile. During the 100 s each of the locations provided CEP's below 12 m. The sudden improvement in location C's CEP at the end of the interval was a result of the missile using a new set of satellites at 94 s. However, it should again be emphasized that the effects of higher-order gravity and the atmosphere were neglected in the CEP calculations. Additionally, the r.b.'s were assumed to be deployed perfectly. The above graph thus gives a

representation of the pure navigational capabilities of a ballistic missile using GPS in terms of CEP.

Figure 5.2 also shows that the CEP's improved the closer the ballistic missile deployment was to the target point. This was in despite the fact that the initial covariance matrix for location C was the largest due to residual thrusting and higher-order gravity prior to the GPS measurements. The initial CEP's reflected this difference, but with only one set of GPS measurements these differences were eliminated. CEP's were smallest for the locations nearest to the target because orbital dynamics had less time to increase the uncertainties in the free-fall phase. In fact, the farther from the target the more sensitive CEP is to velocity errors in the orbit.

This phenomenon is shown in Tables 5.3. Each of these tables describe the sensitivity of uncertainties in the missile's position, velocity, and time states, to position uncertainties at impact. These are the Φ matrices, (5.1), for each of the three locations. The elements subscripted "0" are the uncertainties at the start of the 100 s measurement phase for the missile. The elements subscripted "f" are the LVLH position uncertainties at impact. The position covariance matrix at impact is eventually used to calculate the CEP. Location A, the farthest distance from the target, was the most sensitive to velocity uncertainties. Velocity uncertainties at this point resulted in large LVLH position uncertainties at impact. This caused location A to have the highest plot in Figure 5.2. Likewise, locations B and C were closer and thus less sensitive to velocity uncertainties. Note that the vertical position uncertainties at impact had zero sensitivities with all of the initial uncertainties since the error ellipsoid had been flattened out for CEP calculations.

Also notice that the effects of position errors in the orbit were negligible in terms of CEP. Time was also minimal in its contribution to impact errors since the clock offset of the missile was estimated on the order of 10^{-9}, 1 σ (Appendix A). Thus, the driving factor for the calculations of CEP was the size of the velocity errors and the

distance from the target. The farther from the target, the more accurate velocity needs to be known in order to maintain a certain level of CEP.

Tables 5.3 Transition (Sensitivity) Matrices for Locations A, B, and C

Location A	Δt_o	Δr_{DRo}	Δr_{VERo}	Δr_{CTo}	Δv_{DRo}	Δv_{VERo}	Δv_{CTo}
Δr_{DRf}	-329	-0.132	1.900	0.0	2475	875	0.0
Δr_{VERf}	0.0	0.0	0.0	0.0	0.0	0.0	0.0
Δr_{CTf}	275	0.050	0.335	-0.411	165	230	1205

Location B	Δt_o	Δr_{DRo}	Δr_{VERo}	Δr_{CTo}	Δv_{DRo}	Δv_{VERo}	Δv_{CTo}
Δr_{DRf}	-329	0.935	0.871	0.0	1465	609	0.0
Δr_{VERf}	0.0	0.0	0.0	0.0	0.0	0.0	0.0
Δr_{CTf}	328	0.036	0.120	0.586	47	94	1003

Location C	Δt_o	Δr_{DRo}	Δr_{VERo}	Δr_{CTo}	Δv_{DRo}	Δv_{VERo}	Δv_{CTo}
Δr_{DRf}	-329	1.069	0.859	0.0	135	106	0.0
Δr_{VERf}	0.0	0.0	0.0	0.0	0.0	0.0	0.0
Δr_{CTf}	297	0.005	0.061	0.990	0.667	7	125

Best 5

The next set of baseline cases represented those for a ballistic missile using the best set of five satellites. Table 5.4 (see next page) shows the satellites used and the average GDOP for each of the locations. In all three locations the missile switched the set of best five satellites at some point during the 100 s interval.

In Appendix B the state uncertainties for location A are shown. As with the best 4 cases, the uncertainties in the missile's states were similar for locations B and C, and therefore only location A is shown. Notice that there was a slight improvement in the missile's knowledge of position and velocity errors when one more satellite was used in the solution. The attitude, accelerometer, and clock state errors did not show any significant improvements in performance. On the other hand, the use of five satellites resulted in some pseudorange bias error information to be obtained. The last two pages

of Appendix B show that the pseudorange bias errors were reduced to as low as 2.25 m for satellites number 20 and 22. This bias estimation then directly helped in the reduction of the position uncertainties.

Also notice that when the satellite selection algorithm switched to a new set of spacecraft there was a distinct improvement in the states' uncertainties. This was a result of the new set offering a different geometry to the ballistic missile, helping to "beat down" its error ellipsoid in new directions.

Table 5.4 Baseline Best 5: GPS S/C Used and Average GDOP

LOCATION	GPS S/C USED AND WHEN	AVERAGE GDOP
A	1-8-11-22-23 @ start 1-4-8-11-20 @ 55 s	1.535
B	7-8-12-14-23 @ start 2-7-8-12-13 @ 53 s	1.445
C	1-4-8-11-20 @ start 1-8-11-22-23 @ 7 s	1.577

Figure 5.3 provides the performance of the missile in terms of CEP for each of the three locations. Like the best 4 cases, notice that location C offered the best CEP performance, while location A provided the worst. Again, the longer the free-fall portion of the trajectory, the more time for velocity errors to enlarge the potential impact region.

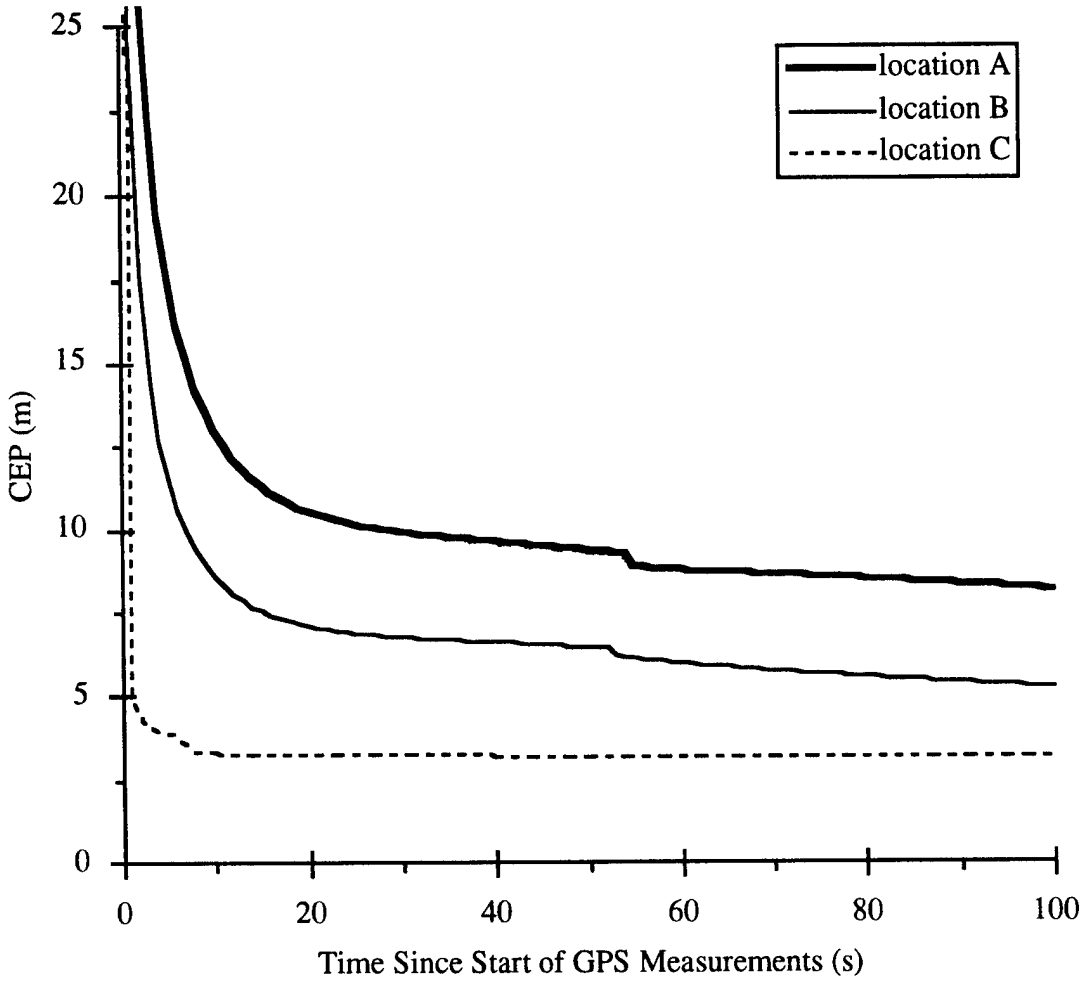

Figure 5.3 Baseline Best 5: CEP vs. Measurement Time

All-In-View

The final set of baseline cases were for a missile using all satellites in view. Table 5.5 (see next page) shows that as many as 19 satellites were used at the highest altitude (location B). The GDOP's associated with the all-in-view cases were significantly reduced from that of using only four or five satellites (Tables 5.3 and 5.4).

Table 5.5 Baseline All-In-View: GPS S/C Used and Average GDOP

LOCATION	GPS S/C USED AND WHEN	AVERAGE GDOP
A	1-2-4-8-10-11-13-14-15-17-22-23-24 @ start add 20 @ 55 s	1.012
B	1-2-4-5-7-8-10-11-12-13-14-15-17-18-20-21-22-23-24 @ start	0.765
C	1-2-4-8-10-11-13-14-15-17-20-22-23-24 @ start drop 20 @ 7 s drop 4 @ 94 s	1.071

Appendix C shows the results of the missile's states using an all-in-view receiver at location A. The uncertainties in each of the states was reduced from that of the four or five best satellite cases. The position and velocity error uncertainties were reduced to 1σ's of roughly 1.3 m and 0.002 m/s, respectively. There was only a slight improvement in attitude error knowledge, and still no estimation of attitude rate errors. However, the clock offset was reduced to approximately 1.0 m, and the clock offset rate to 0.002 m/s. Finally, there was a significant enhancement in the estimation of the pseudorange bias errors. Several of the satellites' biases were reduced to 1σ values as low as 1.5 m.

Figure 5.4 depicts the CEP performance of the all-in-view receiver at the three locations. Notice, like the four and five satellite selection results, that location C provided the best performance.

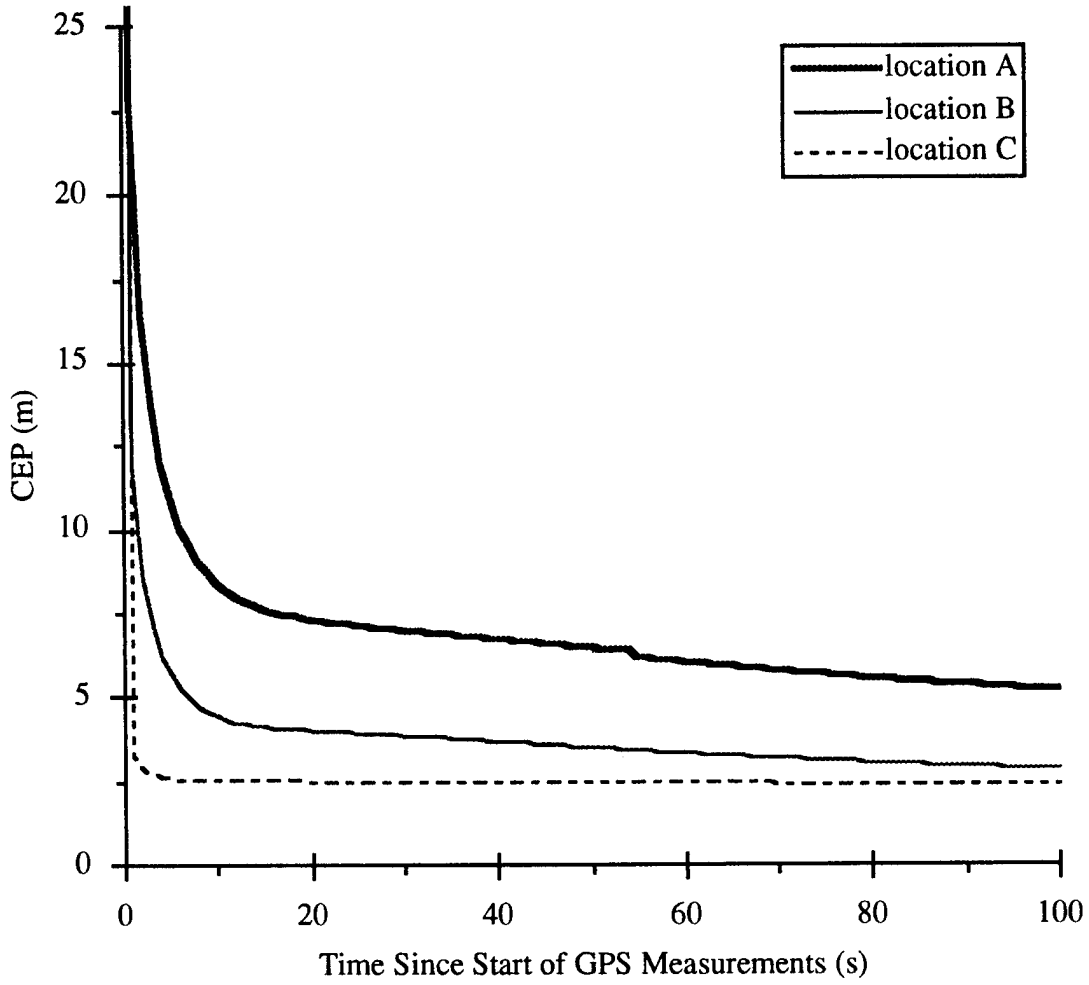

Figure 5.4 Baseline All-In-View: CEP vs. Measurement Time

Comparison of the Best 4, Best 5, and All-In-View Selection Algorithms

One of the questions posed by this thesis is to determine the amount of navigation performance enhancement provided by an all-in-view receiver. Using the information from Figures 5.2 through 5.4 it was possible to quantify this improvement in terms of CEP. The percentage improvement in CEP for a ballistic missile using all-in-view GPS versus the best four satellites is shown in Figure 5.5 on the following page.

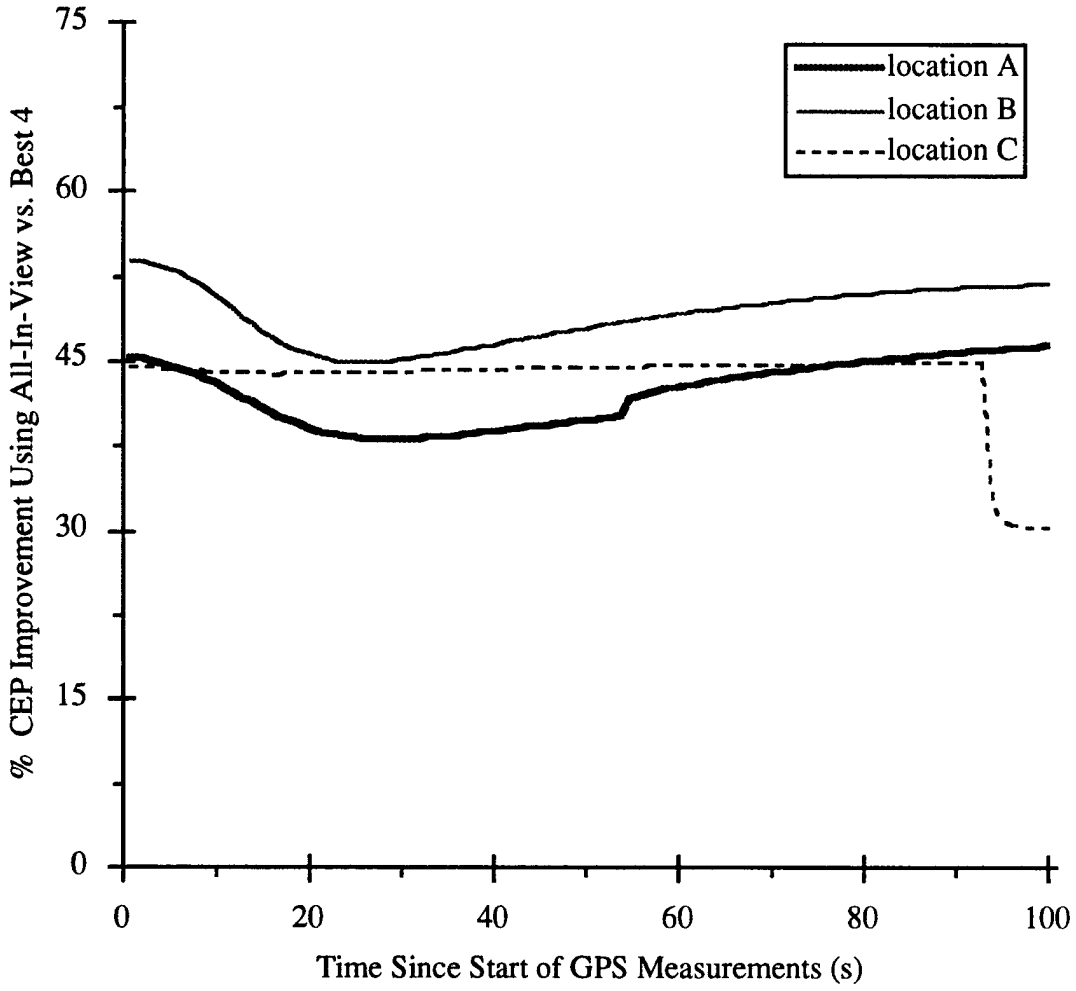

Figure 5.5 Improvement in CEP Using All-In-View vs. Best 4

This data shows that a ballistic missile user could expect to achieve approximately a 45 % (an average of the methods) improvement in CEP with an all-in-view receiver, instead of using only the best four satellites. The location of the missile did not significantly alter this improvement, although location B provided the best CEP's. Location B provides the best improvement because the altitude (apogee) allows the all-in-view receiver to use more satellites than in any other location.

Figure 5.6 shows the CEP enhancement of an all-in-view receiver versus a best five user. Again, with all-in-view a ballistic missile can expect significant navigation performance enhancements, roughly 35 % in this case.

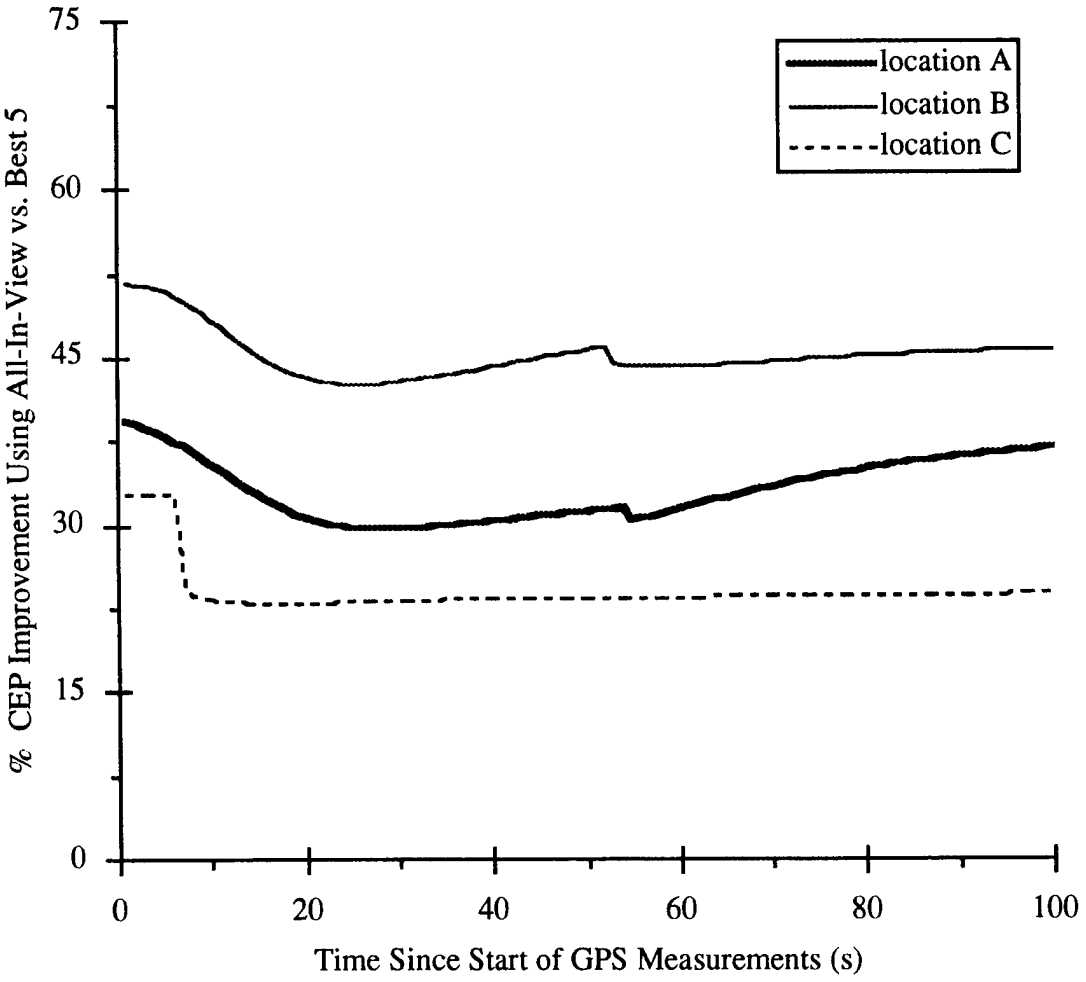

Figure 5.6 Improvement in CEP Using All-In-View vs. Best 5

5.6 Non-Baseline Cases and Navigation Results

In addition to the baseline cases, several other simulations were run with slight variations. These non-baseline cases are presented in the following sections.

5.6.1 No Integrated Doppler Measurements

The first non-baseline case analyzed a ballistic missile's performance without the incorporation of integrated Doppler measurements. In general, it was discovered that the position uncertainties of the ballistic missile were not affected by the lack of

velocity measurements. On the other hand, the velocity uncertainties were reduced at a much slower rate than when Doppler was used. However, it was found that over a long period of time (roughly 5 minutes) the steady-state velocity uncertainties came very close to the cases when Doppler was taken.

The result of the velocity uncertainties being estimated at a much slower rate was to dramatically increase the CEP during the 100 s measurement intervals. The CEP's for each of the selection methods, without velocity measurements being taken, is shown in Figure 5.7.

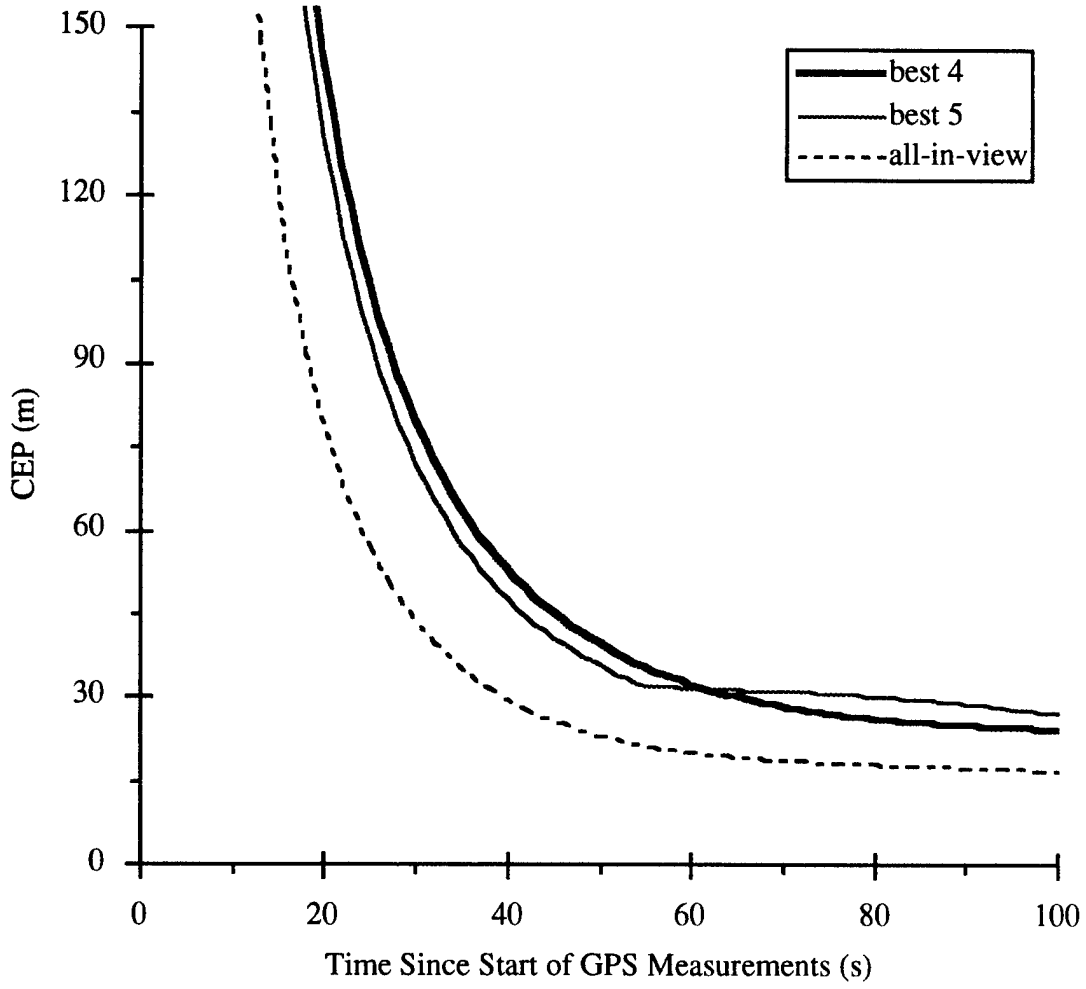

Figure 5.7 Non-Baseline at Location A: No Doppler Measurements

These curves show roughly a factor of three increase in CEP when Doppler measurements are not taken. Also notice that at 55 s the five satellite selection method shows a dramatic change in the CEP plot. This worsening of the CEP curve was a result of the selection method dropping two satellites, numbers 22 and 23, and replacing them with two others, numbers 4 and 20. Although these two new satellites provided a better geometry, they also contributed two new pseudorange bias states (no correlations had been built with these and the other states). These new biases did not affect the position states because even though there were no correlations with the biases, the new geometry was valuable for pseudorange measurements. Yet, with the velocity states the new geometry did not help because Doppler was not being taken. Although, notice towards the latter portion of the plot, when correlations began to build, that the reduction rate of the CEP began to increase.

5.6.2 Deployment Velocity Errors

The CEP calculations in the baseline cases assumed that the r.b.'s were deployed perfectly from the bus. In practice it is impossible to eject these bodies onto their appropriate trajectories with absolute precision. In fact, significant velocity uncertainties are usually given to these bodies through the deployment mechanism, thus increasing CEP.

Two deployment velocity scenarios were run to emphasize the effects of these errors. The first case assumed 1/20 m/s, 1 σ, deployment velocity uncertainties in each of the three orthogonal directions. This spherical distribution was added to the missile's covariance matrix prior to the calculation of CEP. Thus, the only difference between this non-baseline case and the baseline ones was the addition of the velocity errors into the covariance matrix prior to CEP calculation. Figure 5.8 (see next page) shows the performance of the missile using all-in-view at each of the three locations with the deployment velocity errors.

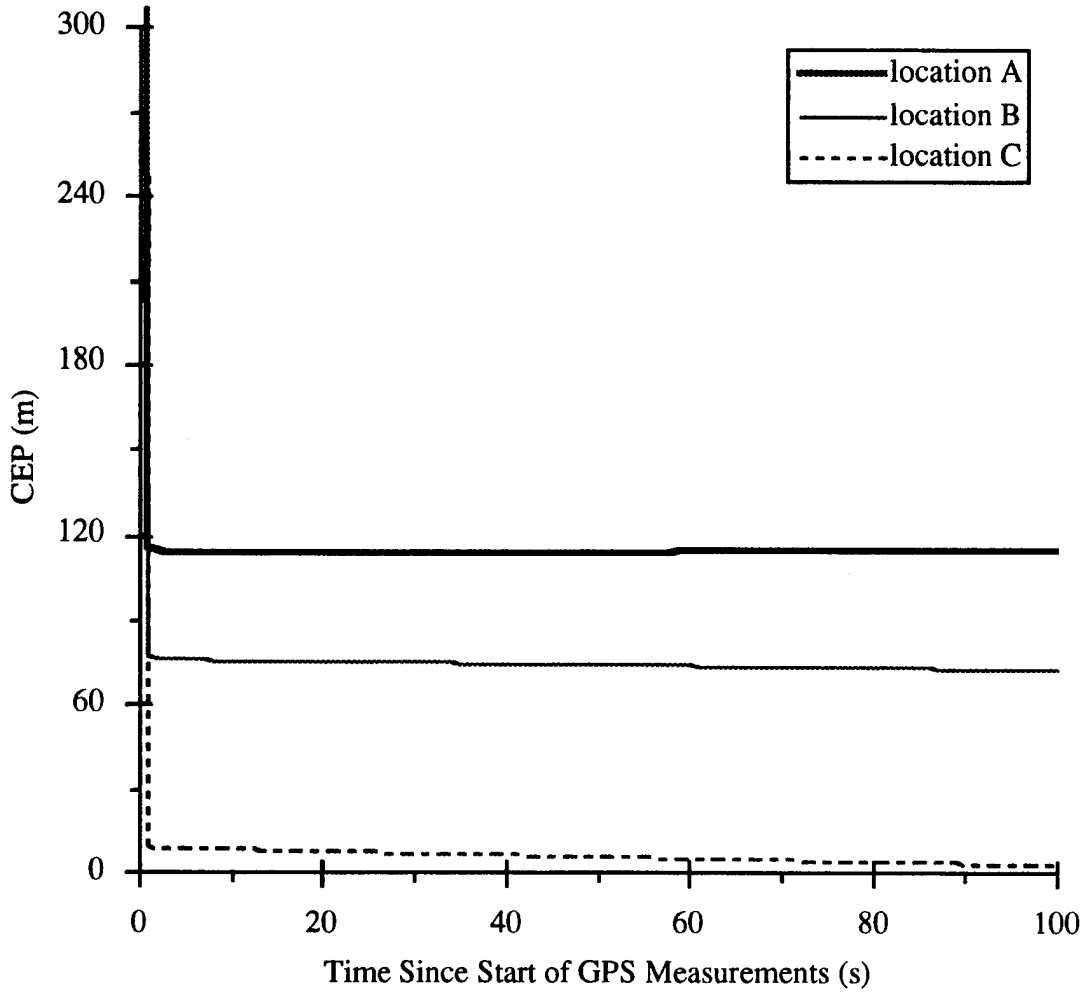

Figure 5.8 Non-Baseline All-In-View: 1/20 m/s Deployment Velocity Uncertainties

The plots clearly show that the farther the missile was from the target the more effect the deployment velocity errors had on the size of CEP. This is again a result of the sensitivity of velocity errors in the orbit to impact CEP. It is thus better to deploy the r.b.'s late in the trajectory.

It should also be noted that the size of the deployment velocity errors essentially "swamped out" the contributions made by the accuracy of GPS. The 1/20 m/s velocity uncertainties from deployment clearly dominated those remaining after taking the GPS measurements, roughly 0.003 m/s.

The second case of deployment velocity errors used 1/10 m/s, 1 σ errors. As expected, the plots in Figure 5.9 reveal even larger CEP's. Clearly, the deployment velocity errors of the missile were the driving factor in its ultimate impact accuracy.

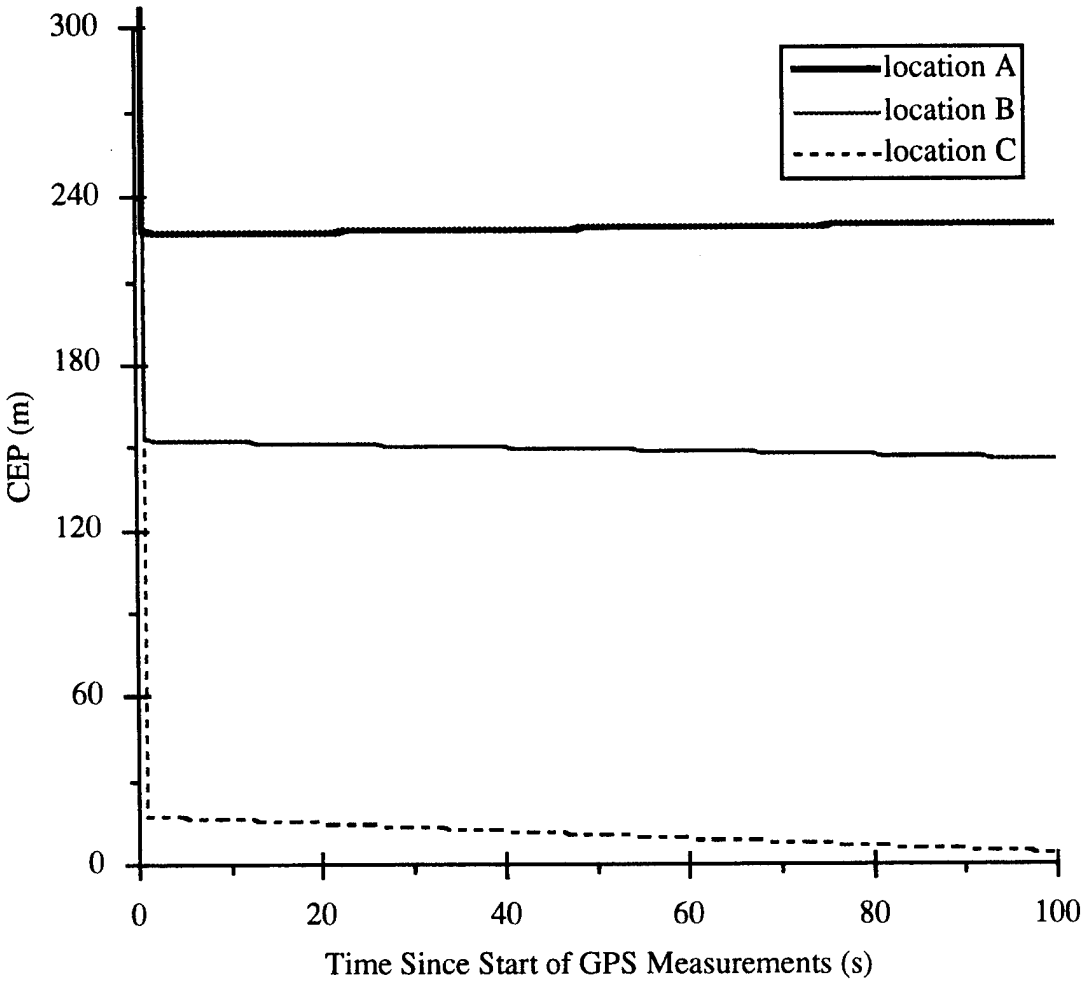

Figure 5.9 Non-Baseline All-In-View: 1/10 m/s Deployment Velocity Uncertainties

5.6.3 Pseudorange Bias States Considered

The next non-baseline case measured the degradation in CEP when the pseudorange bias states to the GPS satellites were considered. That is, these biases were not estimated in the filter. Figure 5.10 (see next page) shows the CEP at location A for each selection method.

Comparing these plots to those when the states were considered (location A of Figures 5.2, 5.3, and 5.4) shows a negligible degradation in CEP. The reasons for this are twofold. First, a measurable improvement in the uncertainties in these biases was seen only when using the five and all-in-view selection methods. The more satellites used in the solution, the better these estimates became. Secondly, even with the pseudorange bias improvements the velocity error uncertainties were unaffected, the driving factor in determining CEP. Instead, only the position states were slightly improved. This is a result of the direct link between the biases and the position states made by the pseudorange measurements.

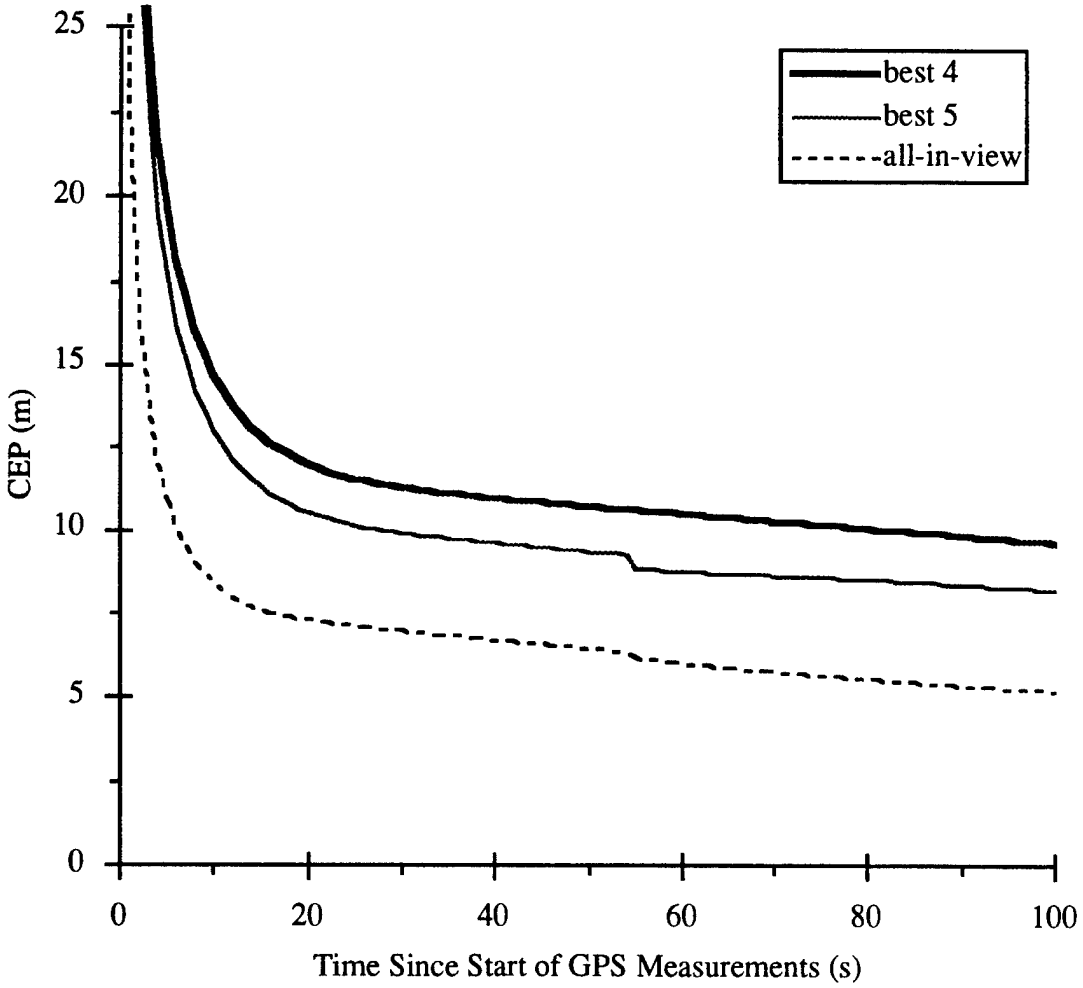

Figure 5.10 Non-Baseline at Location A: Pseudorange Bias States Considered

Even though it appears as if there is no need to include the pseudorange bias states in an on-board system, their use could become important to integrity monitoring. This will be addressed in Chapters 6 and 7.

5.6.4 Quick 4 Selection Method

The final non-baseline case used Soltz' quick four selection method (presented in Section 2.6.2) at the three different locations. The satellites chosen for this method versus the best four are given in Table 5.6.

Table 5.6 Non-Baseline Quick 4: GPS S/C Used (Quick vs. Best 4)

LOCATION	GPS S/C AND WHEN (QUICK 4)	GPS S/C AND WHEN (BEST 4)
A	2-8-11-22 @ start 1-8-11-22 @ 25 s	4-8-11-13 @ start
B	8-18-22-23 @ start 8-12-14-22 @ 52 s	1-5-7-15 @ start
C	8-11-14-22 @ start 2-8-11-22 @ 2 s 1-8-11-22 @ 3 s	4-8-11-13 @ start 2-8-11-22 @ 94 s

The different choices of satellites resulted in average GDOP's less than, but still close, to that of the best four method. The differences in the precisions are shown on the following page in Table 5.7.

As expected, the position uncertainties of the missile were worse with the quick four method. This reflects the fact that GDOP tends to choose the satellites that will most reduce the user's position uncertainties. However, the results shown in Figure 5.11 on the following page reveal that for certain times at each of the locations the CEP's were better using the quick method. This directly reflects the fact that to choose

satellites based solely upon GDOP is not always the best choice for certain applications. More specifically, if CEP were truly the evaluation criterion then the four satellites giving the best CEP could have been used.

Table 5.7 Non-Baseline Quick 4: Average GDOP (Quick vs. Best 4)

LOCATION	AVERAGE GDOP (QUICK 4)	AVERAGE GDOP (BEST 4)
A	1.931	1.768
B	1.732	1.625
C	1.991	1.790

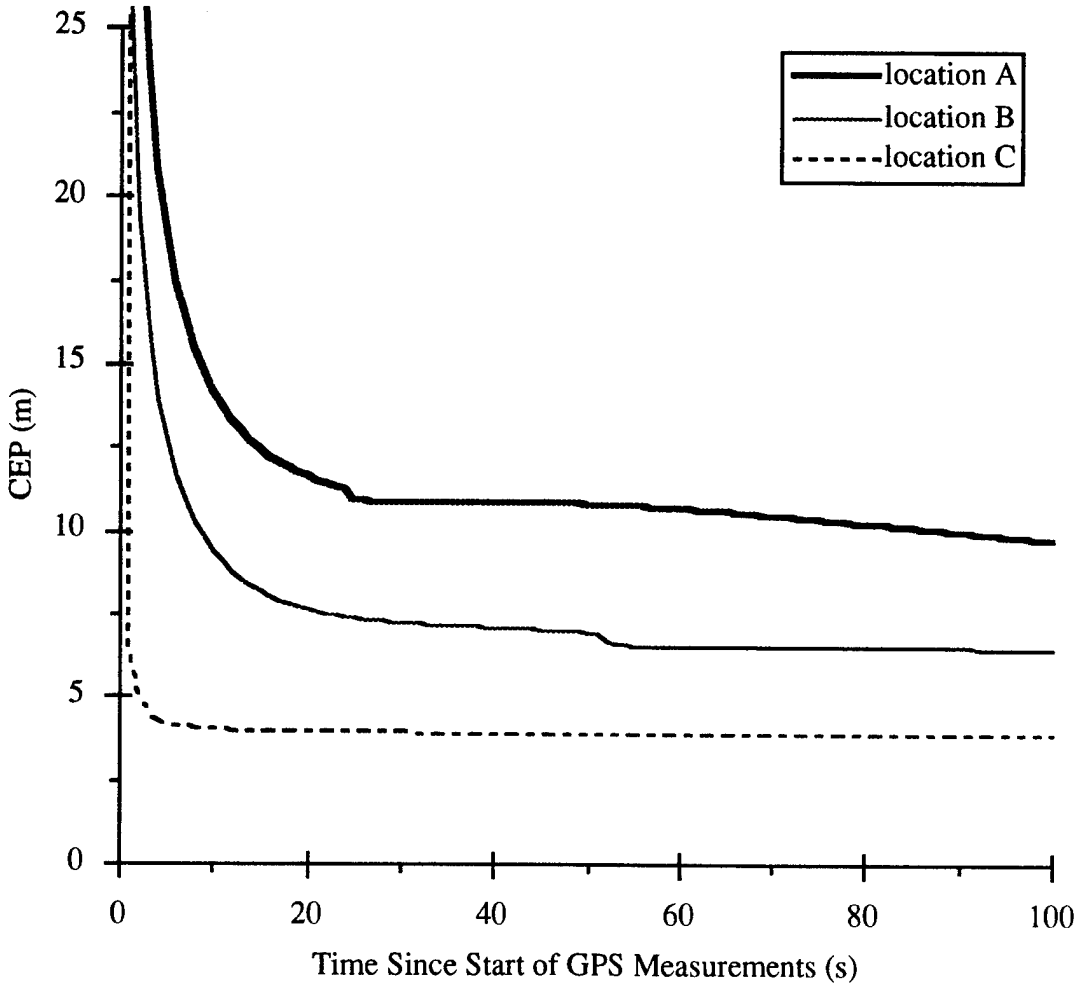

Figure 5.11 Non-Baseline Quick 4: CEP vs. Measurement Time

CHAPTER 6

THE INTEGRITY MONITORING ISSUE

6.1 Introduction

Chapters 6 and 7 are devoted to the integrity monitoring aspect of the thesis. In this first chapter integrity monitoring is presented, with discussion of its background as well as a description of several popular schemes. The last section then details the integrity monitoring approach taken in this thesis.

6.2 Why the Integrity Concern?

The integrity of GPS signals has become a focus of concern among the user community. This is a direct result of the rapid growth in the system's popularity. Its wide-spread use has caused an increased number of individuals and applications to become overly dependent on its accuracy. As the user population continues to grow, detecting a failure in the system has become even more critical.

This is especially true among the military community. The success of GPS in the Persian Gulf Conflict and in high dynamic applications, like fighter aircraft, has contributed to a call for its incorporation into unmanned uses, like missiles. In such scenarios the integrity of GPS is critical to the success of the mission. A flawed satellite left undetected would not only result in the intended target being missed, but would also jeopardize the lives and property of nearby persons.

Even though extensive built-in features and operating procedures have been included in GPS to ensure the integrity of the signals, these measures are not foolproof. For example, such safety precautions as equipment redundancy, communication error detection codes, estimation and prediction consistency checks, and operator

qualification verification could not avert a problem in March of 1993 [16]. In this incident the Master Control Station (MCS) actually induced an error into GPS because of a problem with the Kalman Filter monitoring the satellite. Accuracies were significantly affected for the several days it took for this particular incident to be detected and fixed. During this period significant accuracy problems were seen on Earth [15].

Typically, the biggest problem area lies in the performance of the GPS satellites' atomic clocks. The clocks have the greatest probability of failure. Of particular concern is the detection of a satellite whose clock degrades slowly enough such that measurements to the vehicle are still incorporated into the user's navigation solution. If there was a large and sudden error in the clock, the measurement residual to this satellite would most likely fall out of a threshold range set by the user. Yet, a slowly drifting clock could carry the solution along with it (further discussed in Section 6.3.3) [17].

As evidenced in the March 1993 incident, a significant period of time is needed by the control segment to detect and correct a flawed satellite. At a minimum, a 15 to 20 minute delay exists between an anomaly occurrence and the earliest detection by the ground. It then takes at least one more hour to process the correction and send it to the bad satellite [16]. Only after this period of time, about an hour and 20 minutes, would the satellite be able to broadcast its current status to the user community. The problem would usually be identified to users via the satellite's health bit or User Range Accuracy (URA). However, during this large portion of time users could still be relying on the bad satellite for accurate navigation information, producing potentially disastrous results.

6.3 Integrity Monitoring History and Techniques

Integrity monitoring for GPS has been an issue since the early 1980's. Since that time numerous schemes have been proposed to ensure the integrity of the signals from the satellites. This next section describes its historical development and briefly introduces some of the primary schemes.

6.3.1 Historical Development

Integrity problems relating to the use of GPS first became an issue in the early 1980's. Since that time the direction of integrity monitoring has primarily been guided by the Radio Technical Commission for Aeronautics (RTCA) [16]. This body has acted to establish guidelines and minimum operational performance standards for the development of integrity algorithms. Integrity has been defined as the ability of a system to provide timely warnings to users when GPS should not be used for navigation [16]. Although their focus has generally been limited to providing integrity for the civil aviation arena, the stringent requirements of the FAA has made their work applicable in many other areas.

The RTCA has proposed the development of the GPS Integrity Channel (GIC) as the primary means with which to analyze the quality of the GPS signals. The GIC is a ground-based GPS monitoring system used to track the GPS signals and monitor the satellites for errors. If errors are detected in the constellation this information would then be disseminated by a master control station to GPS users. It has been determined that the use of such a system would allow for early and accurate detection of a flawed satellite. Studies are still being conducted by working groups to determine the best means with which to disseminate the information to GPS users, with both ground-based and satellite communication links being analyzed [16]. The entire GIC concept is still a few years away [14].

In the interim, some form of self-contained integrity monitoring needs to be undertaken by users of the system concerned about the accuracy of the signals. This self-contained checking is typically referred to as Receiver Autonomous Integrity Monitoring (RAIM). In the use of RAIM the user is not dependent on any external communication links to determine the integrity of the GPS signals. Instead, errors are detected solely by algorithms carried by the user. Even with the eventual activation of the GIC, the RTCA has stated that there are good reasons for the continued use of RAIM [14].

Over the past several years many RAIM schemes have been suggested. Each of them falls into one of two primary categories: "snapshot" techniques or Kalman Filter approaches.

6.3.2 "Snapshot" Techniques

"Snapshot" integrity monitoring techniques make use of redundant measurements from the GPS satellites at any given point in time. From the redundancy of the measurements the user is able to determine a failure in the system [14]. "Snapshot" schemes have the advantage of not being dependent on any assumptions with regard to how the user got to their present state [18]. However, the lack of this past information can degrade the performance of the scheme, and also makes the user heavily dependent on the ability to gather numerous measurements.

If there is an abundance of measurements the user might not only be able to "detect" a failure in the system, but also "isolate" the specific satellite going bad. For example, in a two-dimensional problem two noiseless lines of position provide enough information to determine one's position on a plane (where the lines intersect). Now, a redundant or third measurement provides the additional information needed for error detection. More specifically, if all of the lines intersect at one point then there is no failure. Yet, if the crossings are widely separated then a failure has been detected.

However, with three position lines the user only knows there is a failure, but cannot identify which specific satellite is bad. On the other hand, with a fourth measurement the user can "isolate" the position line that is conspicuously inconsistent with the other three [17].

GPS is not quite as simple as the above example, but the general ideas hold true. Since at least four measurements are needed for determining a user's position and clock offset, then five and six satellites are needed for "detection" and "isolation" of a bad satellite, respectively. Matters are also complicated by the fact that noise is inherent in the measurements and S/A can be activated (not a concern for an "authorized" user). Additionally, the user often has high dynamics so the measurements need to be simultaneous. [17].

Three popular "snapshot" schemes have been proposed for GPS integrity monitoring.

Range-Comparison Method

The first "snapshot" solution was developed by Y.C. Lee. Assuming five satellites are visible (with good geometry), the method solves for the user's state using only the first four measurements. Assuming that these measurements were noiseless, the resulting solution could then be used to predict the remaining measurement. If the residual (the difference between the actual and expected) for this fifth measurement was small, then the algorithm would declare "no failure." On the other hand, if the residual was large then the method would have detected a failure in the system. This residual is often termed the "test statistic" [14].

A problem lies in determining the threshold for labeling the residual as being "small" or "large." This is usually developed by considering the ranging accuracies available from GPS, as well as the margin of error needed in the integrity checking. This margin of error is often termed alarm rates, and is defined as the maximum number of reported failures when the system is performing properly [14].

Least-Squares-Residuals Method

The second "snapshot" scheme was developed by B.W. Parkinson and P.A. Axelrad [14]. Assuming that there are five satellites in view gives five equations and four unknowns. This overdetermined case can be solved in a least-squares sense. The least-squares solution can then be used to predict the five measurements, and five residuals can be formed in a similar manner to the range-comparison method [14].

These five residuals can then be grouped together to form a 5x1 vector, **w**. The sum of the squares of the residuals plays the role of the basic observable in this RAIM method. Specifically,

$$S = \mathbf{w}^T\mathbf{w} \tag{6.1}$$

This non-negative scalar quantity, S, has an un-normalized chi-square distribution with only one degree of freedom, not five degrees as one might first expect (provided that the measurement noises are independent zero-mean Gaussian random variables with the same variances). The final step involves determining the threshold for S. This boundary determines whether a failure in the system can be declared and is generally found in a fashion similar to that of the range-comparison method [14].

Parity Method

The final "snapshot" method, proposed by M.A. Sturza and A.K. Brown, is more formal and heuristic than the other two methods [14]. In this method a parity vector is formed, which is ultimately used as the test statistic. This scheme will not be discussed in detail because the results of this method are identical to that of the least-squares-residuals method.

Equivalence of the Three "Snapshot" Methods

As revealed in the description of the parity method, this last scheme produces identical results to that of the least-squares-residuals method. Moreover, the range-comparison method is also identical to the latter two if equal alarm rates are chosen.

Alarm rates are used as one input into determining the threshold boundaries--the point where a test statistic would be labeled a failure. Thus, with similar alarm rates the three "snapshot" methods produce identical results [14].

6.3.3 A Kalman Filter Approach

Brown and Hwang have proposed another means of integrity monitoring in [17] by using the user's on-board navigation system, typically a Kalman Filter. This is a much more natural scheme than any "snapshot" approach because of the immense amount of redundant information in the presence of a rapidly changing geometry [17]. However, the use of a Kalman Filter also makes the accuracy of the scheme dependent on the validity of the model assumptions [18].

One immediate advantage of the use of a Kalman Filter is the ability to eliminate grossly erroneous measurements. This is a result of the measurement residuals calculated in the filter (the difference between the actual measurements and the expected ones). The expected measurement is determined by using all prior information and is weighted to account for its statistical worth and the geometric situation. The filter also contains the variance of this residual as one of its normal computations. Thus, the statistics of the measurement residual can be used to reject a wild measurement (a satellite having gone grossly bad) [17]. Usually this is set to a predetermined level of $\pm 3\sigma$.

It is therefore possible for a Kalman Filter to detect catastrophic failures in the GPS constellation. However, what if the range measurements to a specific satellite degrade in such a fashion as to not create a measurement residual outside the $\pm 3\sigma$ check? In this case the filter would gradually adjust its solution to accommodate the slowly drifting range measurements to the bad satellite. This would tend to drive the solution from the true value.

The slowly drifting scenarios were the situations addressed in [17]. The approach by Brown and Hwang was to rely on the use of a parallel bank of Kalman Filters, forming a multiple hypothesis tester. This scheme was originally formulated by D.T. Magill and is often termed the Multiple Model Estimation Algorithm (MMEA). In this scheme each of the filters was given different error characteristic for a bad GPS satellite. That is, each filter works on the measurement sequence less some hypothesized failure signal. The resulting sequence of measurement residuals output from these filters could then be compared to the failure model. The filter that closest matches the failure signature would then be selected as the truth model [17].

Brown and Hwang found the Kalman Filter scheme to be extremely promising. Using ramp-type failures they found the scheme was able to detect and isolate the bad satellite with great accuracy. The success rate for detecting a failure in the system was extremely high, and the probability for isolating the bad satellite was also very good with even four and five satellites in the solution. However, it appears that the use of a bank of parallel Kalman Filters could be computationally intensive for an on-board system. Further work has been proposed, involving higher dynamic applications (they just looked at low dynamic aircraft) and failures other than ramps [17].

6.4 All-In-View Integrity Monitoring

One of the questions posed in this thesis is: how does the use of all GPS satellites in view help with integrity monitoring? This will be addressed in this thesis by quantifying the degradation in navigation performance by incorporating a bad satellite into the user's solution. The resulting worsening of performance will then be compared to that of using only the four or five best (in terms of GDOP) satellites. The intent is to show how the use of more satellites can mitigate the effects of only one satellite going bad.

In actuality, this is not truly integrity monitoring. Typically integrity monitoring is thought of as a technique to detect a failure in the satellite constellation. If there was a detected failure then GPS should not be used. Integrity monitoring often can proceed one step further by isolating the satellite that is going bad. If this was the case, then the specific satellite identified as bad would simply be thrown out of the user's solution (if the bad satellite had already degraded the solution then some form of recovery might also be necessary). However, it might also be possible to use the bad satellite in the navigation solution, with only a small degradation in performance. This seems especially feasible for a user with all-in-view capabilities because of the sheer number of measurements that would be received. If this were the case, then the classical forms of integrity monitoring could be discarded (saving complexity and computational burden in the system). This then could be considered a form of integrity monitoring.

For this thesis the bad satellite was modeled with two additional states, creating a 46-state environment filter. The two additional states were satellite clock offset and rate. These would affect both range and range rate measurements to the bad satellite. When pseudorange and integrated Doppler measurements were taken to the bad satellite a one was thus placed in the appropriate components of the sensitivity vectors.

Although these states are termed "clock" errors, their modeling was not limited to what would be expected from clock errors on the GPS satellites, but could be associated with any variety of errors. More specifically, the clock rate was modeled as a first-order Markov process. Since the rate was chosen to drive the offset, then the offset became an integrated Markov process. In the form of the Riccati equation this is

$$\frac{d}{dt}\begin{bmatrix} \sigma^2_{\Delta offset} & \sigma_{\Delta offset,\Delta rate} \\ \sigma_{\Delta rate,\Delta offset} & \sigma^2_{\Delta rate} \end{bmatrix} = \begin{bmatrix} 0 & 1 \\ 0 & \frac{-1}{\tau} \end{bmatrix} \begin{bmatrix} \sigma^2_{\Delta offset} & \sigma_{\Delta offset,\Delta rate} \\ \sigma_{\Delta rate,\Delta offset} & \sigma^2_{\Delta rate} \end{bmatrix} + \mathbf{P}\mathbf{F}^T + \begin{bmatrix} 0 & 0 \\ 0 & \frac{2\sigma^2_{ss}}{\tau} \end{bmatrix} \quad (6.2)$$

where: Δoffset = GPS satellite's clock offset error (range equivalent)
Δrate = GPS satellite's clock offset rate error (velocity equivalent)

In Chapter 7 this model was used in several baseline and non-baseline scenarios to evaluate the performance of a ballistic missile if one satellite were to go bad.

CHAPTER 7

INTEGRITY MONITORING PERFORMANCE FOR AN ALL-IN-VIEW RECEIVER

7.1 Introduction

This chapter describes the performance of the ballistic missile when incorporating measurements from a bad satellite. This bad satellite is modeled as described in Section 6.4. Each selection method will be analyzed, with specific emphasis placed on the capabilities of an all-in-view receiver. Similar to the navigation performance chapter, a set of both baseline and non-baseline cases will be simulated.

7.2 Integrity Monitoring Input Deck

The baseline integrity monitoring input deck describes which states were considered and the initial covariances and Markov process values for the bad satellite states. First, both the clock offset and rate states for the bad satellite were considered (not estimated). These states were chosen to be part of the environment model only because the missile would not know which satellite was going bad. Therefore, the on-board system could not associate the two bad satellite states with the appropriate GPS spacecraft.

The bad satellite's clock offset and rate covariances were initially set to zero. This scenario thus assumed that a certain GPS satellite just started to go bad when the missile began to take measurements. Clearly, worse situations are possible, and several other cases (non-baseline) were modeled in Section 7.4.

Finally, the first-order Markov process values for the bad satellite's clock rate were chosen such that the clock offset would drive up to a 1 σ range equivalent value of

10 m at the end of the 100 s of GPS measurements. Setting the time constant to 1/2 day resulted in a steady-state (maximum) 1 σ value of 2.5487 m/s for the clock rate. These values are summarized in Table 7.1.

Table 7.1 Satellite # 11's Baseline Markov Process and Clock Values

1 σ Initial Clock Offset	0 m
1 σ Initial Clock Offset Rate	0 m/s
1 σ Final (100 s) Clock Offset	10 m
1 σ Final (100 s) Clock Offset Rate	0.1732 m/s
Markov Process Steady-State Value	2.5478 m/s
Markov Process Time Constant	1/2 day

7.3 Baseline Integrity Monitoring Results

The baseline integrity monitoring cases looked at the performance of the missile when one satellite, with the characteristics described in the prior section, was going bad. The three selection algorithms were compared at location A to quantify the resulting CEP degradation from incorporating measurements from the bad satellite. Location A was chosen since it is most sensitive to velocity errors, a parameter that could be directly driven by the bad satellite's clock rate.

The satellite chosen to go bad was satellite # 11. This was one of only two satellites common to all of the selection algorithms at location A. This particular satellite was chosen over the other common one because it offered the more dramatic degradation of CEP when it went bad. The CEP's with satellite # 11 bad are shown in Figure 7.1 for each of the selection algorithms.

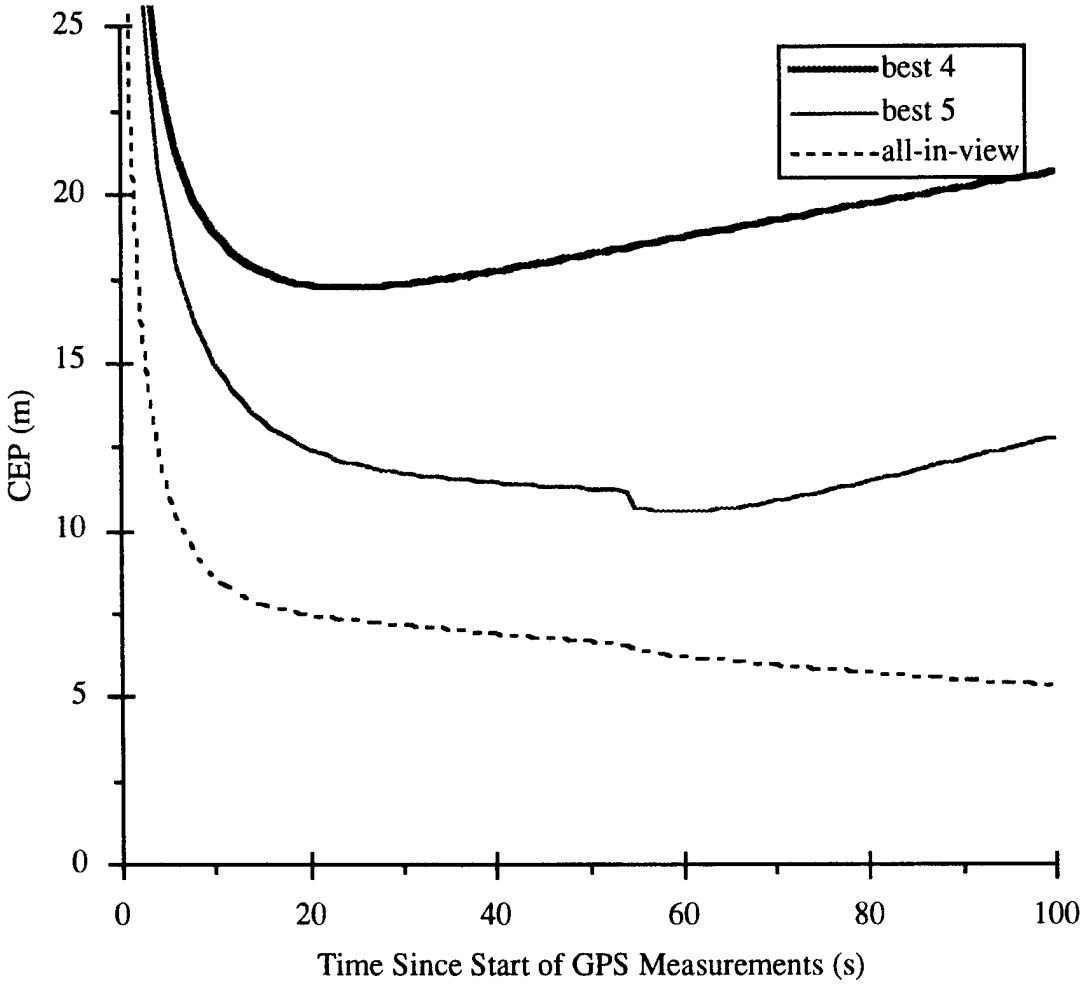

Figure 7.1 CEP vs. Measurement Time with Satellite #11 Bad

For the best four selection algorithm the CEP's were initially driven down, then steadily rose over the 100 s interval. This was a result of the early GPS measurements substantially reducing the missile's covariance, yet not being able to overcome the effects of the bad satellite's clock offset and rate state errors as they grew over time.

However, with the addition of one satellite, the best five selection algorithm provided substantial CEP improvement. Although, notice that at 55 s (when two satellites were switched) the CEP suddenly began to increase. It might have been better to keep the same set of five satellites throughout the 100 s measurement interval. This will be discussed further as the first non-baseline case in Section 7.4.1

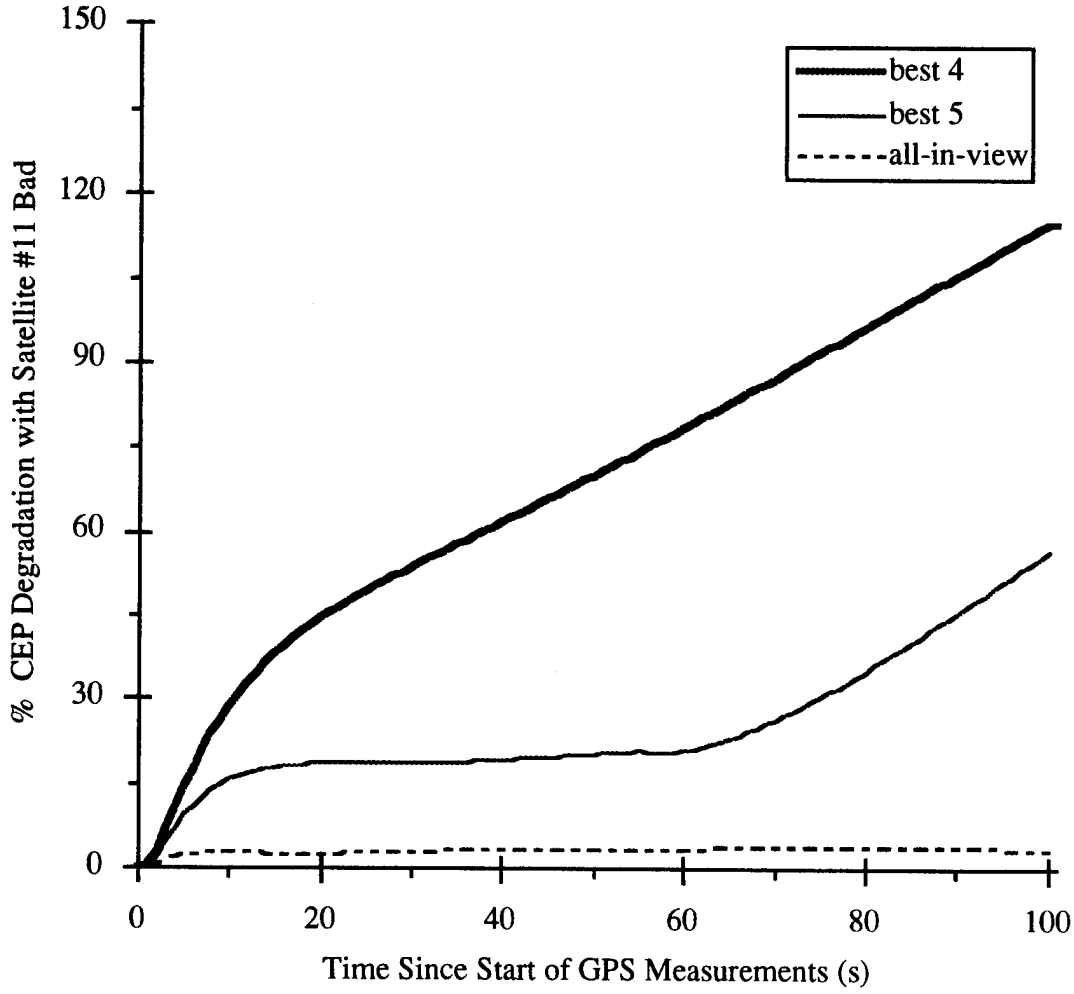

Figure 7.2 CEP Degradation for Each Selection Method with Satellite #11 Bad

The all-in-view case provided the best CEP results. This was to be expected because of the large number (13, then 14 at 55 s) of satellites used in the solution, providing excellent geometrical coverage. The effects of one bad satellite are mitigated by other satellites in the same general direction. Figure 7.2 (above) provides an excellent depiction of just how well the all-in-view receiver performed with the bad satellite. These plots represent the percentage degradation in CEP caused from the GPS satellite going bad. While the four and five satellite cases reached a CEP degradation of 115 % and 57 %, respectively, the all-in-view case only degraded 3.6 %. Thus, if the baseline scenario was truly a representative model of the characteristics of a bad GPS

satellite, then by using all the satellites in view a missile would essentially be "immune" to the degradation. This was studied further in the non-baseline cases.

7.4 Non-Baseline Integrity Monitoring Results

These next sections describe variations from the baseline integrity monitoring scenario.

7.4.1 Best 5 Selection Method with No Switching

The first non-baseline case analyzed the performance of the missile using a five satellite receiver with no satellite switching. The first set of five satellites chosen for the best GDOP would be used throughout the 100 s measurement phase (as long as they all remained in view). This case was simulated because from Figure 7.1 it was shown that the best 5 case switched two satellites at 55 s and worsened the CEP.

Figure 7.3 on the next page presents a comparison of these best five cases, i.e. with and without the satellites being switched. These plots show that the CEP performance was much better after 55 s if the original five satellites were kept in the solution set.

The performance of the missile was degraded when switching satellites apparently because of the addition of the two new pseudorange bias states to the filter (for the two new satellites brought into the best five set). Although a better geometry for range and range rate measurements was achieved, the two new pseudorange biases were not initially correlated with any of the other states. Therefore, the filter apparently relied more heavily on those satellites where correlations still existed, one of which was the bad spacecraft. This increased reliance on the bad satellite probably resulted in the worsening of the CEP.

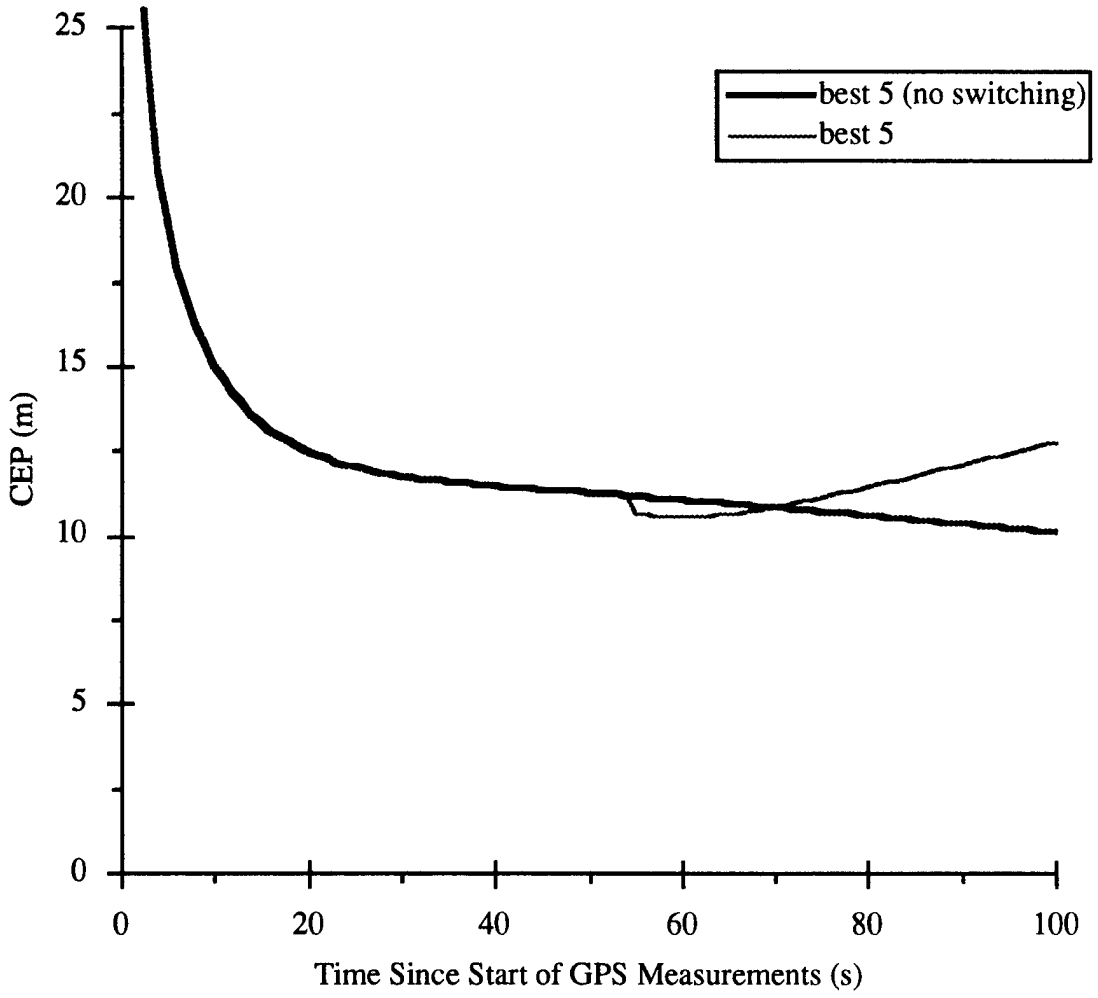

Figure 7.3 CEP for Best 5 (Switching vs. No Switching)

7.4.2 Pseudorange Bias States Considered

An on-board system lacking the 24 pseudorange bias states was the next non-baseline case modeled. As presented in Section 5.6.3, the pseudorange bias states add little to the performance of the missile in terms of its pure navigational capabilities. When these states were also considered (not estimated) in the baseline integrity monitoring cases the results were similar.

Figure 7.4 shows the degradation in CEP when the pseudorange bias states were considered. The all-in-view case revealed the worst degradation. This is a function of

the fact that, because of the sheer number of satellites used, this case was able to estimate the pseudorange biases to a greater extent than any of the other selection methods. As a result, not estimating these states tended to hurt the all-in-view case the most. However, a maximum degradation of only 1.3 % (at the end of the 100 s) would most likely not justify the extra computational burden of carrying the pseudorange bias states in an on-board system.

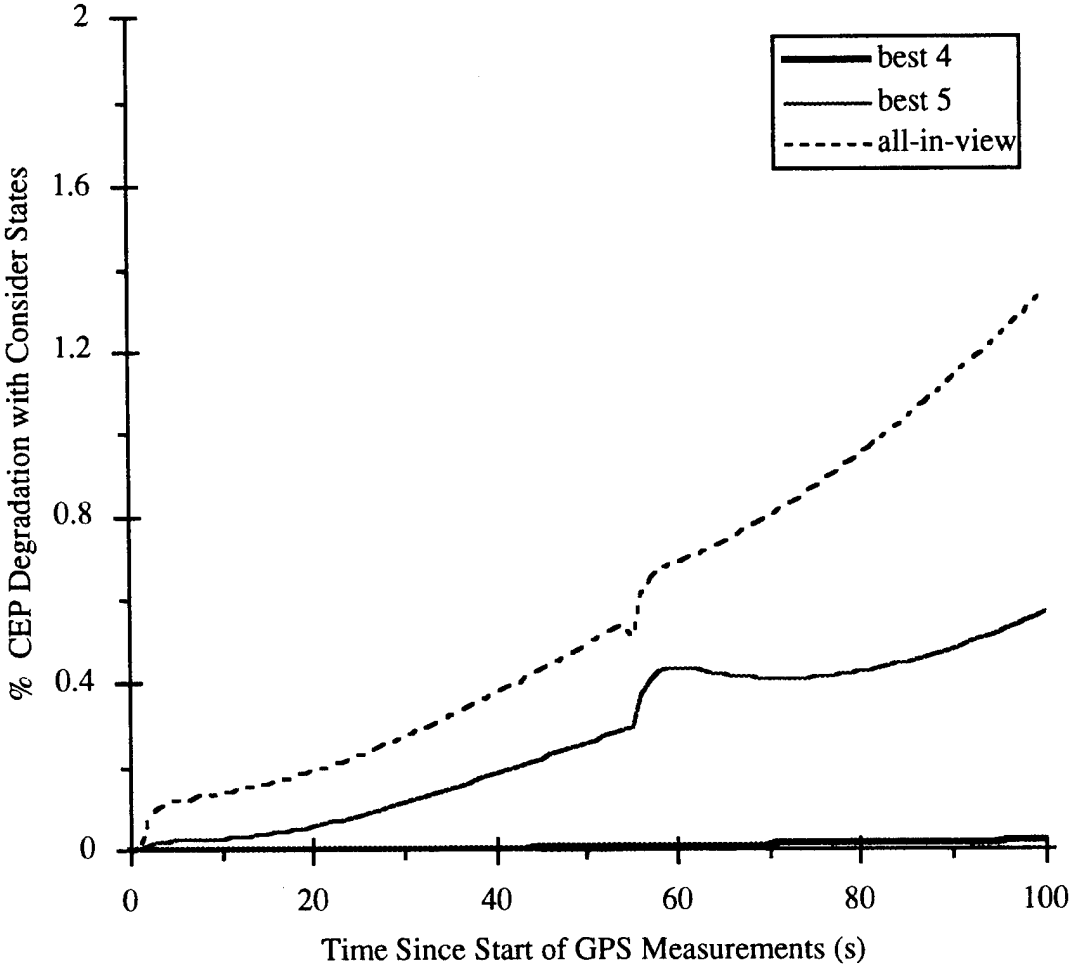

Figure 7.4 CEP Degradation with Pseudorange Bias States Considered

7.4.3 Worst Case Scenarios for All-In-View

The baseline integrity monitoring cases revealed that, by using an all-in-view receiver, little CEP degradation could be expected from using a bad GPS satellite. At what point does this performance "break?" That is, how bad does the satellite have to be to cause a serious degradation of CEP? This is the question answered in the remaining non-baseline cases.

It was found that the severity of the bad satellite had little affect on the all-in-view receiver performance. This was determined by worsening the baseline characteristics of the bad satellite. For example, instead of using Markov process values to give the clock offset 10 m of drift in the 100 s of measurements (the baseline case), more severe conditions were chosen. For the first case, Case I, values were chosen such that the bad satellite's clock rate drove from 0 to 2 m/s during the measurement phase. This represents a final velocity equivalent clock rate 100 times greater than the accuracy of the missile's integrated Doppler measurements.

For the second case, Case II, even more severe conditions for the bad satellite were used. This worst case started the bad satellite's clock offset and rate at 1000 m and 100 m/s, respectively (1σ). This would be representative of a spacecraft that had been severely degrading prior to its use by the missile. To make matters even worse, the Markov process values were then chosen to drive the clock rate to 200 m/s during the measurement interval. The values for both of these cases are shown in Table 7.2 on page 129.

The severity of the initial conditions in Case II were so great that measurements to this particular satellite would most likely have been thrown out by an actual user. This is because the measurement residual to this satellite would likely have fallen outside of a standard deviation threshold set by the user (usually 3σ), with the σ being determined by the current covariance matrix and estimated noise on the measurements.

However, it is also possible that big initial position and velocity uncertainties (like that of the ballistic missile) would allow for the measurements to be used, at least initially.

Table 7.2 Sat # 11's Non-Baseline Markov Process and Clock Values (Cases I & II)

	Case I	Case II
1 σ Initial Clock Offset	0 m	1000 m
1 σ Initial Clock Offset Rate	0 m/s	100 m/s
1 σ Final (100 s) Clock Offset	116 m	14177 m
1 σ Final (100 s) Clock Offset Rate	2 m/s	200 m/s
Markov Process Steady-State Value	29.428 m/s	25505.5 m/s
Markov Process Time Constant	1/2 day	1/2 day

The degradation in CEP for both Case I and II are shown in Figure 7.5 (see next page). Reflecting the results of Section 7.4.2, the pseudorange bias states for these simulations were considered.

For both Cases I and II the degradation in CEP was minimal. For Case I the final change in CEP versus the case with no bad satellites was merely 3.8 %. Case II increased to only 5.6 %. Recall that the final degradation for the non-baseline (pseudorange bias states considered) case was 3.6 %.

The figure suggests that no matter how bad the clock was on satellite # 11, the resulting CEP change was minimal. This was apparently a result of the fact that an all-in-view receiver at location A had 13 satellites from which to take measurements (14 after 55 s). The sheer number of satellites in the solution would work to eliminate even the worst measurements from one bad satellite. This is presumably a result of the fact that 12 sets of accurate range and range rate measurements from 12 different, hence well dispersed, directions could eliminate the bad contributions from any one direction.

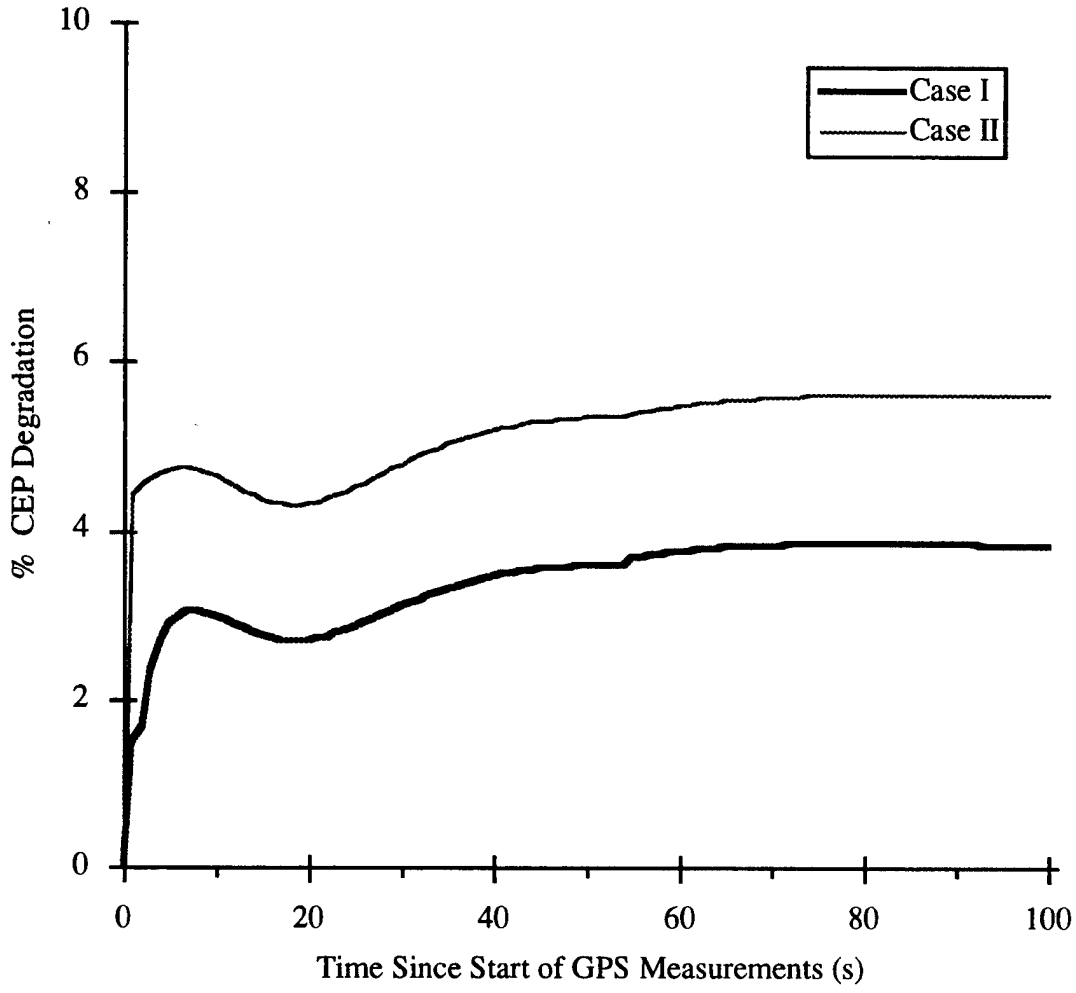

Figure 7.5 CEP Degradation for All-In-View Cases I and II

It is also hypothesized that the above results would be independent of which specific satellite went bad. Unlike the best four or five selection algorithms, it seems that the geometry from an all-in-view receiver generally prevents the user from becoming too dependent on any one particular satellite. However, this could also be a result of the specific geometry seen at location A, and not necessarily valid for other points along the trajectory.

Under the assumptions made in this thesis, these results seem to suggest a simple and effective manner in which to mitigate the effects of a bad satellite for an all-in-view receiver--a plausible integrity monitoring scheme. However, the results are also quite

optimistic because of the assumptions in the thesis, with more in-depth analysis needed to verify the results. This will be discussed in detail in the conclusions chapter, Chapter 8.

CHAPTER 8

CONCLUSIONS

8.1 Summary of Navigation Performance Results

The first portion of this thesis quantified and compared the navigation performance of a ballistic missile using various satellite selection algorithms, emphasizing the power of all-in-view. Using a 44-state environment model, the navigation performance was analyzed in terms of CEP at three different locations along a nominal missile trajectory. At each location 100 s of GPS measurements were taken.

It was found that a substantial improvement in CEP could be obtained by using an all-in-view GPS receiver. Specifically, using all-in-view resulted in a 45 % improvement versus the best four satellites, and a 35 % improvement versus the best five. It was also found that CEP was most sensitive to velocity uncertainties, becoming more dramatic the farther from the target point (more coasting time).

The non-baseline cases also yielded several interesting results. First, the pseudorange bias states do not need to be carried by the on-board filter. Estimating these states resulted in a negligible enhancement of performance. A second non-baseline case emphasized the need for Doppler measurements if GPS was available only for a short period of time. Although in the steady-state there was little difference, it was found that the lack of Doppler measurements resulted in a degradation in the missile's ability to estimate velocity errors in a 100 s interval. The rate of convergence to a solution was diminished because of the missing velocity measurements. This then directly contributed to a worsening of CEP, especially at the locations most distant from the target.

A last non-baseline case analyzed the missile's performance with deployment velocity errors placed on the r.b.'s. These velocity errors are a result of the inability of the bus to accurately eject the r.b.'s. In general it was found that the deployment velocity errors "swamped out" the GPS error contributions. If a user wants to take full advantage of GPS, alternatives must be found. At least three possible actions could be taken:

(1) The deployment mechanism could be improved so that less velocity errors are given to the r.b.'s.

(2) The r.b.'s could be deployed closer to the target, making CEP less sensitive to the deployment velocity errors.

(3) GPS could be used by the r.b.'s (making them re-entry vehicles (r.v.'s) because they would now have maneuvering capabilities) until impact with the target or signal loss in the atmosphere.

8.2 Summary of Integrity Monitoring Results

The integrity monitoring portion of the thesis quantified the navigation degradation (in terms of CEP) experienced by a ballistic missile when incorporating measurements from one bad satellite. The bad satellite was modeled by including states in the environment model for clock offset and rate, with the rate state modeled as a first-order Markov process. In this fashion, both pseudorange and Doppler measurements to this particular satellite would be affected.

A comparison of all-in-view versus the best four and five satellite selection methods revealed substantial improvement by using all spacecraft in view. Starting the bad satellite's states at zero, and choosing Markov process values such that the clock offset reached 10 m after 100 s, the all-in-view CEP degraded by under 5 %. On the other hand, at this same particular location the four and five satellite cases degraded by over 50 and 100 %, respectively.

The non-baseline cases also provided some interesting conclusions. First, it was shown that with the five satellite receiver it might be better to remain with the same set of five throughout the mission. This case revealed that when two of the satellites were switched, at about midpoint in the mission, there was a substantial degradation in CEP. From these results it can be hypothesized that if satellites are going to be switched during a mission, the less spacecraft swapped, relative to the total number used, the better (assuming the bad satellite isn't changed). This then apparently favors receivers with more channels, i.e. all-in-view.

Another non-baseline case showed that the pseudorange bias states to the 24 GPS satellites did not need to be carried in the on-board filter as an aid to integrity monitoring. As a consequence (since they didn't help with the general navigation performance either), under the assumptions made in this thesis, carrying the extra states is not beneficial to a ballistic missile.

The most interesting results of the thesis come from the final non-baseline scenarios. In these last cases the results suggested that, regardless of the degree with which a single satellite were to go bad, the resulting CEP degradation to an all-in-view receiver would be minimal. This was concluded by analyzing the performance of the missile with outrageously poor conditions for the clock offset and rate states of the bad satellite. It was also suggested that the small degradation could very well hold true for any one of the satellites in view going bad. However, it needs to be stressed that these results are optimistic, with much more study needed (outlined in the future research section).

8.3 Recommendations for Future Research

As is often the case in the practice of engineering, the gaining of knowledge and insight into certain applications leads to an abundance of new questions. This is the case with this thesis. Several interesting issues have been identified, all of which need

further research to fully understand their potential use to a ballistic missile. The following recommendations primarily address the integrity monitoring portion of this thesis. However, they are also equally valid for further study into the navigation performance of an all-in-view receiver.

Although the results suggest that an all-in-view receiver might inherently offer an immunity to one bad satellite, a form of integrity monitoring, the conclusions only hold under the assumptions made in the thesis. Further analysis is required. First, more cases need to be analyzed. An initial approach could be to vary the bad satellite's characteristics, the satellite going bad, the missile's location, and some of the other models used in the simulations. This thesis just analyzed one specific case.

Besides varying the characteristics of the cases studied, a more significant benefit could come from varying the covariance analysis equations themselves. Recall in Chapter 4 that an optimal-suboptimal filter was used for the simulations. This update equation represents the best that an on-board system could theoretically be tuned. This may be the primary reason that makes this thesis' integrity monitoring results extremely optimistic. More specifically, because of the manner in which the suboptimal weighting vector is created, the optimal-suboptimal filter is essentially being told which satellite is going bad and the characteristics of that bad satellite. Future research should analyze the missile's performance by maintaining two separate filters, a suboptimal and environment (this technique was described in Section 4.2.3 as "off-line system error analysis"). In this fashion, the suboptimal filter has no knowledge of the bad GPS satellite. The suboptimal filter would then have to be tuned to give the best performance under a variety of bad satellite conditions.

As a follow-on to the above research, even more extensive analysis could be undertaken by the use of data editing techniques. In this fashion measurement residuals from the bad satellite could be eliminated by σ threshold checks, and algorithms could be developed for detecting a failure and isolating the bad spacecraft. This data editing

would require the use of a Monte Carlo Kalman Filter simulation approach because of the non-linearities created from the editing and the need to process actual measurements to the satellites.

A sequence of possible follow-on research steps is summarized as:

- Analyze more cases within the framework of this thesis' simulation model, developing the performance statistics through numerous runs.
- As a follow-on to the optimal-suboptimal filter, analyze the missile's performance through the technique of off-line system error analysis.
- For integrity monitoring analysis, develop a Monte Carlo Kalman Filter simulation to include data editing techniques, and detection and isolation capabilities.

APPENDIX A

TIME HISTORY OF STATE UNCERTAINTIES

POSITION & VELOCITY ERRORS

Baseline Best 4 at Location A

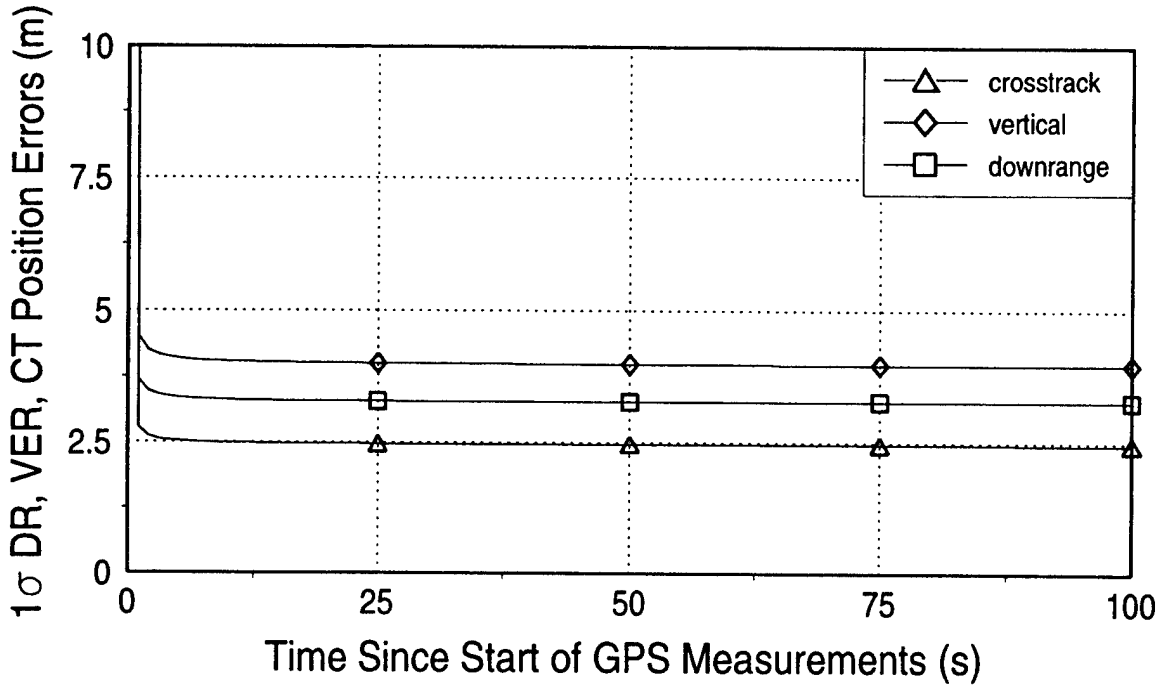

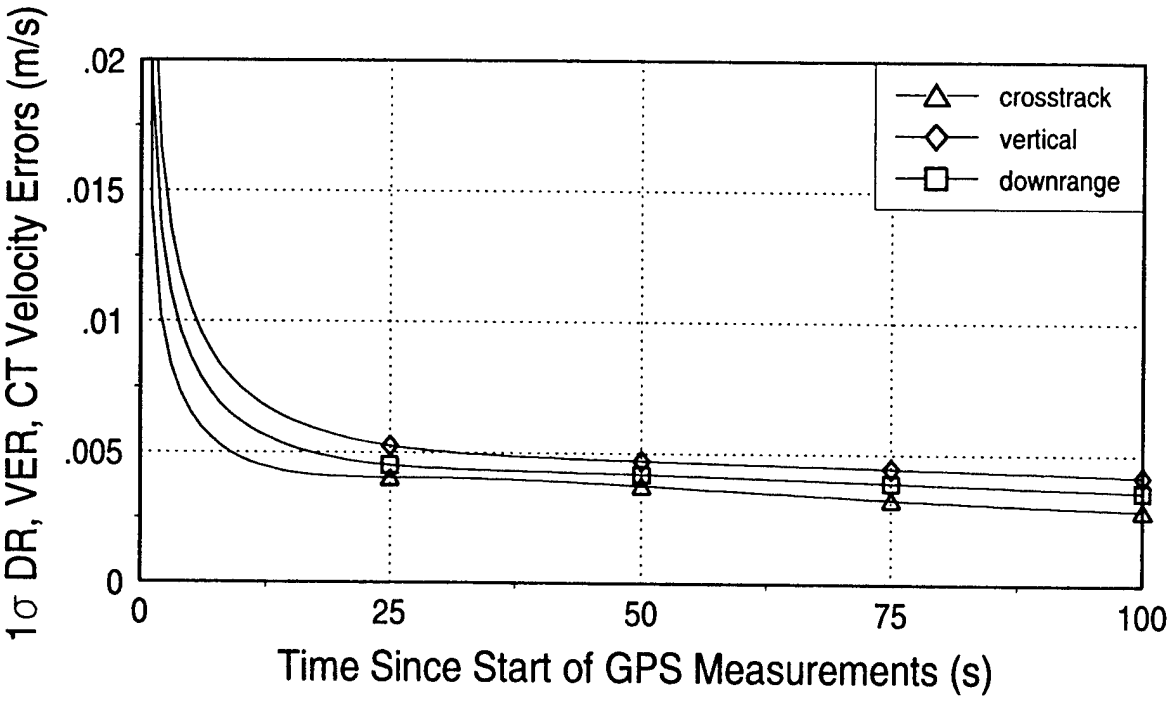

ATT. & ATT. RATE ERRORS

Baseline Best 4 at Location A

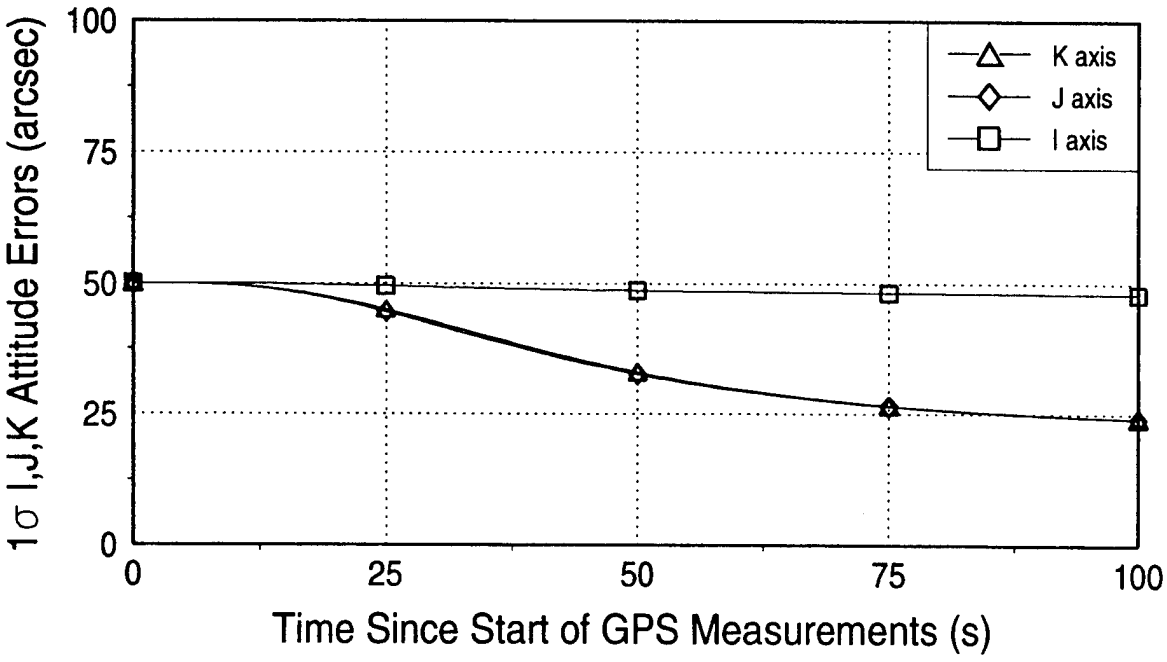

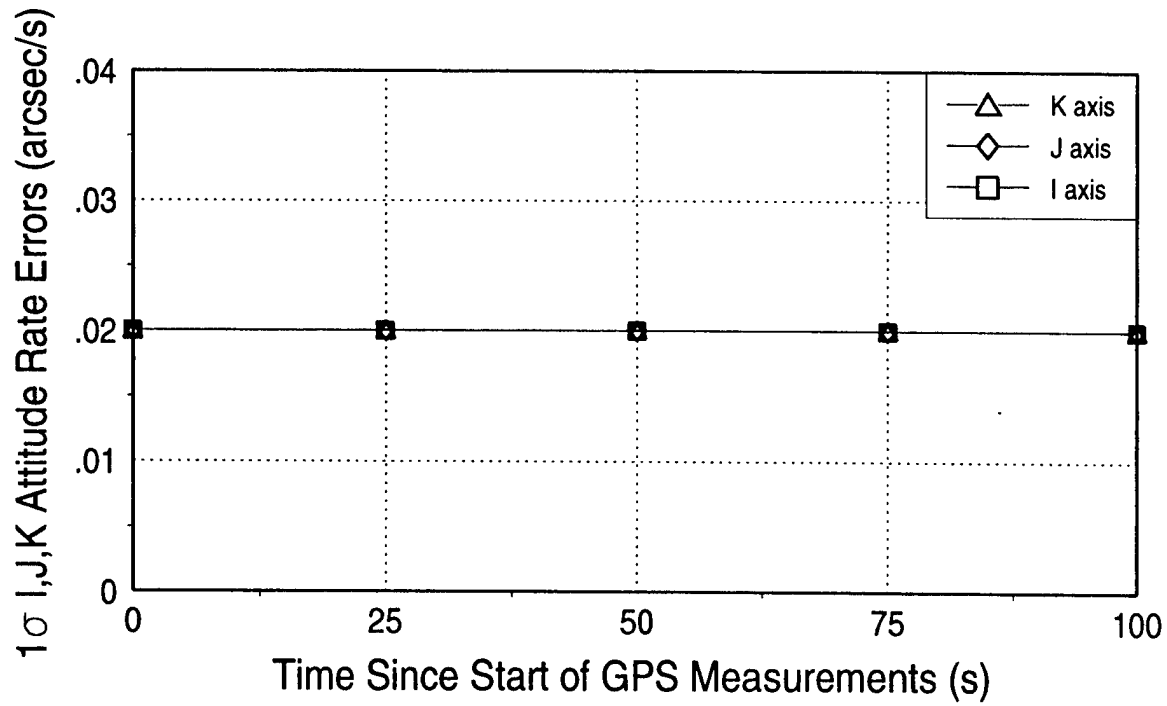

ACC. BIAS & CLOCK ERRORS

Baseline Best 4 at Location A

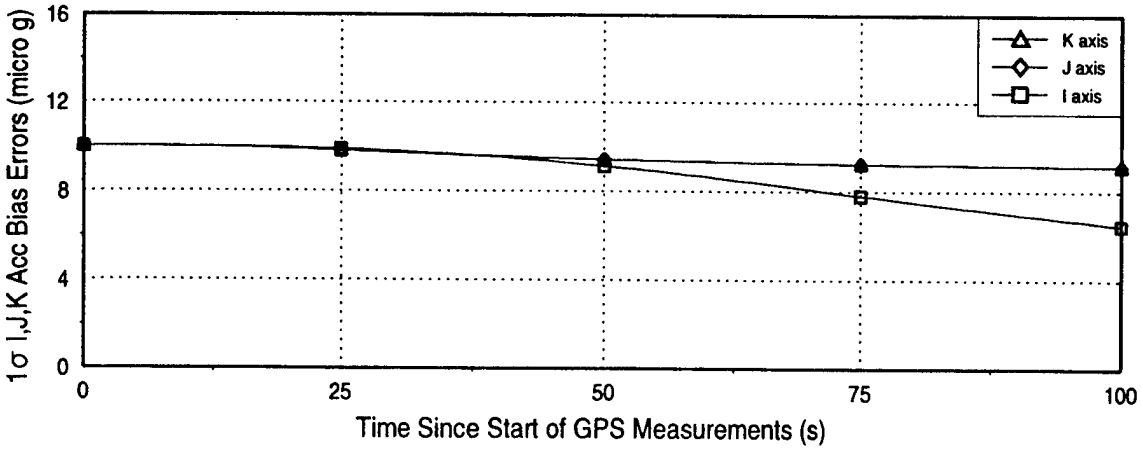

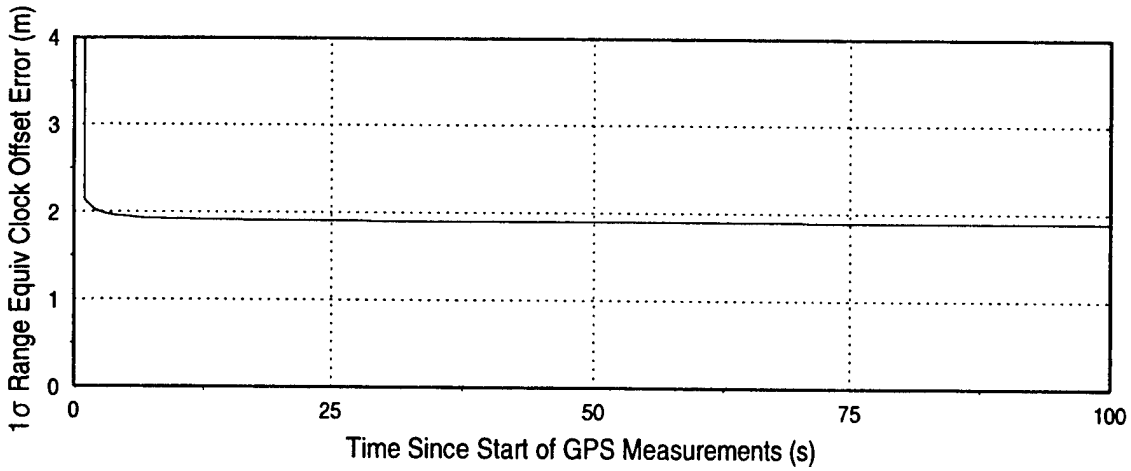

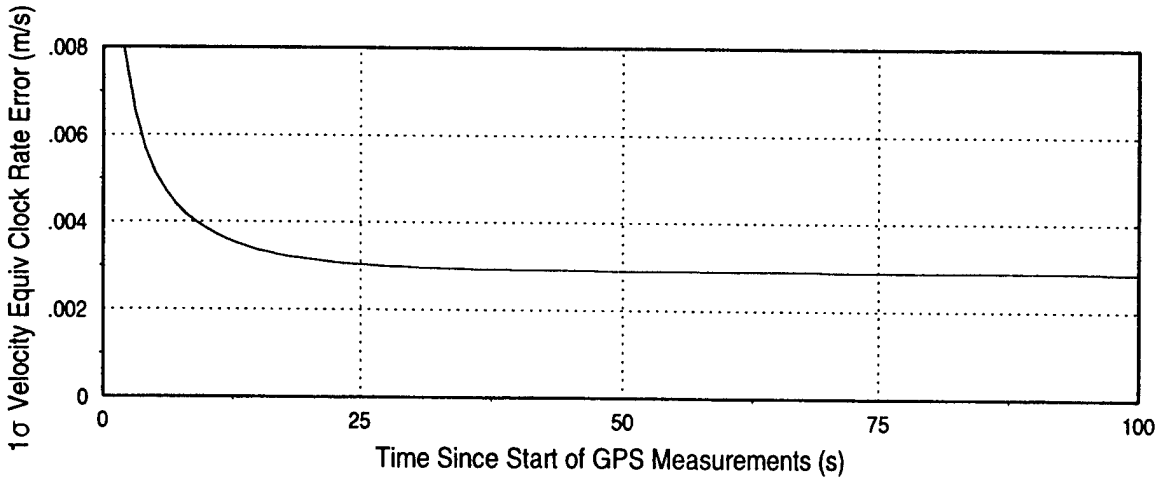

PSEUDORANGE BIAS ERRORS

Baseline Best 4 at Location A

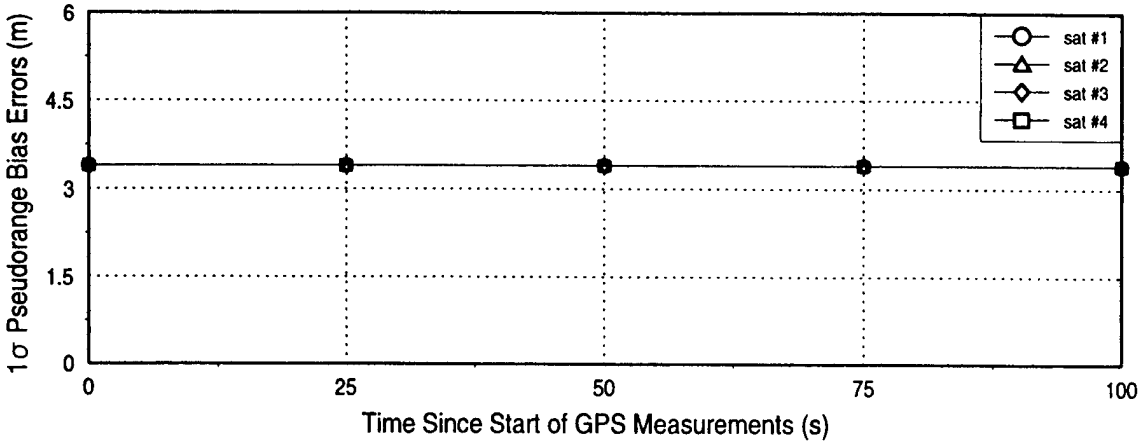

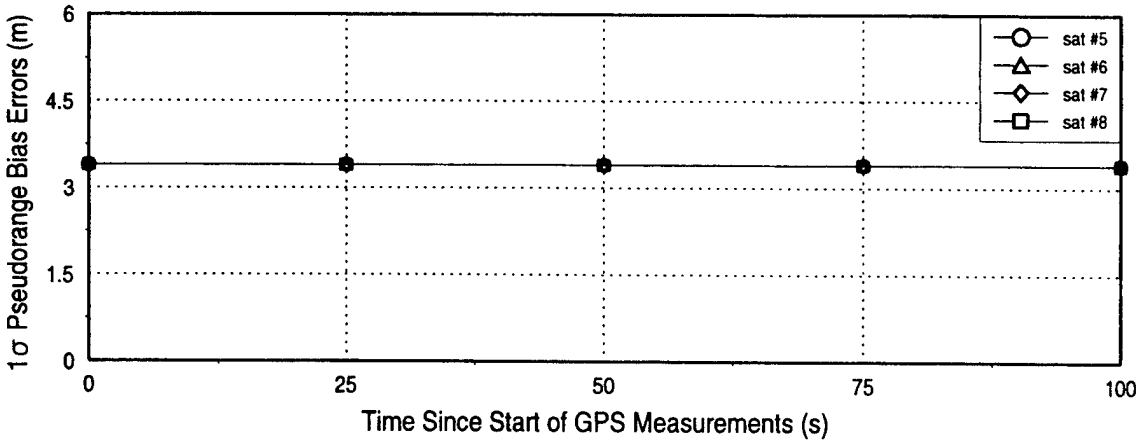

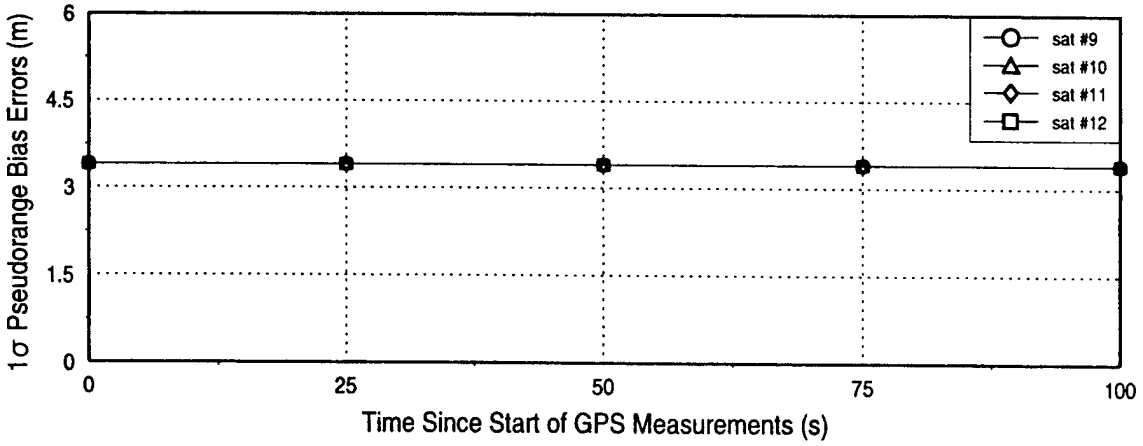

PSEUDORANGE BIAS ERRORS

Baseline Best 4 at Location A

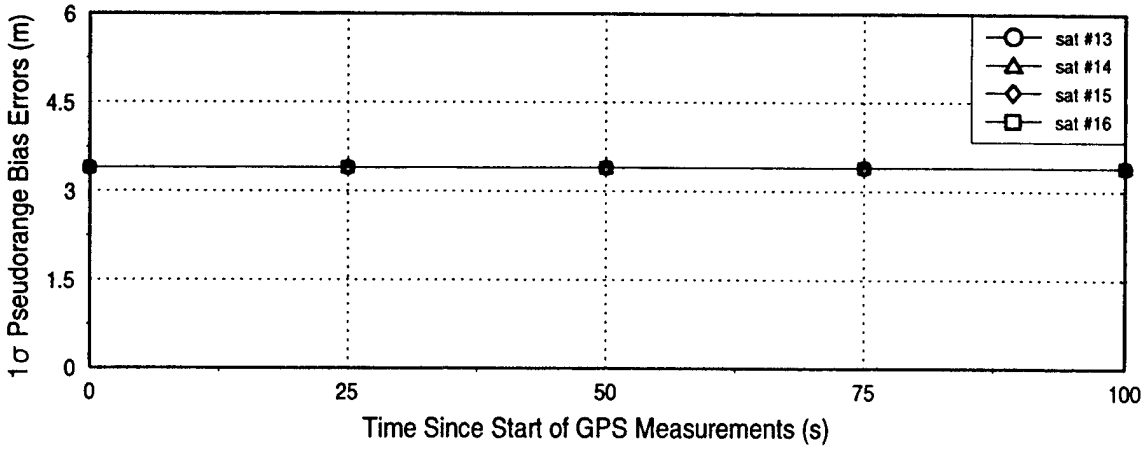

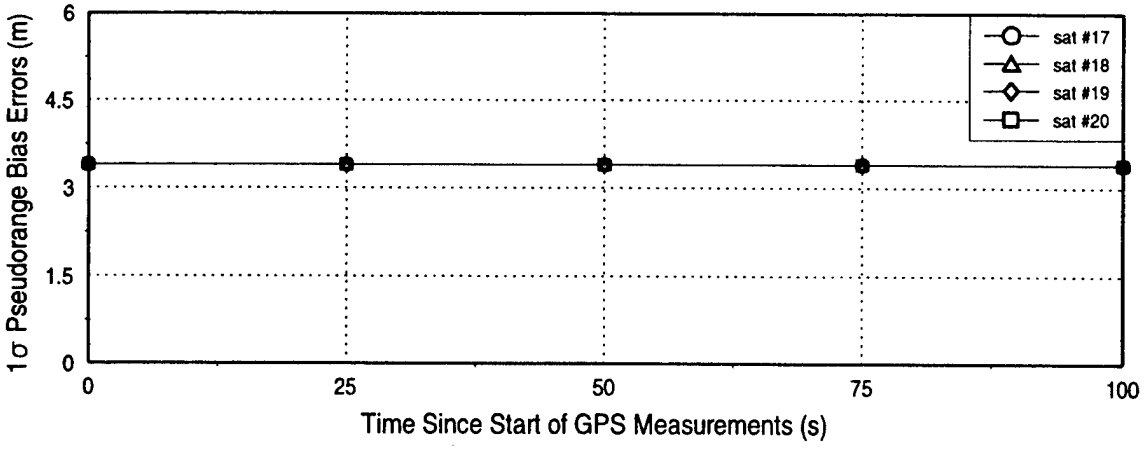

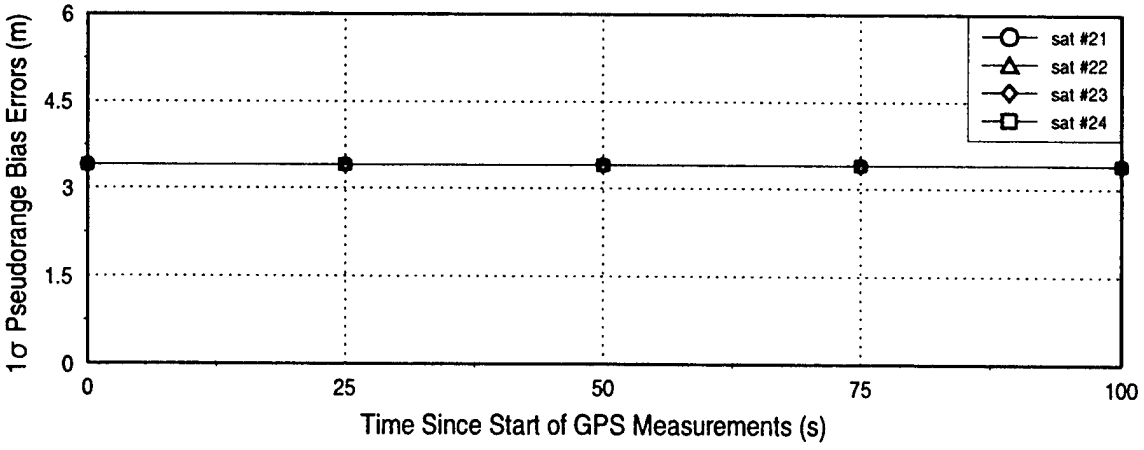

POSITION & VELOCITY ERRORS

Baseline Best 5 at Location A

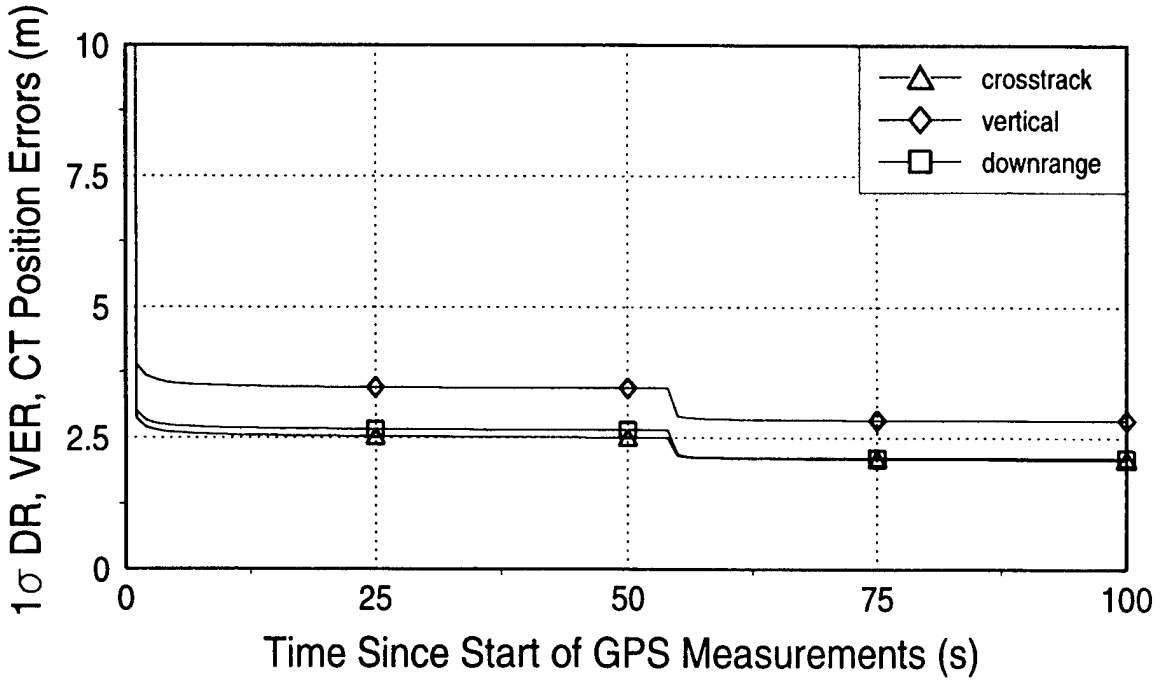

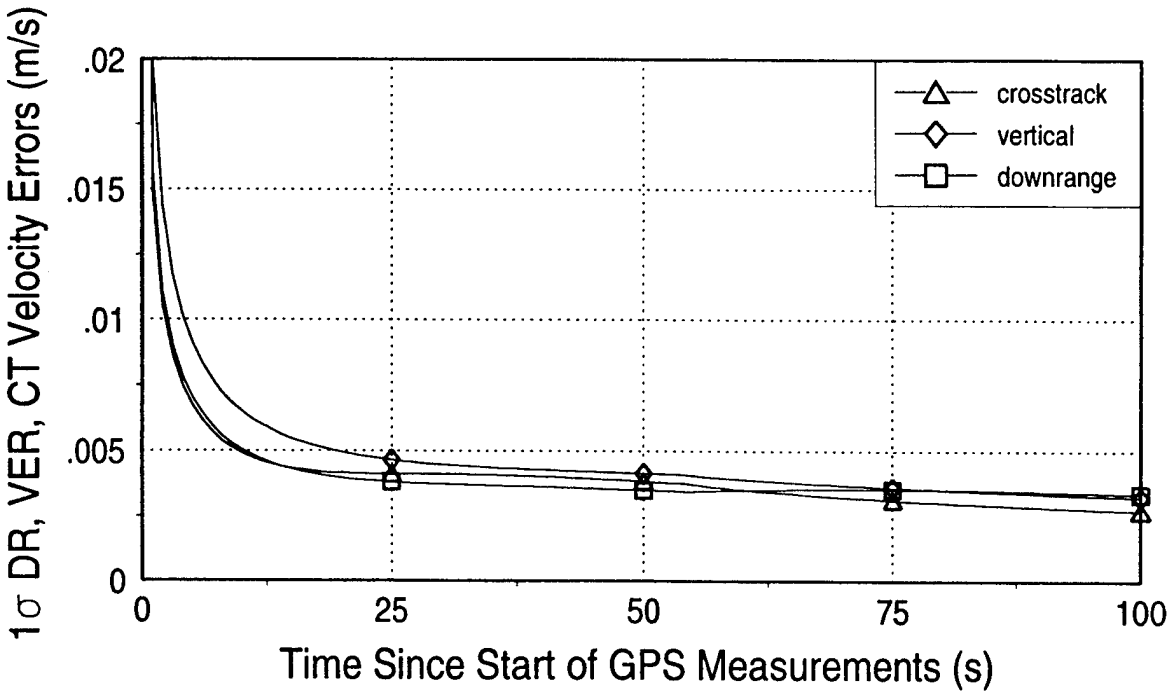

ATT. & ATT. RATE ERRORS

Baseline Best 5 at Location A

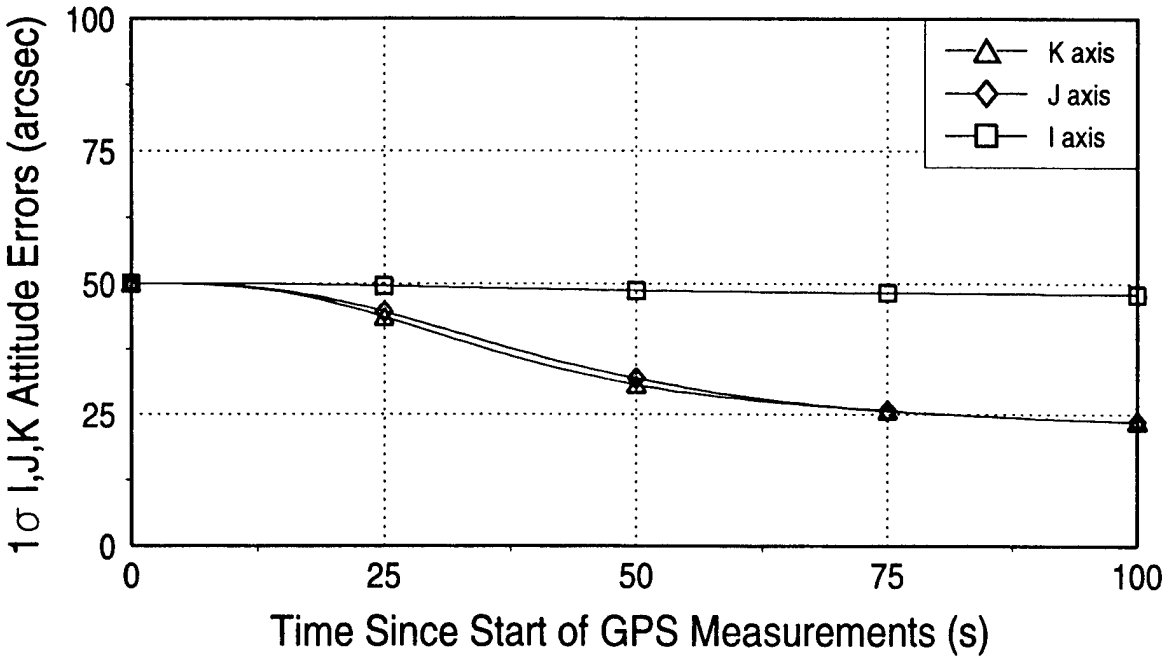

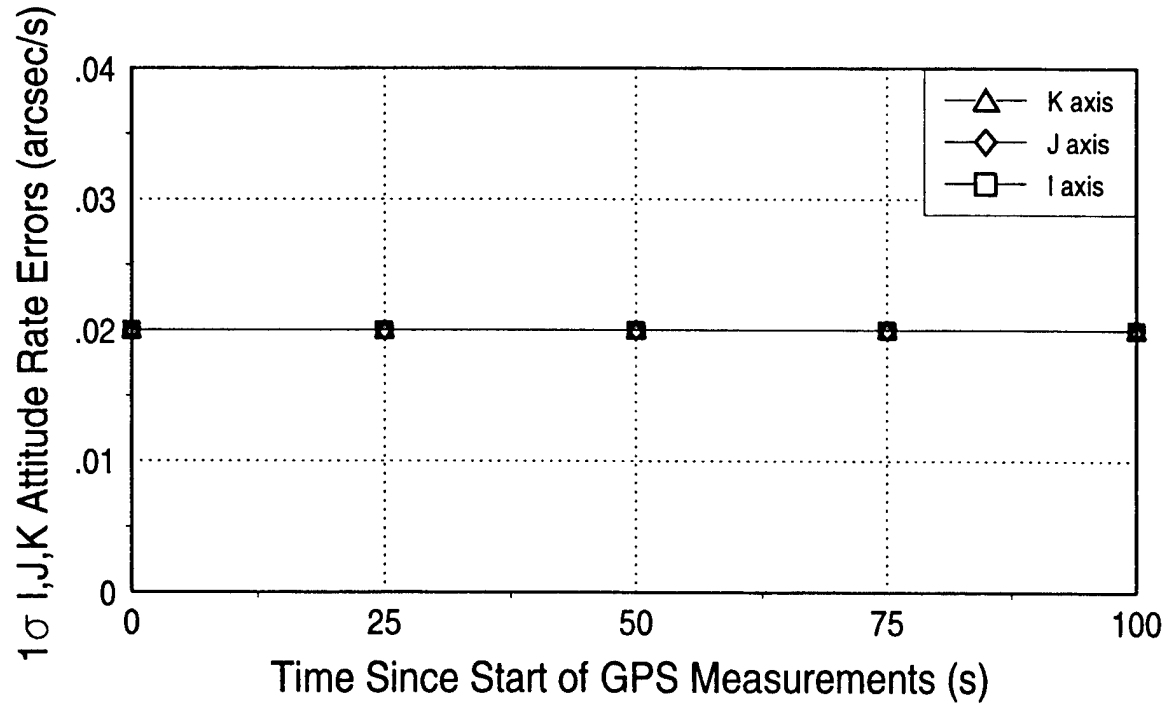

ACC. BIAS & CLOCK ERRORS

Baseline Best 5 at Location A

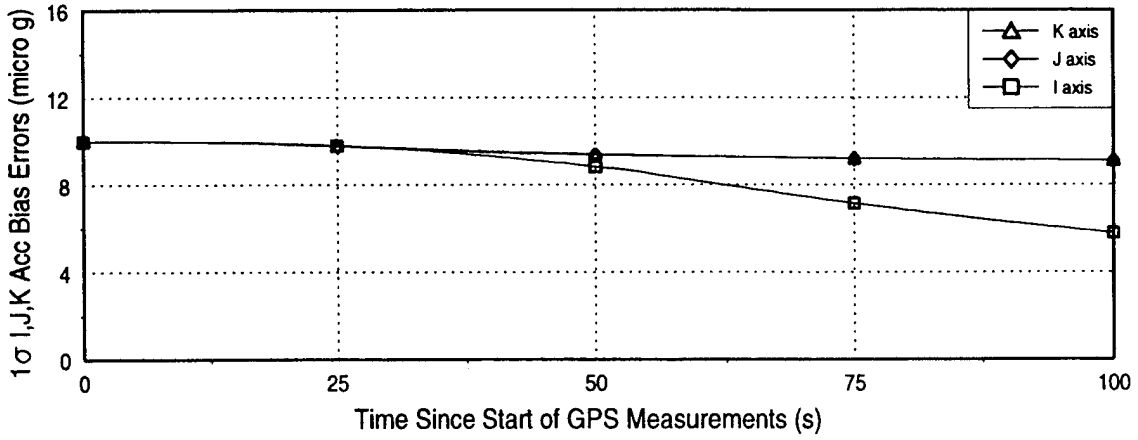

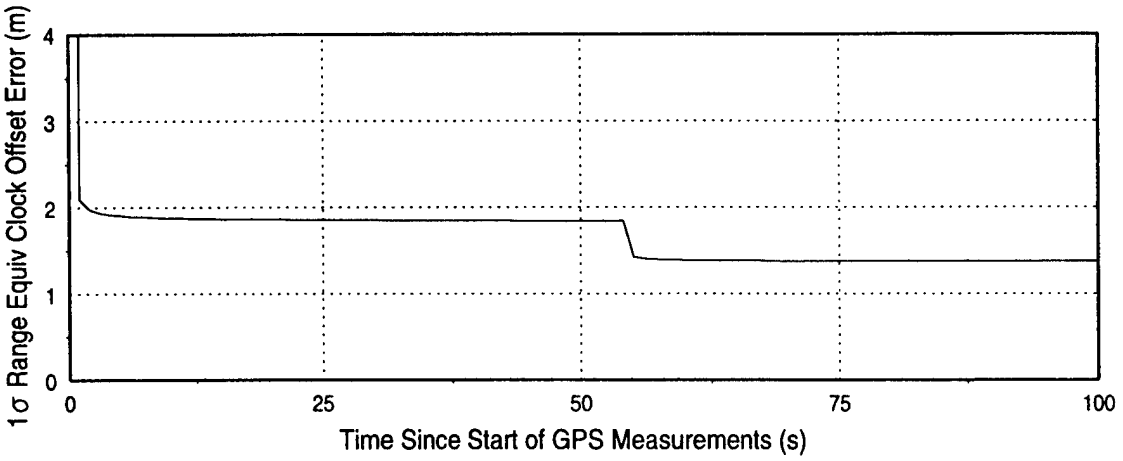

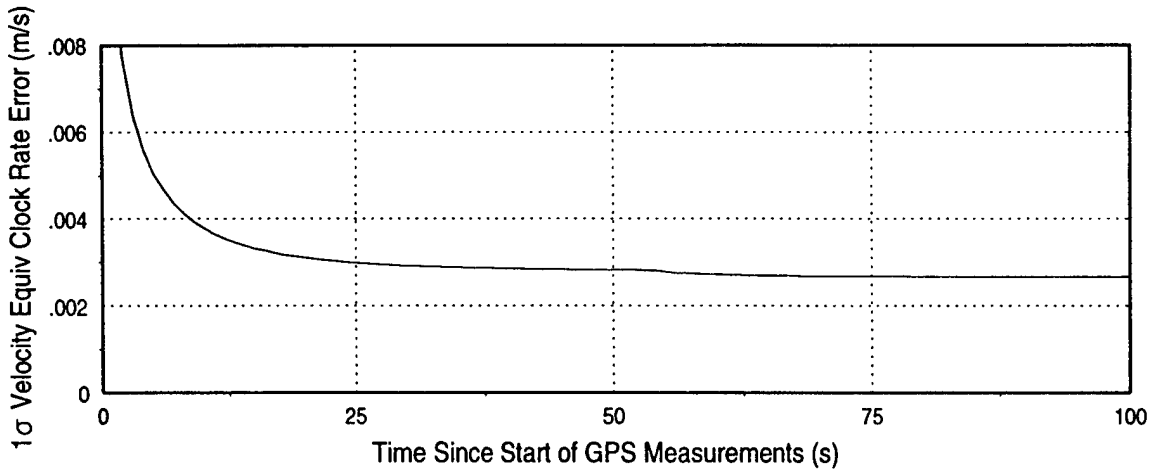

PSEUDORANGE BIAS ERRORS

Baseline Best 5 at Location A

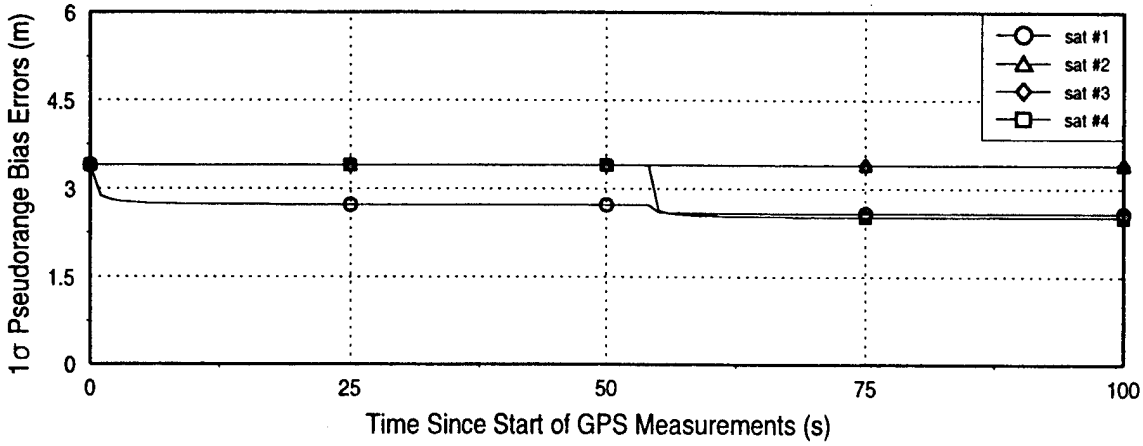

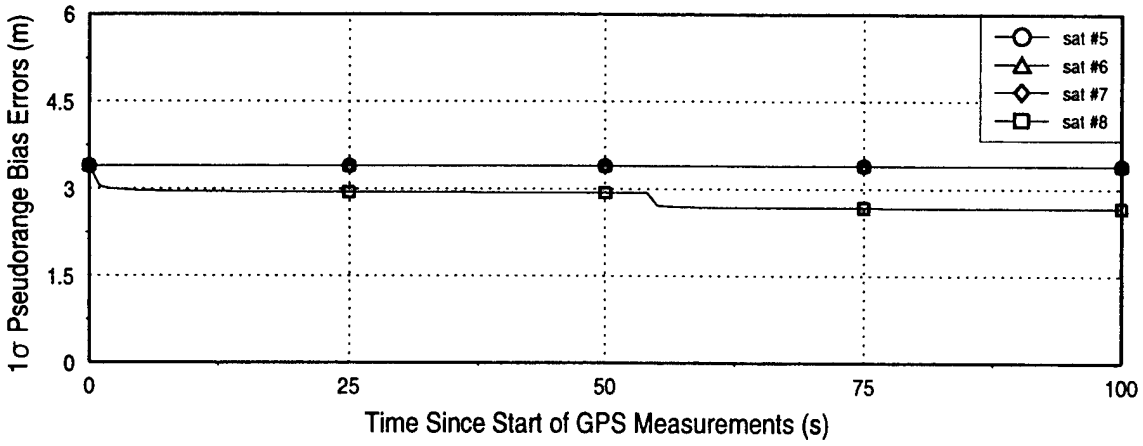

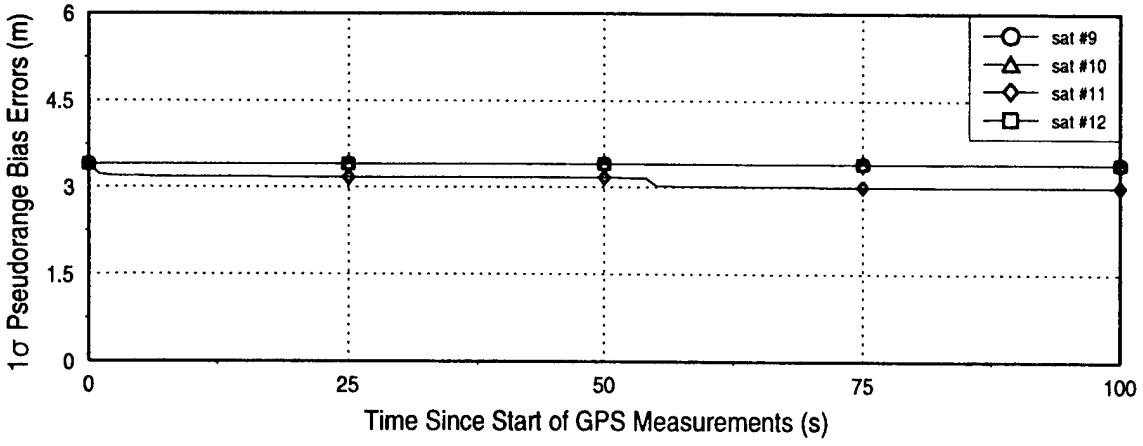

PSEUDORANGE BIAS ERRORS

Baseline Best 5 at Location A

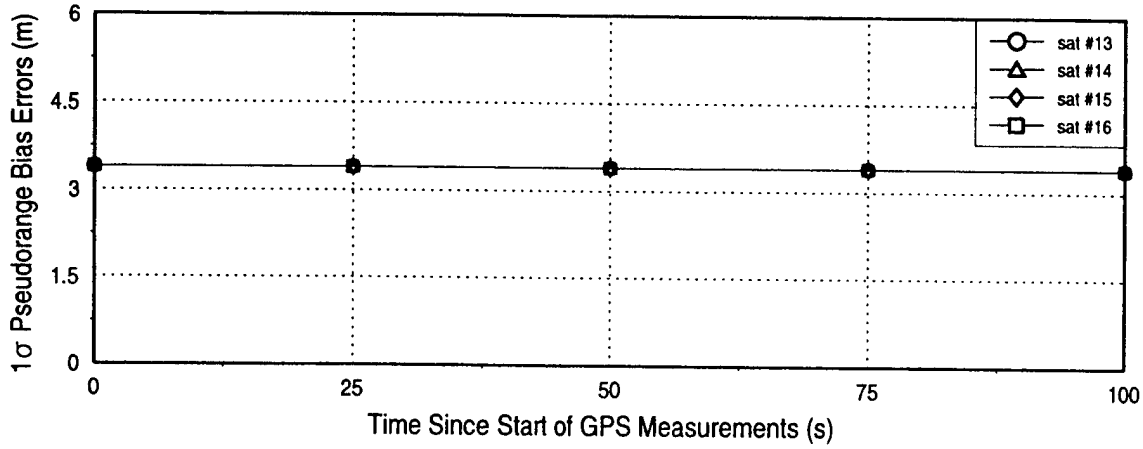

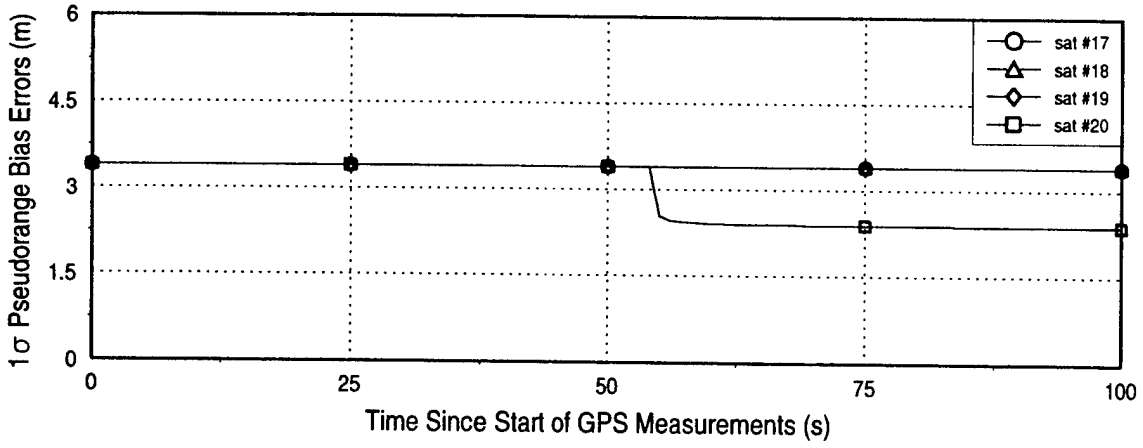

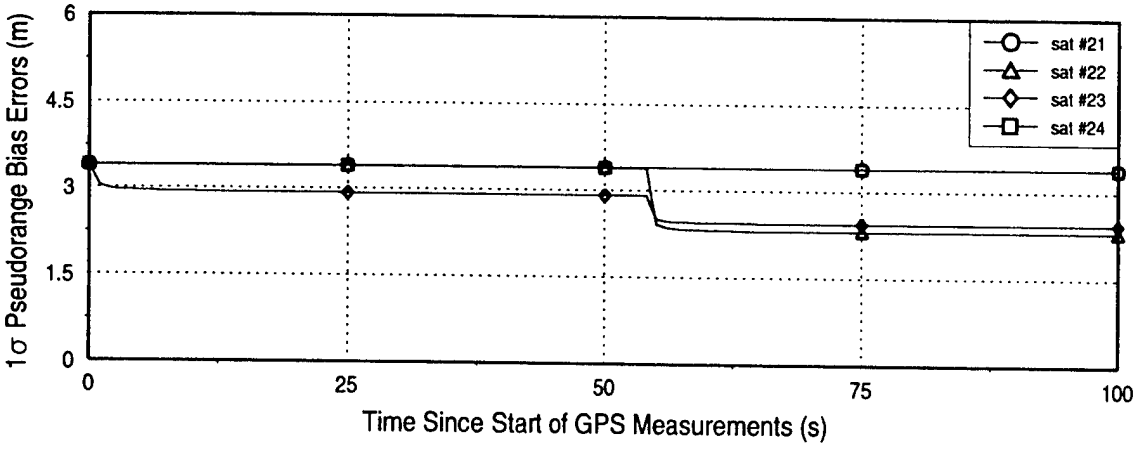

POSITION & VELOCITY ERRORS

Baseline All-In-View at Location A

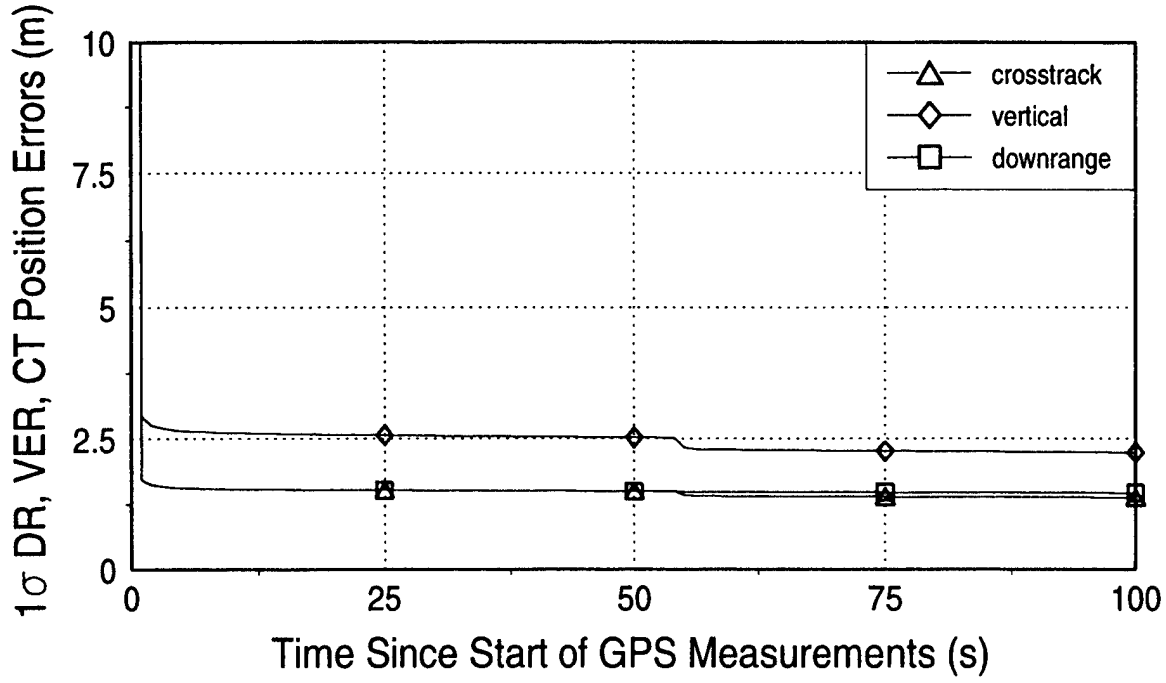

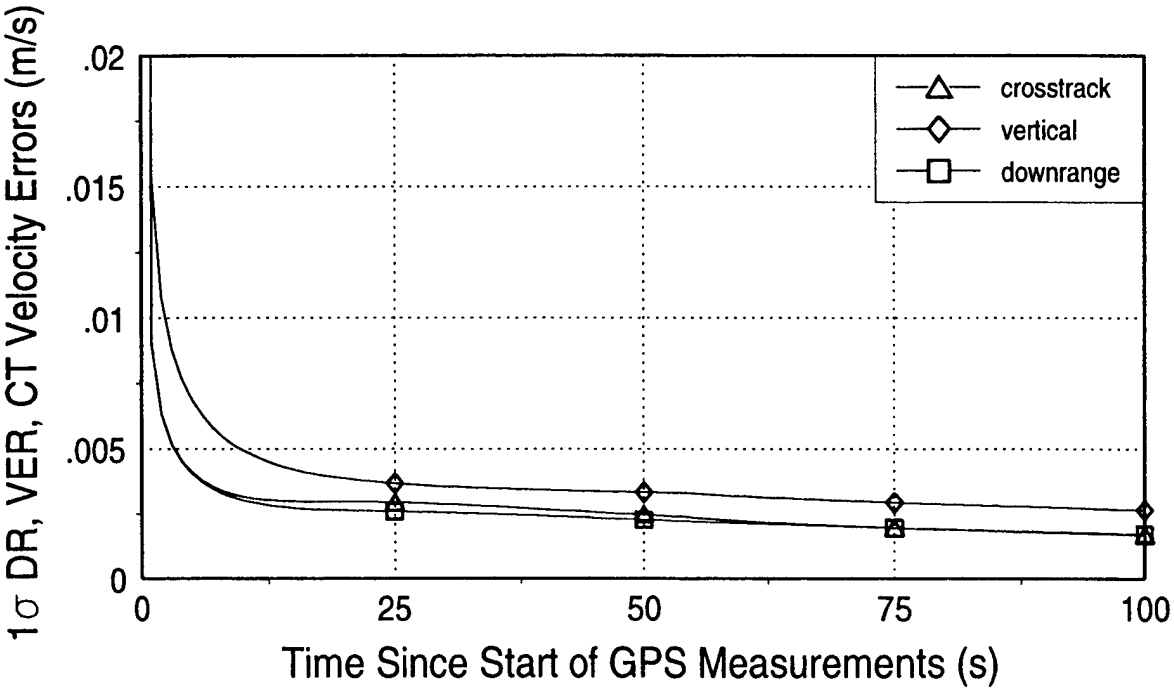

ATT. & ATT. RATE ERRORS

Baseline All-In-View at Location A

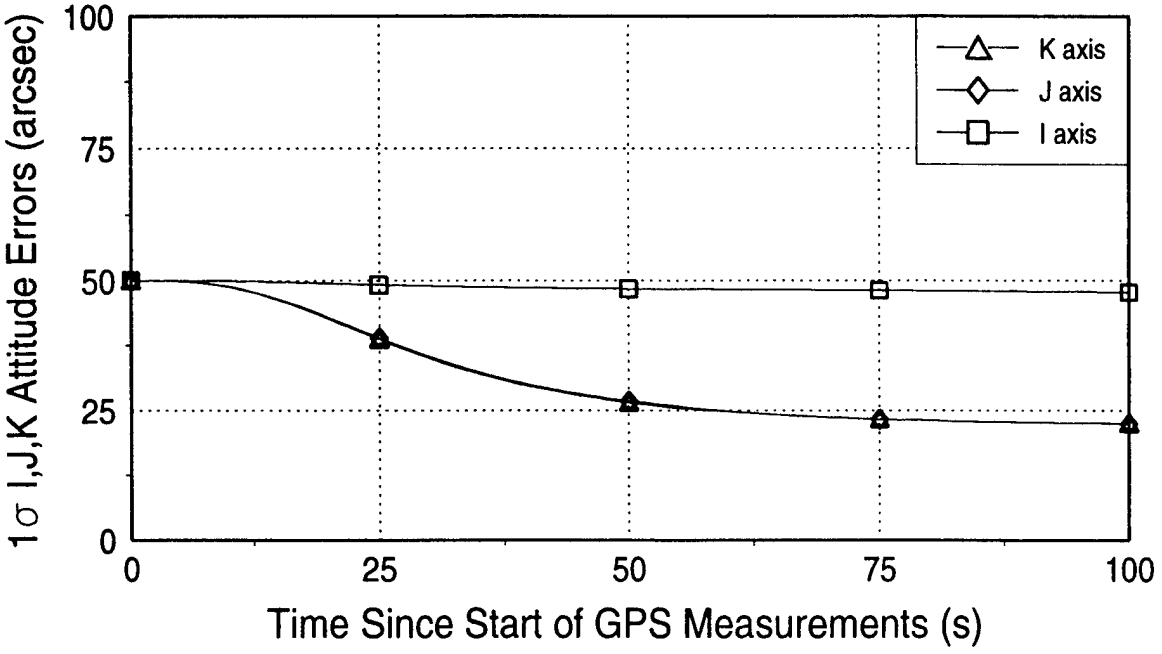

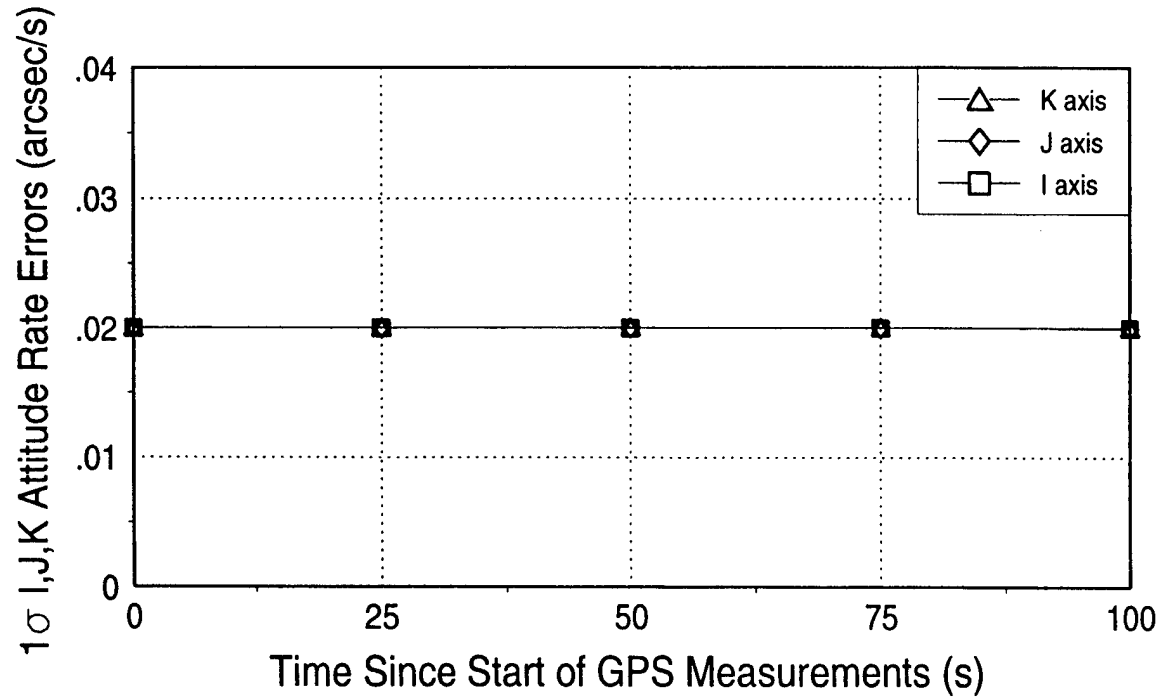

ACC. BIAS & CLOCK ERRORS

Baseline All-In-View at Location A

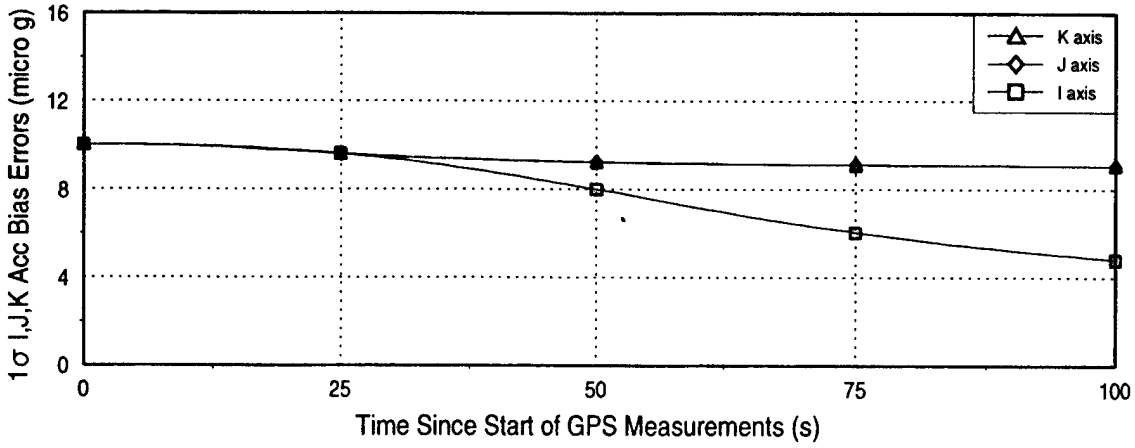

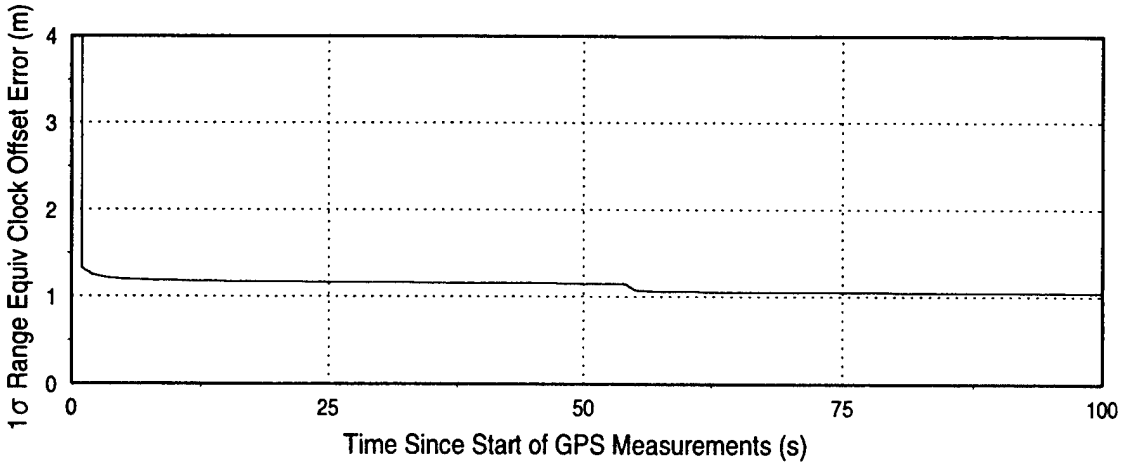

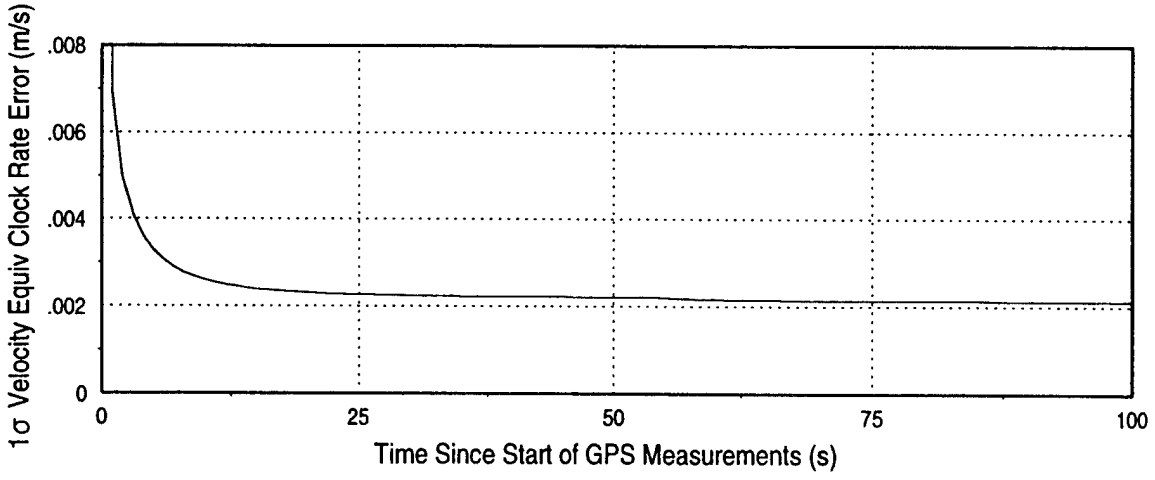

PSEUDORANGE BIAS ERRORS

Baseline All-In-View at Location A

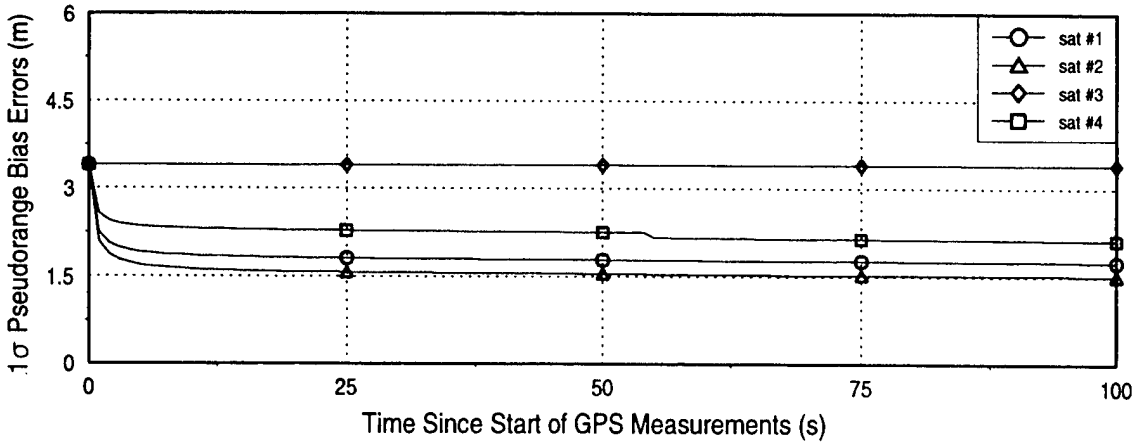

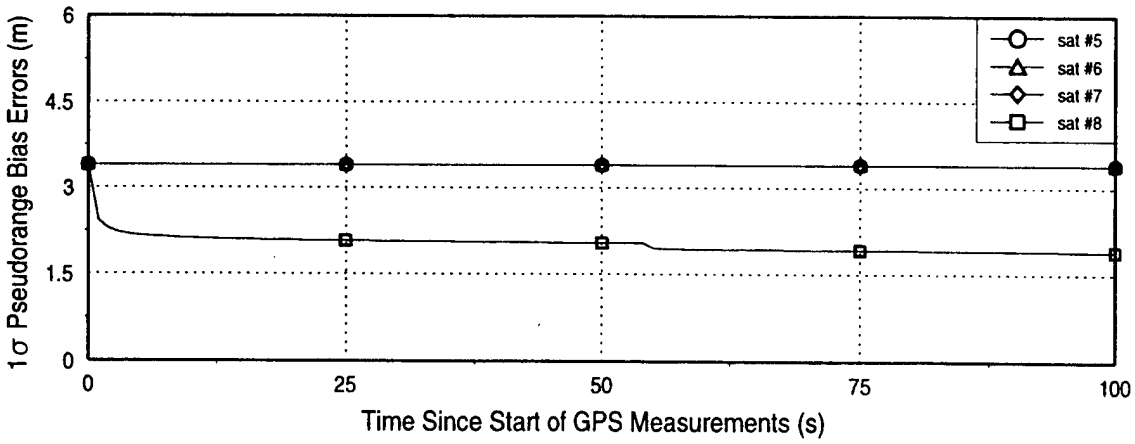

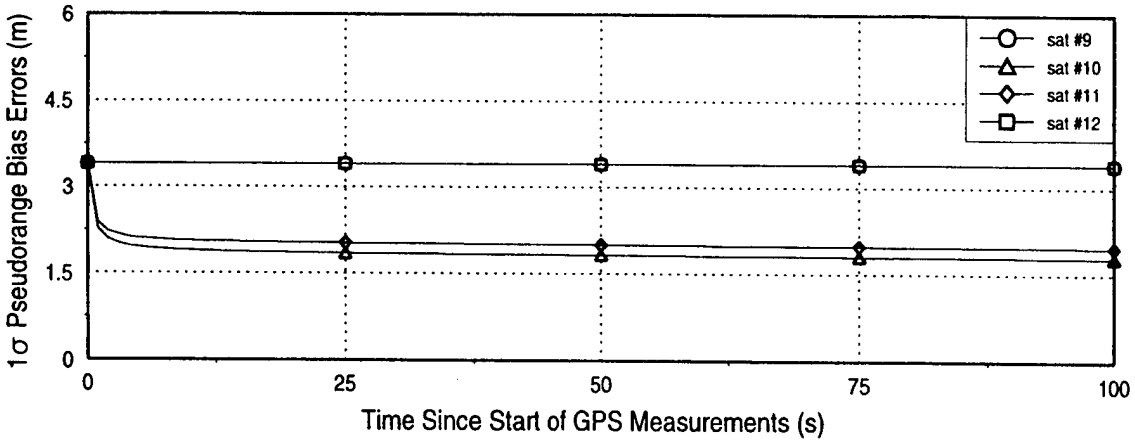

PSEUDORANGE BIAS ERRORS

Baseline All-In-View at Location A

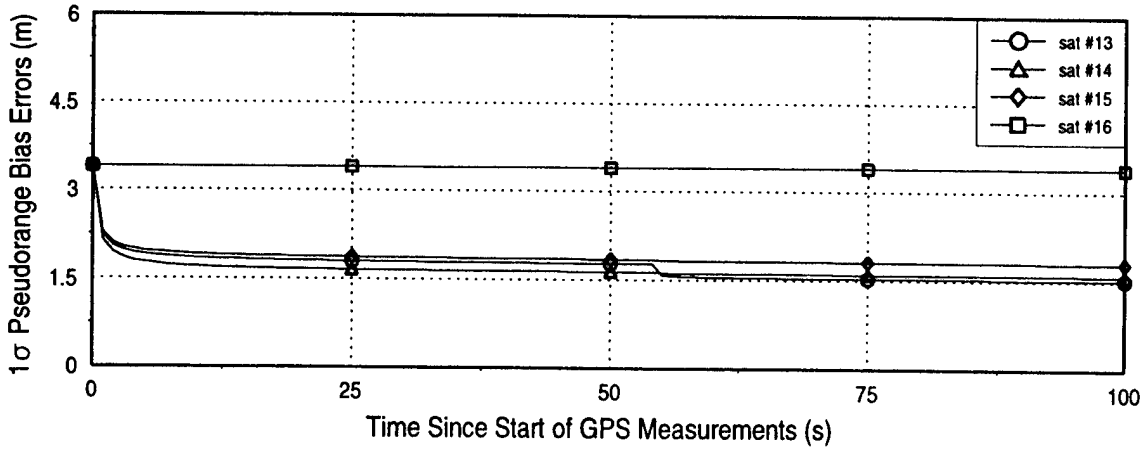

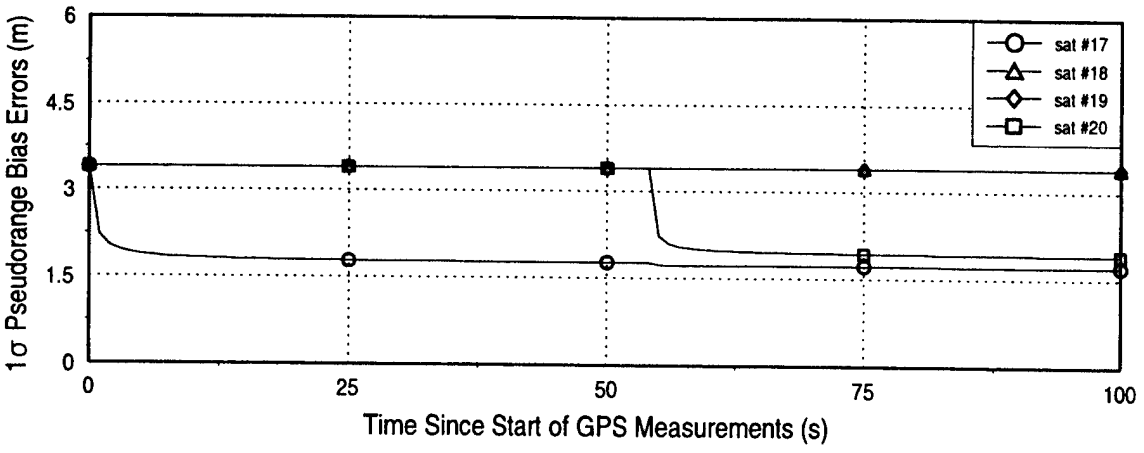

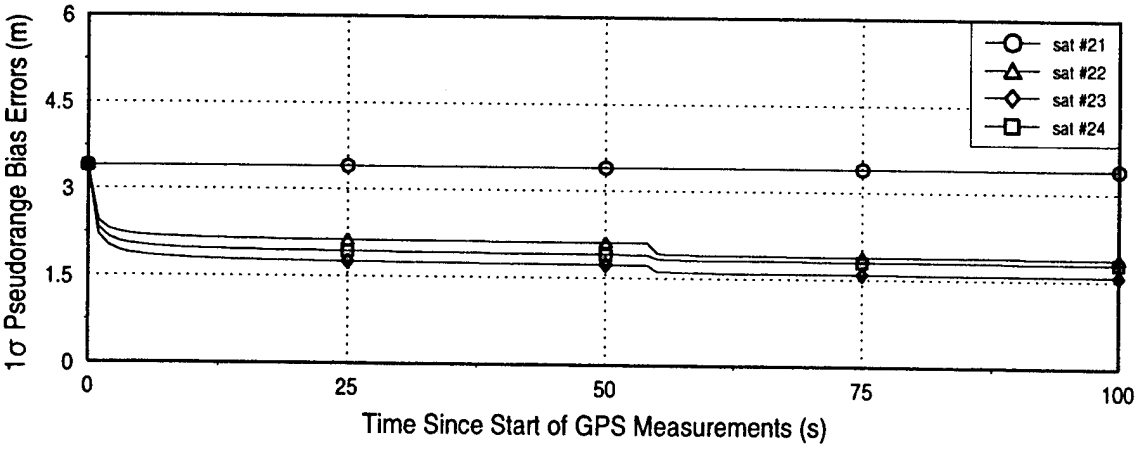

APPENDIX B

VALUES OF PHYSICAL CONSTANTS USED IN THE SIMULATIONS

Description	Value
Equatorial Radius of the Earth	6378137.0 m
Gravitational Parameter of the Earth	3.986012×10^{14} m^3/s^2
Rotation Rate of the Earth	$7.292115856 \times 10^{-5}$ rad/s
Speed of Light	2.99796×10^{8} m/s

REFERENCES

[1] Leick, A., *GPS Satellite Surveying*, Wiley, New York, 1990.

[2] The NATO Team, *NAVSTAR GPS User Equipment: Introduction*, Public Release Version, NAVSTAR-GPS Joint Program Office, Los Angeles Air Force Station, February 1991.

[3] Logsdon, T., *The NAVSTAR Global Positioning System*, Reinhold, New York, 1992.

[4] "GPS and DGPS Topics for C.S. Draper Laboratory," Navtech Seminars, Cambridge, MA, October 22-28, 1993.

[5] Personal communications with R.L. Greenspan, The Charles Stark Draper Laboratory, April 1994.

[6] Col. Green, G.B., and Dr. N.W. Massatt, "The GPS 21 Primary Satellite Constellation," NAVSTAR GPS Joint Program Office and The Aerospace Corporation, El Segundo, CA, 1989.

[7] Lavrakas, J.W., and 1Lt C. Shank, "Satellite Navigation and Surveillance Systems Beyond Year 2000," The Institute of Navigation 49th Annual Meeting, Cambridge, MA, June 21-23, 1993.

[8] Personal communications with J.A. Soltz, The Charles Stark Draper Laboratory, April 1994.

[9] Soltz, J.A., "Fast Near-Optimum GPS Satellite Selection Algorithm," Memo No. ESD-94-213, The Charles Stark Draper Laboratory, April 20, 1994.

[10] Personal communications with M.V. Boelitz, The Charles Stark Draper Laboratory, March 17, 1994.

[11] Langley, R.B., "Time, Clocks, and GPS," *GPS World*, November/December 1991.

[12] Personal communications with S.W. Shepperd, The Charles Stark Draper Laboratory, August 1992 - May 1994.

[13] Personal communications with D.J. Pasik, The Charles Stark Draper Laboratory, December 1993 - May 1994.

[14] Brown, R.G., "A Baseline GPS RAIM Scheme and a Note on the Equivalence of Three RAIM Methods," *NAVIGATION: Journal of The Institute of Navigation*, Vol. 39, No. 3, Fall 1992.

[15] Briefing from 1Lt. C. Shank, USAF, 2nd Space Operations Center, November 5, 1993.

[16] Brown, A.K., "Civil Aviation Integrity Requirements for the Global Positioning System," *NAVIGATION: Journal of The Institute of Navigation*, Vol. 35, No. 1, Spring 1988.

[17] Brown, R.G., and P. Hwang, "GPS Failure Detection by Autonomous Means Within the Cockpit," *NAVIGATION: Journal of The Institute of Navigation*, Vol. 33, No. 4, Winter 1986-87.

[18] Brown, R.G., Chin, G.Y, and J.H. Kraemer, "RAIM: Will It Meet The RTCA GPS Minimum Operational Performance Standards," Proceedings of the 47th Annual National Technical Meeting on Using Synergism to Strengthen Navigation Systems, Phoeniz, AZ, January 22-24, 1991.

[19] Brown, R.G., and P. Hwang, *Introduction to Random Signals and Applied Kalman Filtering*, 2nd edition, Wiley, New York, 1992.

[20] Personal communications with T.A. Spitznagel, PaineWebber, May 1994.